River Training and Sediment Management with **Submerged Vanes**

A. Jacob Odgaard, Ph.D., P.E.

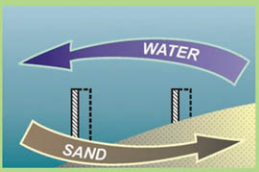

ASCE PRESS

River Training and Sediment Management with Submerged Vanes

Other Titles of Interest

***Protection and Restoration of Urban and Rural Streams,* edited by Michael Clar, Donald Carpenter, James Gracie, and Louise Slate** (ASCE Proceedings, 2002). Collection of technical papers covering many facets of stream restoration, from planning to post-construction monitoring. (ISBN 978-0-7844-0695-3)

***Environmental Fluid Mechanics: Theories and Applications,* edited by Hayley H. Shen, Alexander H. D. Cheng, Keh-Han Wang, Michelle H. Teng, and Clark C. K. Liu** (ASCE Committee Report, 2002). Comprehensive survey of fluid mechanics information most relevant to environmental engineers, including principles and contemporary applications in river, lake, coastal, and groundwater areas. (ISBN 978-0-7844-0629-8)

***Hydraulic Design of Labyrinth Weirs,* by Henry T. Falvey** (ASCE Press, 2003). Handbook on the hydraulic design of labyrinth spillways, from theory to current practice. (ISBN 978-0-7844-0631-1)

***Sedimentation Engineering: Processes, Measurements, Modeling, and Practice,* edited by Marcello Garcia** (ASCE Manuals and Reports on Engineering Practice No. 110, 2008). Companion to *Sedimentation Engineering: Classic Edition,* updating selected topics and exploring new ones. (ISBN 978-0-7844-0814-8)

***Sedimentation Engineering: Classic Edition,* by Vito A. Vanoni** (ASCE Manuals and Reports on Engineering Practice No. 54, 1975/2006). Classic reference for understanding the nature and scope of sedimentation problems, methods for their investigation, and practical approaches to their solution. (ISBN 978-0-7844-0823-0)

River Training and Sediment Management with Submerged Vanes

by

A. Jacob Odgaard, Ph.D., P.E.

ASCE PRESS

Library of Congress Cataloging-in-Publication Data

Odgaard, A. Jacob.
River training and sediment management with submerged vanes / by A. Jacob Odgaard.
p. cm.
Includes bibliographical references and index.
ISBN 978-0-7844-0981-7
1. Stream channelization. 2. Sediment control—Equipment and supplies. 3. Hydrofoils.
I. Title.

TC529.O34 2009
627'.12—dc22

2009000706

Published by American Society of Civil Engineers
1801 Alexander Bell Drive
Reston, Virginia 20191
www.pubs.asce.org

ISBN 978-0-7844-0981-7
Manufactured in the United States of America.

17 16 15 14 13 12 11 10 09 1 2 3 4 5

Contents

Preface

All throughout the ages, rivers have played an important role in society. They have provided means of transportation, water for irrigation, water supply, power generation, and many other uses. They have also caused disasters, primarily during floods when they inundate portions of the floodplain and destroy property and infrastructure. The sediment they transport from the watershed to the ocean often interferes with both navigation in the rivers and infrastructure along them. One of the river engineer's major tasks is to help facilitate optimum usage of this resource and at the same time provide protection against disasters. River training is the common solution. Traditional river training strategies include construction of dikes, wing dams, weirs, various types of revetments, and dredging. Unfortunately, many of these strategies are expensive and sometimes even a detriment to the environment. The submerged-vane technique presented in this book offers an alternative that protects the environment and facilitates sustainable developments around the river. In certain river environments, vanes are less expensive than traditional techniques and are equally effective.

The book is written because design guidelines are not readily available to the profession. Several papers have been published over the years describing the technique, and field installations have proved its feasibility. However, there is no single source outlining the steps necessary for design. Written for both students of hydraulics and water resources engineering and practicing engineers, in particular river engineers, the book offers a simple, step-by-step approach to the development of a submerged-vane design for a given application. The book presents the most up-to-date design guidelines. Recognizing that there is always room for further developments of the vane concept and for further improvements of the design guidelines, the book also summarizes the most important aspects of the underlying theory and laboratory tests validating the theory. By including part of the underlying theory, readers will be able to better understand the concept and make adjustments along the way as new ideas, tools, and techniques emerge.

Four different design objectives or scenarios are described: (a) stabilization of river bank; (b) stabilization of river bed; (c) sediment control at water intake or diversion; and (d) stabilization of river channel alignment. Chapter 1 presents illustrations of these four objectives. Chapter 2 describes the theoretical background

for these objectives, and presents the governing equations and a set of relatively simple design graphs applicable to all of these objectives.

The purpose of the laboratory tests described in Chapter 3 is to not only demonstrate validity of the theory, design equations, and graphs but also to show that results obtained in a laboratory model can be scaled to prototype conditions. Scalability of laboratory tests is important because prototype boundary conditions are often so complex that a model study is required for the development of final design.

In Chapter 4, the four design objectives and guidelines are illustrated with numerical examples, five in total. These examples include data typical of projects that are already completed, and they may serve as model examples for new, similar projects.

Select field installations are reviewed in Chapter 5. The installations are selected to cover the four design objectives and a wide range of flow and sediment conditions. The selection includes a few early designs even though, in retrospect, they are less efficient than the newer designs. Important lessons were learned from these early designs, and readers may value the progression in design development. Photos are used extensively to illustrate design features. However, vane installations cannot be photographed in design condition when they are fully submerged. Therefore, all photos of vane installations were taken at extreme low flow when the tops of the vanes extended above the water surface.

The book concludes with a summary of the design guidelines, in Chapter 6. The summary includes a list of typical dimensions, which are listed only to provide readers with a benchmark. Many variables affect the dimensions, some of which are summarized in this chapter. The chapter also summarizes the primary design considerations for the four design objectives or scenarios. The summary may serve as a checklist in preliminary design. The different vane materials that have been used so far in applications are also reviewed. They range from simple wooden planks to sheet-piling to double-curved, reinforced concrete panels. The chapter concludes with a brief summary of the main limitations to vane use.

Acknowledgments

The material in this book is based on work supported by the following sponsors: U.S. National Science Foundation; U.S. Army Corps of Engineers; U.S. Geological Survey; Electric Power Research Institute, State of Iowa; and the Iowa Department of Transportation. Figures and photographs were made available from several individuals and organizations, including Robert DeWitt, River Engineering International; Paul Collingsworth, FPL Energy Duane Arnold, LLC; Robert Ettema, University of Wyoming; Rhoël M. Tierra, Nebraska Public Power District; Keh-Chia Yeh, National Chiao Tung University; Adnan Alsaffar, Consultant; J. Oosterman, DHV Consulting Engineers; Genesis Energy, New Zealand; and Shive-Hattery, Inc., Iowa. Michael Kundert, IIHR, prepared the line drawings and concept renderings.

Many University of Iowa graduate students were involved in the development of the vane technology. They are, in alphabetical order: Brian Barkdoll, Mary Bergs, Hong-Yuan Lee, Carlos Mosconi, Vince Neary, Sanjiv Sinha, Anita Spoljaric, and Yalin Wang.

John F. Kennedy, University of Iowa, helped formulate the first theoretical approach, and he continued to support subsequent developments of the technology. Frank Engelund, Technical University of Denmark, the author's academic advisor and mentor, spurred the author's interest in river engineering and fluid mechanics in general.

A. Jacob Odgaard
IIHR-Hydroscience and Engineering
College of Engineering, University of Iowa

This page intentionally left blank

Notation

The following symbols are used in this book:

A = area of flow cross section, or area of vane field
a = amplitude of meander wave
b = channel width
c = constant (Eq. 2-23)
c_L = lift coefficient for force by vane on flow (Eq. 2-5)
D = median diameter of sediment
d = flow depth
d_c = centerline flow depth
d_o = pre-vane cross-sectional average flow depth
d_m = maximum flow depth at outer bank of river curve
d_v = vane-induced flow depth within vane field or at outer bank of river curve (Figs. 2-11, 2-12, 2-13)
F = function of m and d/H (Eq. 2-31)
$\mathbf{F}_D$ = sediment Froude number = $u_o/\sqrt{(gD)}$
F_D = vane-induced drag force
F_L = horizontal vane lift force
f = Darcy-Weisbach friction factor
g = acceleration due to gravity
g_r = ratio of bed-load transport into diversion per unit width g_i to bed-load transport in main channel per unit width
H = vane height (above pre-vane streambed)
H/L = vane aspect ratio
k = meander-wave number
L = vane length
ℓ = meander length, measured along channel centerline
M = function of m (Eq. 2-20)
m = resistance parameter = $\kappa u_o/\sqrt{gSd_o} = \kappa\sqrt{8/f}$
N = number of vanes in vane system
n = lateral distance from channel centerline, or Manning's number
Q = discharge

Q_i = intake/diversion discharge
q = discharge per unit width (specific discharge)
q_i = unit discharge of water into intake or diversion
q_r = ratio of unit discharge of water into intake or diversion to unit discharge of water in main channel = q_i/q
R = hydraulic radius
r = radius of curvature, or radial distance from vortex axis
r_c = centerline radius of curvature
S = longitudinal (streamwise) slope of water surface and/or channel bed
S_{tc} = transverse bed slope at channel centerline
s = longitudinal (downstream) distance along channel centerline, or downstream distance along vortex axis
T = vane submergence below design water level
t = time
u = depth-averaged flow velocity
u_o = pre-vane cross-sectional average velocity
u_m = maximum depth-averaged flow velocity at outer bank of river curve
v = transverse velocity component
v_θ = tangential velocity in vane induced vortex
α = vane angle of attack
β = vane system angle with bankline (Fig. 3-14) or area-averaging factor (Eqs. 2-12 and 2-13)
λ = meander wavelength, or vane interaction coefficient
Δh = increase in bed level (decrease in flow depth) outside vane field
Δd = decrease in bed level (increase in flow depth) outside vane field
κ = von Karman constant (≈ 0.40)
δ_b = distance from bank to vane
δ_s, δ_n = vane spacings in streamwise and transverse directions, respectively
δ_v = width of vane field or width of accretion created by vane field
φ = phase lag (angle) between channel curvature and transverse bed slope (Fig. 2-19)
θ = included angle of channel segment (Eq. 2-30), or critical Shields stress
ε = eddy viscosity
τ = bed shear stress
Γ = vane-induced horizontal circulation

CHAPTER 1

Introduction

1.1 Objective

Sediment management, in particular the control of sediment movement, scour, and deposition, is one of the most difficult problems encountered by river engineers. Bed scour along the outer bank of river curves frequently causes undermining of the banks and loss of soil and infrastructure (Figs. 1-1 and 1-2). Deposition of sediment often reduces flood-conveyance capacity of rivers and interferes with navigation (Fig. 1-3). Deposition of sediment is also a recurring problem at many water intakes and diversions (Fig. 1-4). The main difficulty in the engineering treatment of these problems is the absence of effective, affordable measures to control the movement of sediment.

Traditionally, sediment management, and river training in general, are accomplished by construction of revetments, dikes, wing dams, weirs, and by dredging. These techniques function by adjusting bank resistance and/or bank erodibility and/or flow and bed topography. They have been perfected over many years, and experience and design guidelines are well documented in the literature (Biedenham et al. 1997; Petersen 1986; Jansen et al. 1979; and numerous reports by the U.S. Army Corps of Engineers).

The submerged-vane technique is a new and not so well documented technique whose promise is becoming more evident every day. Both laboratory and field tests (Odgaard and Kennedy 1983; Odgaard and Spoljaric 1986; Odgaard and Mosconi 1987; Wang 1990; Fukuoka 1989; Fukuoka and Watanabe 1989) suggest that this technique has a broad range of applications. Vanes have already been installed in many rivers throughout the world, including the Nile River, Egypt; Waikato River, New Zealand; Kosi River, Nepal (Fig. 1-5); Kuro River, Japan; Feng-Shan Creek, Taiwan; Missouri River, United States; and a number of smaller rivers in the midwest states of the United States. Figure 1-6 shows an early version of the vane design installed in East Nishnabotna River, Iowa. Feedback from these and other sites have resulted in an improved understanding of the functioning of vanes and improved design basis.

The cost of a vane installation is generally lower than that of a comparable traditional river training structure. The cost of the East Nishnabotna installation was

Figure 1-1. Stream bank erosion in East Nishnabotna River, Iowa. *Source:* Odgaard (1987).

Figure 1-2. Abutment scour at Bulls Bridge over Rangitikei River, New Zealand. *Source:* Raudkivi and Ettema (1985), ASCE.

Figure 1-3. Shoaling in Kaoping River, Taiwan, China, 2007.

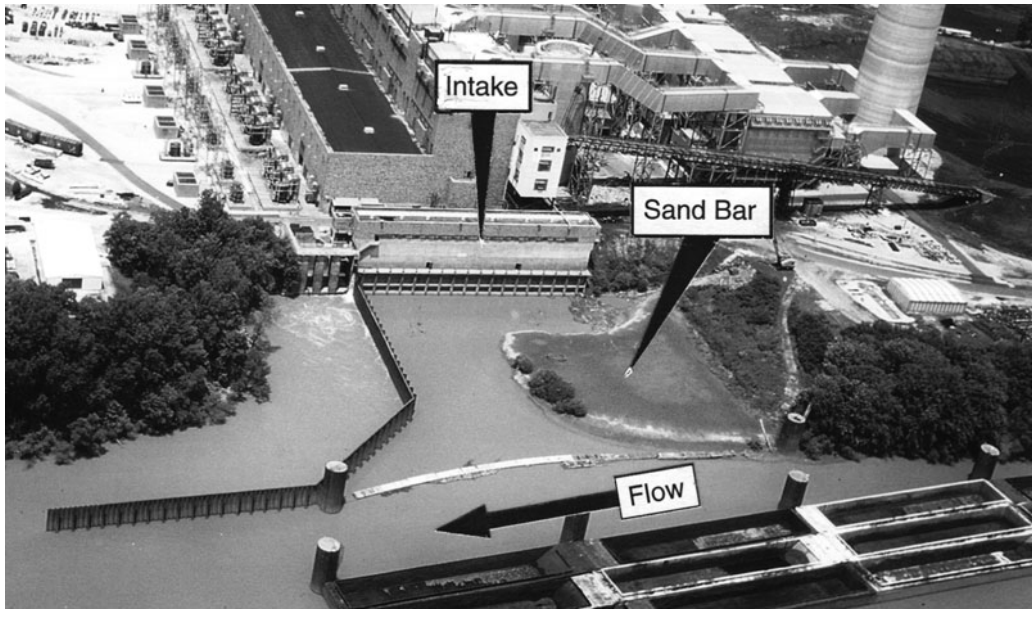

Figure 1-4. Sedimentation in forebay of intake adjoining Ohio River, U.S.A.
Source: Neary et al. (1999), ASCE.

Figure 1-5. Submerged vanes being installed at water intake on Kosi River, Nepal. View is downstream and inside of coffer dam (right). The vane system will prevent sediment from being entrained into the intake (left). Courtesy of J. Oosterman, DHV Consulting Engineers.

Figure 1-6. Submerged vanes (early version) in East Nishnabotna River, Iowa, protecting stream bank against erosion. View is downstream at extreme low flow, showing vane-induced sediment deposition along right bank. The sediment deposits provide natural toe protection at the bank.

(per meter bank) about half the cost of a rock riprap embankment installed at the same time along a comparable reach of the nearby Raccoon River.

1.2 Concept

Submerged vanes are small flow-training structures (foils) designed to modify the near-bed flow pattern and redistribute flow and sediment transport within the channel cross section. The structures are installed at an angle of attack of typically 10 to 20 degrees with the flow, and their initial height is 0.2 to 0.4 times the local water depth at design stage.

The vanes function by generating secondary circulation in the flow. The circulation alters magnitude and direction of the bed shear stresses and causes a change in the distribution of velocity, depth, and sediment transport in the area affected by the vanes. As a result, the riverbed aggrades in one portion of the channel cross section and degrades in another (Fig. 1-7).

To illustrate the concept, consider two vanes placed near the centerline of a long, rectangular channel as shown in Fig. 1-8. The view in the figure is toward downstream and before water is admitted to the flume. The vanes are 7 cm tall and 16.5 cm long and angled at 20 degrees with the centerline of the flume. Figure 1-9 is a top view of the same two vanes with water flowing through the flume (from top of photo to the bottom). Water depth is about 15 cm, slightly more than twice the vane height. The figure also shows two dye traces from dye injected upstream from the vanes. Neutrally buoyant blue dye is being injected at the bottom and neutrally buoyant red dye on the surface. The figure shows the circulation that the vanes induce in the flow downstream from the vanes. (In the grayscale photograph, the red dye appears as the darker of the two dye traces.) Figure 1-10 shows an array of four vanes placed across the channel with blue dye being injected on the bottom upstream of the array. As seen, the vane array causes the blue

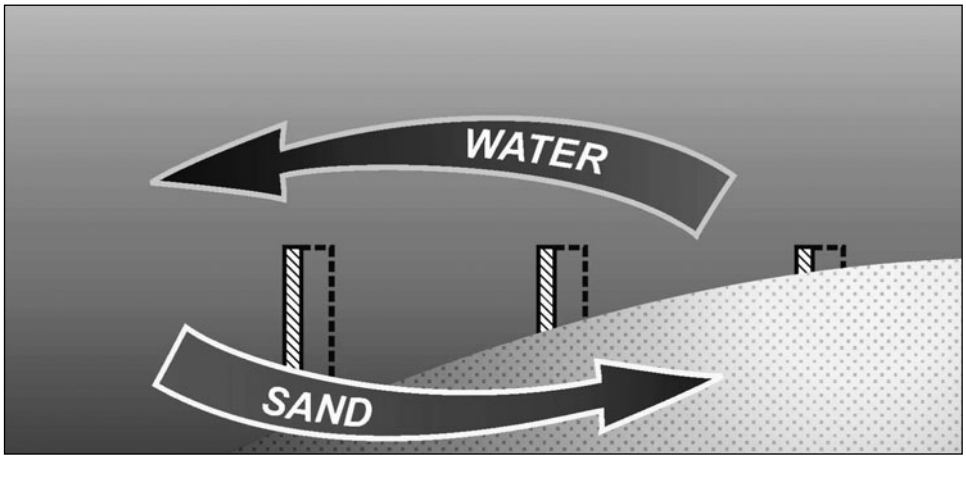

Figure 1-7. Submerged vanes redistribute flow and sediment transport within a channel cross section.

Figure 1-8. Two vanes at centerline of open channel. View is downstream before water is admitted.

dye to be deflected to the left, illustrating what an array like this could do to sand moving along the bed. Near-bed flow is being deflected toward the left side, and surface flow toward the right. The effect of a vane on bed sediment is shown in Fig. 1-11. The vane in this figure is 7 cm tall and angled 20 degrees with the flow. With water flowing through the flume at a depth of about 18 cm, the vane effectively diverts bed load toward one side, creating a longitudinal ridge of sand along one side of the channel and a trough along the other side.

Typically, vanes are installed in arrays along one side (or both sides) of a river channel over a reach long enough to create a desired flow redistribution. Their advantage over traditional training structures, such as dikes and groins, is that they can produce a given redistribution of flow at less resistance to the flow and at less cost. Whereas groins and dikes, which are usually placed normal to the flow, produce flow redistribution by simple continuity and drag force, vanes produce flow redistribution by vorticity. Because they are nearly aligned with the flow, the associated drag force is relatively small. Their alignment also eliminates the problem of structural stability associated with local scour, which is often a concern with the traditional structures. An important point in regard to flow resistance is that the resulting lower velocity within the vane field not only causes a reduction in flow depth, but also results in dunes in the vane field that are smaller than prior to the installation of vanes. So, in the vane field, the increase of flow resistance due to vane-induced drag is partially outweighed by the decrease of flow resistance due to smaller size of bed forms. As a result, the overall change in water-surface slope is often negligible. This feature makes the vanes ideally suited for sustainable adjustments of flow in the river.

Figure 1-9. Top view of vane pair with water flowing (from top of photo to bottom) at depth about twice the vane height; dye injected upstream (blue at the bottom and red at the surface) shows vane-induced circulation.

1.3 Developments

Although the literature indicates that vanes, or panels, similar to those discussed here have been used in the past for river-channel stabilization (Potapov and Pyshkin 1947; Chabert et al. 1961; Jansen et al. 1979), little is documented on vane design and performance. Only recently have efforts been made to optimize

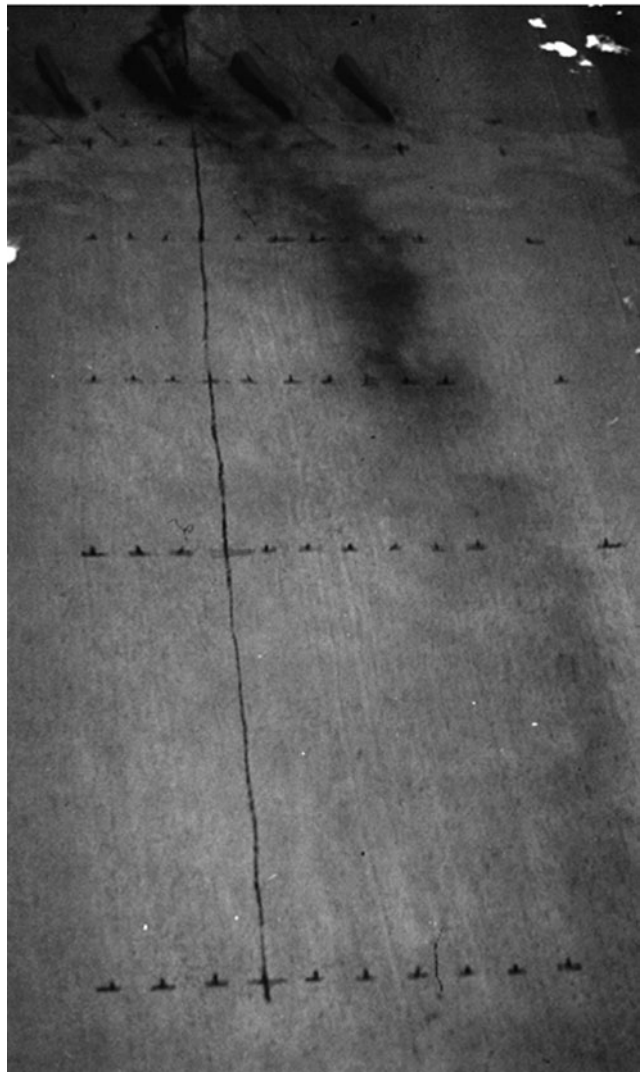

Figure 1-10. Vane array deflecting near-bed flow (blue dye) toward left side in open-channel flow.

vane design and document performance. These efforts have targeted three broad areas of application: (a) bank protection, (b) shoaling amelioration, and (c) sediment control at diversions and water intakes.

1.3.1 Areas of Application

The first known attempts to develop a theoretical design basis are by Odgaard and Kennedy (1983) and Odgaard and Spoljaric (1986). Odgaard's and Kennedy's efforts are aimed at designing a system of vanes to stop or reduce bank erosion

Figure 1-11. Vane in sand-bed channel deflecting sediment to one side of the channel.

in river curves. In such an application, the vanes are laid out so that the vane-generated secondary current eliminates the centrifugal-induced secondary current, which is the root cause of bank undermining (Fig. 1-12). The centrifugally induced secondary current in river bends, also known as the transverse circulation or helical motion, results from the difference in centrifugal acceleration along a vertical line in the flow because of the nonuniform vertical profile of the velocity. The secondary current forces high-velocity surface current outward and low-velocity near-bed current inward (Fig. 1-12a). The increase in velocity at the outer bank increases the erosive attack on the bank, causing it to fail. By directing the near-

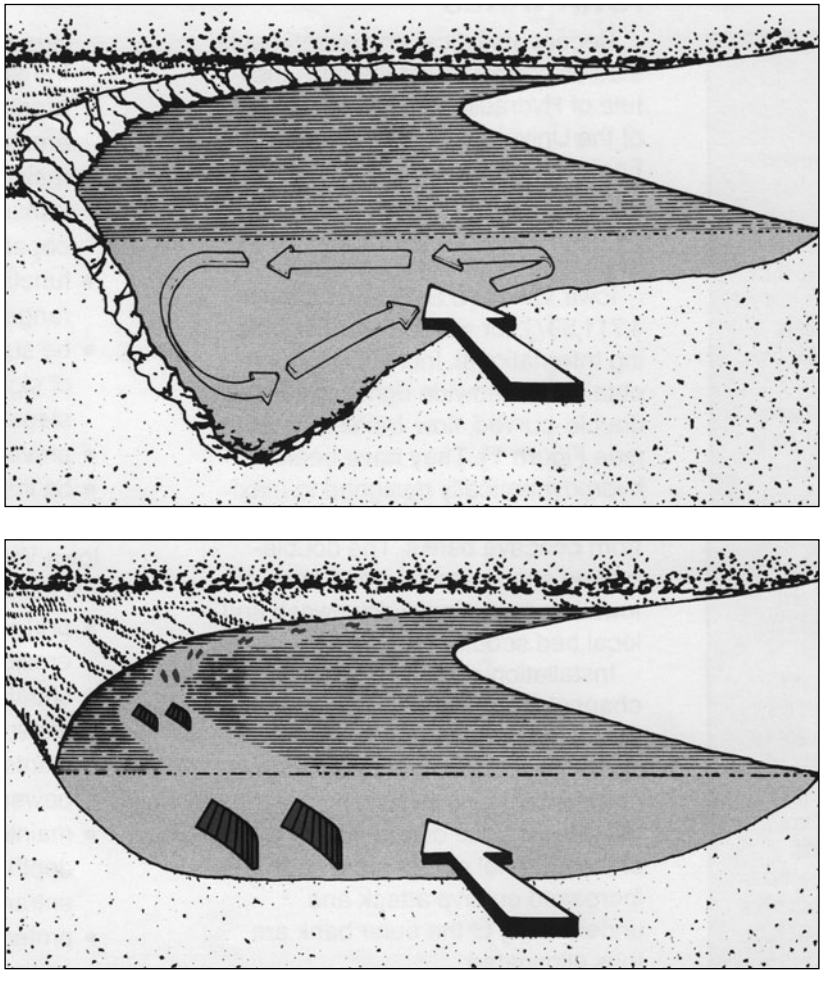

(a)

(b)

Figure 1-12. Submerged vanes for mitigating bank erosion. (a) Naturally occurring secondary current in river bend; (b) vane-induced secondary current eliminates the naturally occurring secondary current and stabilizes the bank.

bed current toward the outer bank, the submerged vanes counter the centrifugally induced secondary current, thereby inhibiting bank erosion. The vanes stabilize the toe of the bank (Fig. 1-12b). Laboratory tests by Odgaard and Wang (1990) have confirmed that a vane layout can be designed that makes the water and sediment move through a river curve as if it were straight.

Figure 1-13 shows how vanes might be laid out to stabilize a meandering river reach. Field tests with this application have been conducted by Odgaard and Mosconi (1987), Fukuoka and Watanabe (1989), and others. Select field tests are described in detail in Chapter 5.

The technique has been further developed to ameliorate shoaling problems in rivers (Fig. 1-14). This application is suggested by laboratory tests (Odgaard

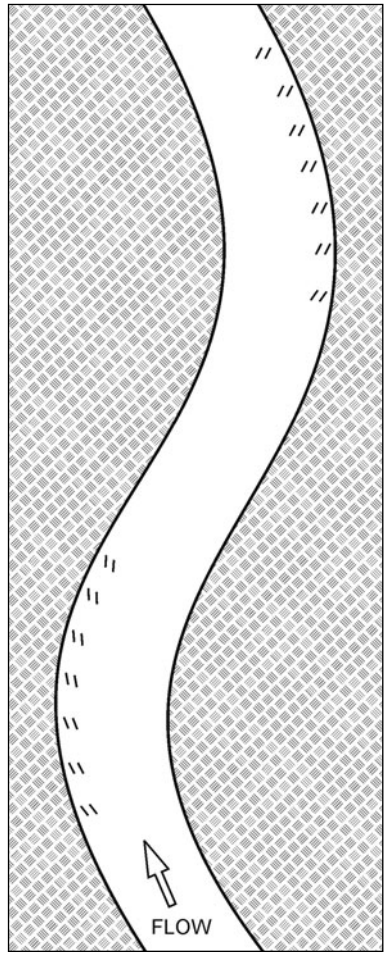

Figure 1-13. Layout of vane systems in meander curves.

and Spoljaric 1986) in which vanes are laid out to change the cross-sectional profile of the bed in a straight channel. The tests show that significant changes in depth can be achieved without causing significant changes in cross-sectional area, energy slope, and downstream sediment transport. The changes in cross-sectional average parameters are small because the vane-induced secondary current changes the direction of the bed shear stresses by only a small amount. These findings were validated in subsequent tests by Odgaard and Wang (1991).

The vanes' effectiveness in sediment redistribution is particularly useful at diversions and water intakes. Strategically placed, the vanes are effective in preventing bed-load transport from entering the diversion or water intake (Fig. 1-15). Guidelines for this application, first developed by Odgaard and Wang (1991), have been refined through several laboratory studies and field tests (Wang et al. 1996; Barkdoll et al. 1999; Nakato and Ogden 1998; Muste and Ettema 2000; Michell et al. 2006).

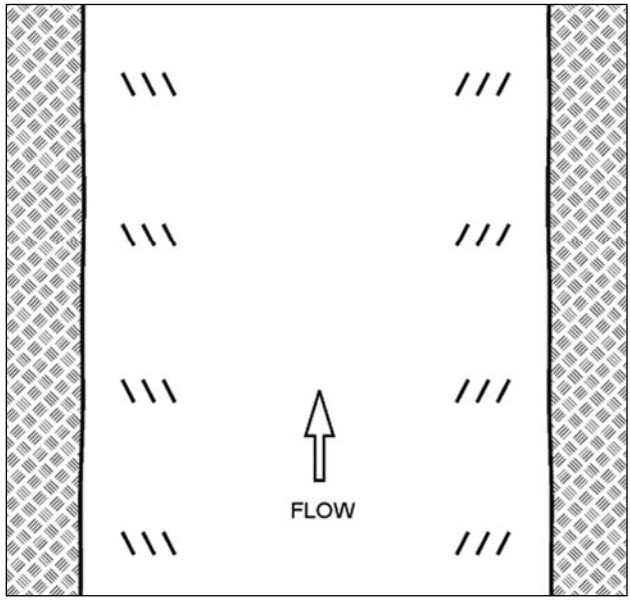

Figure 1-14. Layout of vane systems to ameliorate shoaling problems.

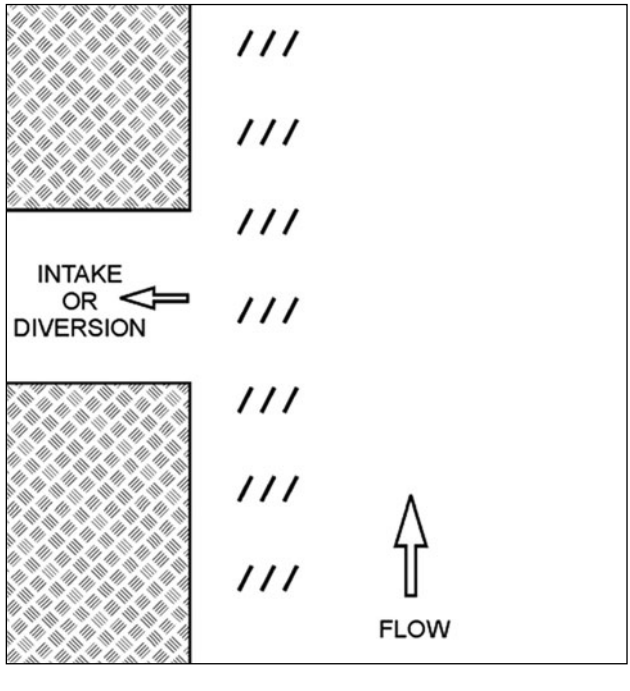

Figure 1-15. Layout of vane system to prevent bed load from entering water intake.

Finally, vanes may be used effectively in conjunction with traditional river training strategies. For example, protecting a river bank using a system of submerged vanes together with a moderate toe protection with riprap is, in many cases, less expensive than and equally effective as a full-height riprap embankment. The vane–riprap solution is also more environmentally attractive because both vanes and riprap will be submerged most of the time, allowing the upper bank to maintain its natural structure and ecosystem. As will be demonstrated in Chapter 5, vanes also work well in combination with dikes and wing dams. In this case, the dikes and wing dams are installed upstream to stabilize a river segment and provide optimum approach-flow conditions for the vane system.

1.3.2 Vane Profile

Most applications so far have been with a simple, flat-panel design. Laboratory studies (Spoljaric 1988; Odgaard and Spoljaric 1989) have shown that vane efficiency can be improved by a redesign of the vanes. These studies were conducted in a flume with the vanes mounted on a separate bottom panel that allowed measurements of horizontal lift and drag. Figure 1-16 shows the experimental setup

Figure 1-16. Lift and drag measurements on vane profiles in laboratory flume resulted in improved vane design.

and Fig. 1-17 the different designs tested. The final design is sketched in Fig. 1-18. Figure 1-19 shows the improved vane prototype.

Efforts are currently underway to further optimize the vane profile using genetic algorithms. Reference is made to Ouyang et al. (2006). Another effort is related to applications in the coastal zone. Here, vanes are being designed so when they are placed in the upper part of the water column and aligned with a specific angle of attack to the incoming waves, they induce a radiation stress component that affects the long-shore sediment transport. Reference is made to Marelius (2001).

1.3.3 Rock Vanes and Bend-Way Weirs

In their first analyses, Odgaard and Kennedy (1983) suggested that if vertical vanes (say, in the form of sheet-piling) were objectionable for one reason or another, it is likely that so-called rock vanes, constructed from rows of dumped rock with steep side slopes, would achieve much the same result, although more and longer vanes of this type likely would be required because of the smaller transverse force per unit area that would be exerted on them. It still remains to be seen whether rock vanes designed with the principles described herein will perform satisfactorily. One of the potential concerns with rock vanes is that they may cause too large a local reduction in water-surface slope. Such a reduction would cause a slowdown in near-bank velocity. However, downstream from the rock vanes, slope would increase again, causing higher near-bank velocity and, potentially, bed scour. Channel-alignment instability may result. As will be demonstrated subsequently, vertical vanes placed at a small angle of attack have negligible effect on water-surface slope.

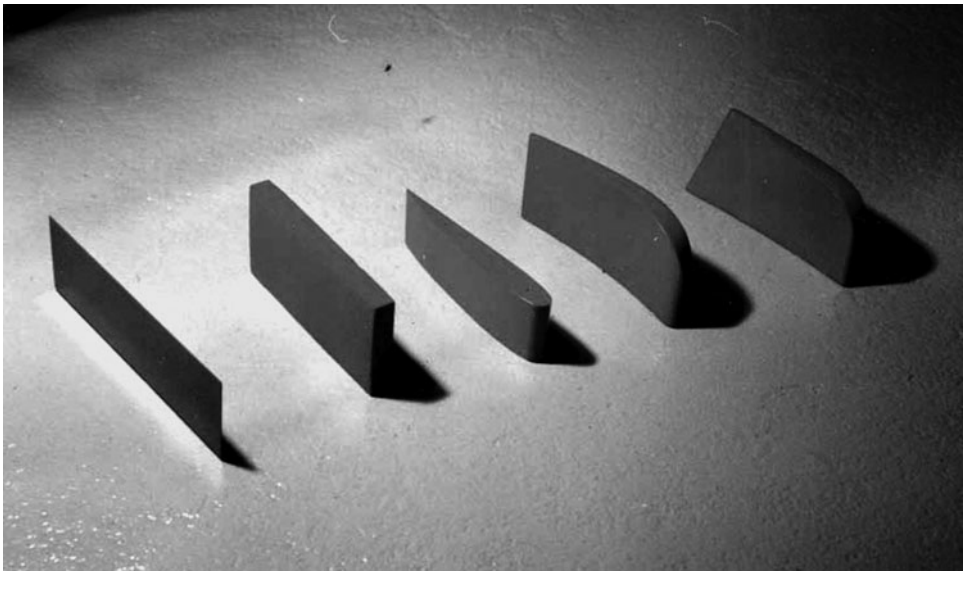

Figure 1-17. Different vane designs tested in the laboratory flume in Fig. 1-16.

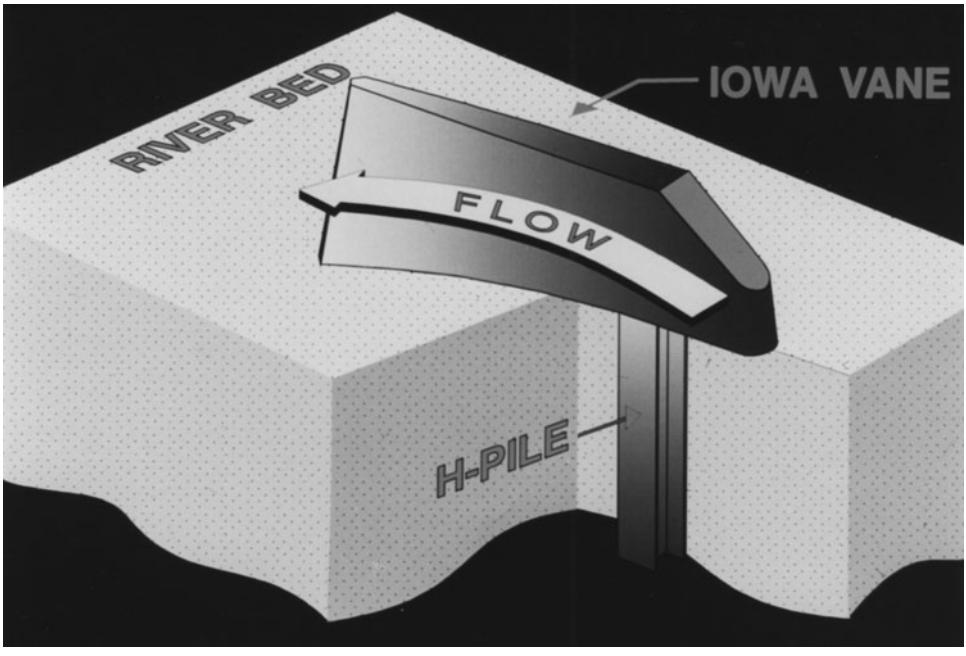

Figure 1-18. Sketch showing improved final design. Courtesy of Robert DeWitt, River Engineering International.

Figure 1-19. Improved vane prototype. Courtesy of Robert DeWitt, River Engineering International.

A unique type of rock vanes have been developed and are being promoted by the U.S. Army Corps of Engineers, the so-called bend-way weirs (Fig. 1-20). Bend-way weirs are conceptually quite different from the vanes discussed in this book. Both types are designed to redirect the near-bank surface current away from the bank. However, the submerged vanes do it by inducing a secondary current in the flow, eliminating the naturally occurring secondary current, whereas the bend-way weirs do it by "weir effect." The weirs cause water flowing over them to be redirected at an angle perpendicular to the axis of the weirs. With the weirs angled slightly upstream, flow is directed away from the outer bank of the bend and toward the point bar. As will be clear subsequently, the alignment of the Corps's bend-way weirs is at odds with the design guidelines presented in this book.

1.4 Sustainability

As suggested earlier, vanes are ideally suited for sustainable adjustments of the flow in a river channel. This is because the adjustments are made without causing significant changes in the variable that has probably the greatest effect on channel stability, namely, water-surface slope or energy expenditure per unit length. By preserving slope and rate of energy expenditure of the river flow, vanes also

Figure 1-20. U.S. Army Corps of Engineers's bend-way weirs.
Source: U.S. Army Corps of Engineers (2008).

help preserve the ecosystem of the river and its environment. However, at the same time, it is important to recognize that the vane-induced adjustments are static. River channels are dynamic. Many river channels maintain their dynamic equilibrium by the natural process of meandering, that is, a certain amount of bankline migration may be part of the natural process of maintaining dynamic equilibrium. Therefore, in certain river environments, vane design must be preceded by a channel stability analysis so the vanes can be laid out to anticipate migration and provide long-term stability.

A channel stability analysis is also important when new channel alignments are being designed, for example, in channel restoration projects and in re-meandering of previously straightened channels. An example of a stability analysis is given in Chapter 2. The example shows how a stable meander plan form is obtained by perturbation stability analysis, and how vanes may be used to preserve the stable plan form. However, channel restoration is still an area of much research, and a stability analysis based on a single-thread meander plan form may not always be sufficient for a sustainable solution. Reference is made to Ward et al. (2001) and Bledsoe and Watson (2001).

This page intentionally left blank

CHAPTER 2

Theory

2.1 Airfoil Analogy

This section summarizes the theoretical analysis that was used for developing the design guidelines. Flow around a single vane is described first, using the theory of flow around airfoils. This description is followed by an analysis of flow around a vane pair. In this case, flow around one vane affects the flow around the other, and an interaction coefficient is introduced. The section concludes with a brief description of flow in a field of vanes arranged in arrays along one side of a channel.

2.1.1 Single Vane

A submerged vane at a small angle of attack with the flow, α, induces a horizontal circulation in the flow downstream (Fig. 2-1). The circulation arises because the vertical pressure gradients on the two surfaces of the vane cause the fluid flowing along the high-pressure (upstream) side to acquire an upward velocity component, whereas on the low-pressure (downstream) side there is a downward velocity component. The resulting vortices (vortex sheet) at the trailing edge of the vane roll up to form a large vortex springing from a position near the top of the vane. This vortex is carried with the flow downstream, where it gives rise to a secondary or helical motion of the flow and associated changes in bed shear stress and bed topography (Fig. 2-2). These changes can be calculated (see Odgaard and Wang 1991; Wang and Odgaard 1993). The following is a brief summary of the calculation, which is based on ideal flow around a vane.

The vane-induced vortex is described as a steady potential (Rankine) vortex (Eibeck and Eaton 1987). Its strength decays because of viscous diffusion as the vortex is transported downstream. In an unbounded flow field, the tangential velocity perpendicular to the core axis of such a vortex is (Lamb 1932):

$$v_\theta = \frac{\Gamma}{2\pi r}\left[1 - \exp\left(-\frac{u}{4\varepsilon s} r^2\right)\right] \tag{2-1}$$

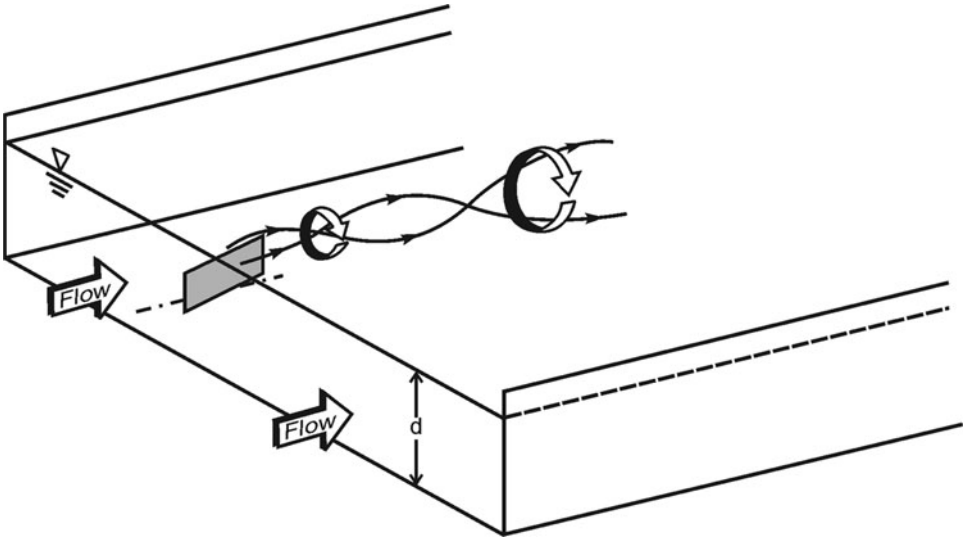

Figure 2-1. Schematic showing vane-induced circulation.

in which r = radial distance from vortex axis; ε = eddy viscosity; s = downstream distance along the vortex axis; u = velocity of fluid transporting the vortex or velocity approaching vane; and Γ = horizontal circulation at $s = 0$. This description is good only when the vortex is far from the flow boundaries. The presence of the bed and free surface distorts the vortex and gives rise to larger tangential velocities near the boundaries than are predicted by Eq. 2-1. The effect of the boundaries on the tangential velocity is accounted for analytically by using the method of images. The transverse velocity component, v, is obtained by summing the horizontally projected velocities of the vortex and images:

$$v = \sum_{i=1}^{\infty} v_i \tag{2-2}$$

where $v_i = v_{\theta_i} \cos(v_{\theta_i}, n)$; v_{θ_i} = tangential velocity due to vortex (or image) i; and (v_{θ_i}, n) = angle between velocity vector v_{θ_i} and the axis (n) along the bottom perpendicular to the s-axis. The summation includes the ideal vortex and all the

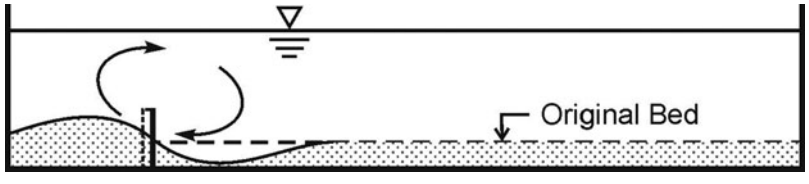

Figure 2-2. Schematic showing vane-induced change in bed profile.

images above the water surface and below the bed (see Wang 1991 for the distribution). Assuming ideal flow around the vane, the horizontal circulation, Γ, is calculated by relating it to the horizontal lift force, F_L, which the vane exerts on the flow. This lift force has the same magnitude as the force that the flow exerts on the vane, which, according to the Kutta-Joukowskii theorem (Sabersky and Acosta 1964), is proportional to the vertical circulation around the vane associated with the shift of the rear stagnation point to the trailing edge of the vane. This vertical circulation, in turn, is equal to the horizontal circulation, Γ (Helmholz's second theorem). Consequently,

$$F_L = \rho \Gamma u H \tag{2-3}$$

where ρ = fluid density and H = vane height. F_L may also be related to dynamic pressure as

$$F_L = \frac{1}{2} c_L \rho L H u^2 \tag{2-4}$$

in which L = vane length and c_L = lift coefficient. By assuming that the distribution of vertical circulation around the vane is elliptical (maximum at the bed and zero at the top of the vane), the lift coefficient is (Odgaard and Spoljaric 1986; Odgaard and Mosconi 1987):

$$c_L = \frac{2\pi\alpha}{1 + \frac{L}{H}} \tag{2-5}$$

Equations 2-3, 2-4, and 2-5 yield

$$\Gamma = \frac{\pi \alpha L u}{1 + \frac{L}{H}} \tag{2-6}$$

As seen in Chapter 3, with this relation for Γ, Eqs. 2-1 and 2-2 provide a reasonably good description of the distribution of vane-induced transverse velocity. The calculated transverse velocity does not include the contribution from the bound vortex (vertically around the vane) and, thus, is slightly less than the actual value. The measurements reported in Chapter 3 show that the decay rate of the vortex is simulated well by using the depth-averaged value of eddy viscosity corresponding with the measured friction factor.

The vane-induced transverse bed shear stress, τ_{vn}, is calculated by assuming that it has the same ratio to the streamwise bed shear stress, τ_{bs}, as the near-bed value of ν has to the near-bed value of streamwise velocity, u:

$$\frac{\tau_{vn}}{\tau_{bs}} = \frac{\nu}{u} \tag{2-7}$$

By substituting Eq. 2-2 into Eq. 2-7, the transverse bed shear stress is

$$\tau_{vn} = F_L f_v \tag{2-8}$$

where f_v = function of m and H (see Odgaard and Wang 1991). It follows that the streamwise (s) component of the induced bed shear stress is

$$\tau_{vs} = F_D f_v \tag{2-9}$$

where F_D = drag force associated with F_L. Relating F_D to dynamic pressure yields

$$F_D = \frac{1}{2} c_D \rho L H u^2 \tag{2-10}$$

where c_D = drag coefficient. It follows that $F_D = (c_D/c_L)F_L$, and

$$c_D = \frac{1}{2\pi} \frac{L}{H} c_L^2 \tag{2-11}$$

As mentioned, this description is for ideal flow around a vane. In reality, for angles of attack larger than about 5 degrees to 7 degrees, flow separates from the suction side of the vane before reaching the trailing edge. In the separated zone, the pressure is higher than elsewhere on the suction side; it is essentially the same as on the pressure side. Consequently, F_L is less than if no separation occurred (i.e., less than calculated by Eq. 2-3). In addition, the separation, together with the small vane–aspect ratio, may also make the vortex shedding more complex than described by the simple Rankine equation (Eq. 2-1). Nevertheless, experimental data (Odgaard and Spoljaric 1986) support the aforementioned relations.

2.1.2 Vane Pair

The area of stream bed affected by a single vane is limited. To generate a larger, coherent vortex that affects the flow pattern over a wider area of the channel cross section, several vanes must be employed. If the vanes are arranged in an array as shown in Figs. 2-3 and 2-4, the width of the affected area is increased. The question arises as to how the vanes should be spaced so that a coherent vortex is formed without diminishing the effectiveness of individual vanes. Transverse spacing is denoted δ_n.

To define the problem, consider flow around an array of two vanes (i.e., two vanes placed side-by-side with the same orientation). If the distance between them, δ_n, is very large, the effect of one of the vanes on the flow around the other is very small. Each vane generates its own distinct vortex, and the associated circulation is about the same as that due to one isolated vane. However, in this case, the two vortices do not merge to form a combined vortex, so the objective is not met. If the spacing δ_n is small, the two vanes generate a combined vortex downstream. In this situation, interaction between the vanes becomes pronounced. The vortex generated by one vane interferes with the vortex generated by the other.

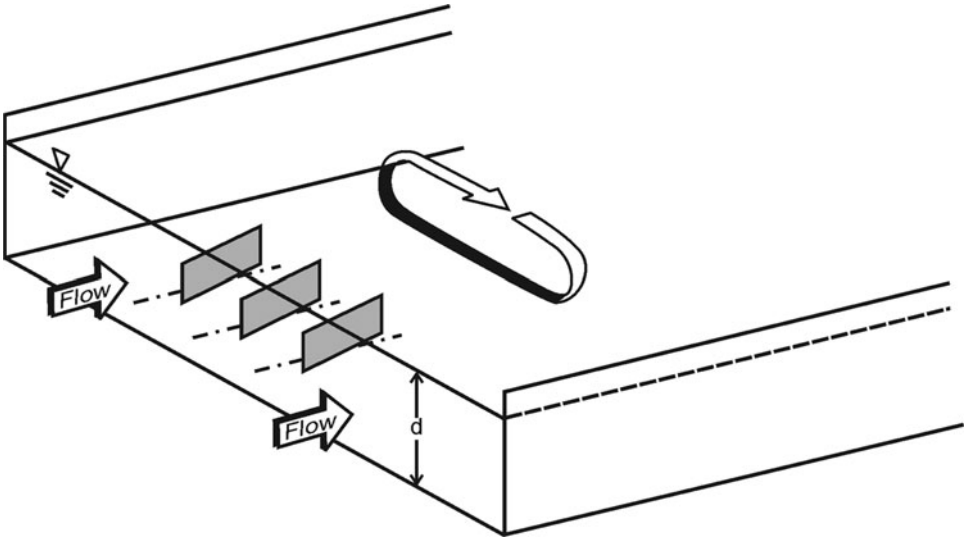

Figure 2-3. Schematic showing circulation induced by an array of three vanes.

This interference causes a reduction in total circulation because of the shear layer in the area between the vortices. Consequently, the total circulation induced by two closely spaced vanes is less than twice that due to an isolated vane. The smaller the spacing, the stronger is the interaction and the greater the reduction of total circulation. This effect of interaction reaches a maximum when the two vanes coincide, in which case the two vanes function as a single, isolated vane (provided that vane thickness is small).

The effect of vortex interference on circulation can be evaluated analytically. Consider a finite wing with span and cord being $2H$ and L, respectively. The vortex sheet induced by the wing produces along its span a so-called downwash velocity component, which decreases the effective angle of incidence and consequently circulation. With two finite wings placed in parallel, the vortex induced by one of the wings also produces along the span of the other wing a downwash velocity, thus causing an additional reduction in effective angle of incidence and, subsequently, circulation of the other wing. The effect of this interaction can be

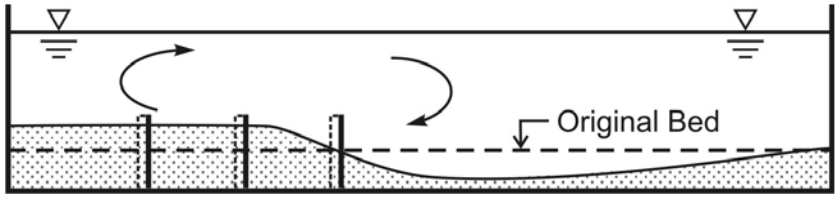

Figure 2-4. Schematic showing change in bed profile induced by an array of three vanes.

described by a model similar to that of the biplane theory (Milne-Thomson 1966). The interaction model for vane arrays, as developed by Wang (1989), assumes that (a) the two vanes, of span $2H$, are represented by two lifting lines that are perpendicular to the approach-flow velocity; (b) each lifting line trails behind it a horseshoe vortex sheet with width equal to the span, $2H$, of the wing; (c) the wings are elliptic in shape; and (d) the distribution of circulation along the span is elliptic. The output of the interaction model is an interaction factor, λ, that relates the circulation associated with an array of vanes with the circulation generated by an isolated vane. The factor λ is a function of vane spacing and dimensions. Calculated values are shown in Fig. 2-5. By introducing this factor, the circulation and associated transverse velocity components generated by an array of vanes are obtained by simple superposition. Similarly, by incorporating λ in the function f_v, the resulting stress distribution downstream for a vane array is obtained by summation of the stress distributions associated with the individual vanes in the array.

The calculations and experiments described in Chapter 3 show that a vane spacing of two to three times vane height is appropriate for the vortices induced by a vane pair to merge into a distinct, common vortex with relatively large transverse velocity in the region between the vane axes and not too large reduction of circulation per vane due to vortex interference. As seen in Fig. 2-5, when the spacing is two to three times vane height, λ is on the order of 0.9.

2.1.3 Vane Arrays

To sustain a certain induced circulation and induced bed shear stress downstream, the vane array must be repeated at intervals in the downstream direction. The dis-

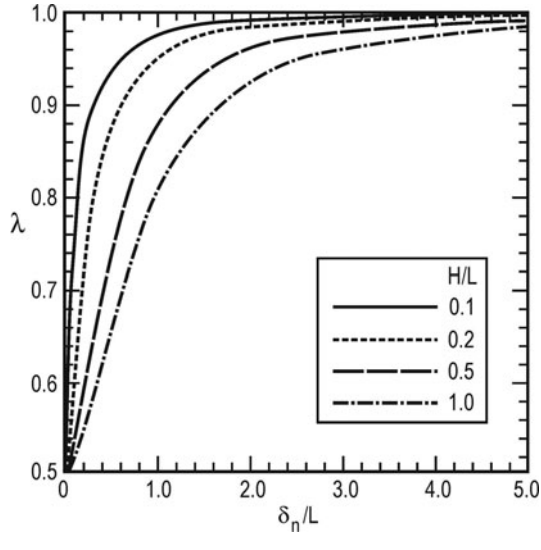

Figure 2-5. Calculated values of vane-interaction factor, λ.

tance between the arrays, δ_s, depends on the design objective, which must stipulate lower limits on induced stresses. Within a vane field consisting of equal-sized, equal-spaced vanes, the area-averaged induced bed shear stresses are

$$\tau_{vn} = \lambda \beta_n \frac{F_L}{A_v} \tag{2-12}$$

and

$$\tau_{vs} = \lambda \beta_s \frac{F_D}{A_v} \tag{2-13}$$

in which $A_v = \delta_n \delta_s$, and β_n, β_s = factors arising from the area-averaging process (Wang 1990). It follows that if the vane field covers an area A, and the total number of vanes is N, then $A_v = A/N$.

With ideal flow around the vanes, factors β_n and β_s are equal. However, because of flow separation around the vanes, the ideal-flow formulas for F_L and F_D are inaccurate, and adjustments are generally necessary. These adjustments are accounted for in β_n and β_s. As will be seen in the proof-of-concept tests described in Chapter 3, the aforementioned description provides a reasonable design basis. Other approaches for calculating the induced stress distribution have been proposed (van Zwol 2004; Flokstra 2006).

The impact of a system of vane arrays on a channel's energy slope is estimated using Eq. 2-13. Assuming a system of N vanes is installed in the channel over a length of ℓ and channel width is b, the vane-induced increase in energy slope is approximately

$$\Delta S = \lambda \beta_s \frac{N F_D}{b \ell \rho g R} \tag{2-14}$$

in which g = acceleration due to gravity, and R = hydraulic radius. In wide, open channels, $R \approx$ flow depth, d.

2.2 Flow Equations and Solutions

To calculate the effect of a submerged-vane system on flow and bed topography in an alluvial channel, the vane-induced stress distribution is introduced into the equations for conservation of mass (water and sediment) and momentum. The resulting equations are reduced using order of magnitude analysis and applying a stability criterion for sediment particles on the stream bed (Odgaard and Wang 1991). The coordinate system used is curvilinear: The s-axis is along the channel centerline, positive in the streamwise direction; the n-axis is perpendicular to the s-axis, positive toward the concave bank; and the z-axis is vertically upward from the bed. The velocity components (time-averaged) in the s-, n-, and z-directions are denoted u, v, and w, respectively.

The following assumptions are made: Flow depth, d, is small compared with width, b, so that $d/b \ll 1$; radius of curvature, r, is larger than width; and flow is fully

developed so that the $\partial/\partial s$ terms are zero. By applying the kinematic boundary conditions at the free surface and bed, the depth-averaged equations of motion read

$$\rho g S d = \tau_{bs} + \tau_{vs} \tag{2-15}$$

$$\rho g S_n d = \tau_{bn} + \tau_{vn} - \rho u^2 \frac{d}{r} \tag{2-16}$$

in which τ_{bs}, τ_{bn} = bed shear stresses in the s- and n-directions, respectively; and S, S_n = water-surface slope in the s- and n-directions, respectively. The effect of the submerged vanes on the flow field is accounted for by the distributed stress field (τ_{vs}, τ_{vn}), as indicated. The unknowns in these equations are u, S_n, d, and τ_{bn}. An additional equation is obtained from a force balance for bed-load particles on a transverse slope. The force balance includes drag, gravity, lift, and friction force. At fully developed conditions, the balance yields (Odgaard 1989a):

$$\frac{d(d)}{dn} = -\frac{1}{B\sqrt{\theta \rho \Delta g D}} \frac{\tau_{bn}}{\sqrt{\tau_{bs}}} \tag{2-17}$$

in which Δ = specific weight of submerged sediment = $(\rho_s - \rho)/\rho$; ρ_s = density of sediment; D = median grain diameter; θ = critical Shields stress; and B = function of Coulomb friction and the ratio of lift force to drag force for a bed particle. Values of B between 3 and 6 were reported by Ikeda and Nishimura (1985) and Odgaard (1989b). Herein a value of 4 is used. For quartz sand, the value of Δ is 1.65. A fourth equation is obtained by evaluating the transverse equation of motion at the water surface.

To further reduce the equations, it is assumed that the vertical profile of u is represented by the power law and the profile of v is a linear distribution made up of centrifugally induced and vane-induced contributions. With these assumptions, the bed shear stresses read

$$\tau_{bs} = \frac{\rho \kappa^2}{m^2} u^2 \tag{2-18}$$

$$\tau_{bn} = -\frac{\rho}{m} M u^2 \frac{d}{r} + \tau_{vn} \tag{2-19}$$

where

$$M = \frac{(2m+1)(m+1)}{m(m+1+2m^2)} \tag{2-20}$$

and m = resistance coefficient, which is related to the Darcy-Weisbach friction factor f as $m = \kappa\sqrt{8/f}$ (Zimmermann and Kennedy 1978); κ = von Karman constant ($\approx$0.4). Hence,

$$m = \frac{\kappa u}{\sqrt{gSd}} \tag{2-21}$$

The four equations are now reduced to the following two:

$$u^2 = \frac{m^2}{\kappa^2}\left(gSd - \frac{\tau_{vs}}{\rho}\right) \tag{2-22}$$

$$\frac{d(d)}{dn} = 2cM\mathbf{F}_D\frac{d}{r} - \frac{2cm}{\rho u^2}\mathbf{F}_D\tau_{vn} \tag{2-23}$$

where $c = 1/(2\kappa B\sqrt{\theta\Delta})$, and $\mathbf{F}_D$ = sediment Froude number defined as

$$\mathbf{F}_D = \frac{u}{\sqrt{gD}} \tag{2-24}$$

The value of c is of the order of 1.0. Note that vane height, H, in the equations for τ_{vs} and τ_{vn} (Eqs. 2-8 and 2-9) is now a function of d. Without vanes (i.e., when $\tau_{vs} = \tau_{vn} = 0$), Eq. 2-22 is the traditional Darcy-Weisbach relation, and Eq. 2-19 is the equation for the transverse bed shear stress associated with the centrifugally induced secondary current in fully developed bend flow.

Odgaard and Wang solve the governing equations using a finite difference scheme. The boundary condition is obtained from the continuity equation. The computation is carried out starting at the bank farthest away from the vanes. In a river curve, this is normally the inner bank. Initially, the flow depth at the starting point is set equal to the pre-vane flow depth, and the cross-sectional distributions are calculated. If these distributions do not satisfy the boundary condition, a new starting depth is selected. The process is repeated until the boundary condition is fulfilled.

The basic vane parameters are vane height, H (height above pre-vane stream bed), vane length, L, aspect ratio, H/L, and angle of attack, α, vane submergence below design water level, T, lateral vane spacing, δ_n, streamwise vane spacing, δ_s, and vane-to-bank distance, δ_b. Vane submergence, T, will often be the distance from the top of the bank to the tops of the vanes. See Fig. 2-6.

The basic flow and sediment parameters are channel width, b; depth, d; depth-averaged velocity, u; pre-vane cross-sectional average flow depth, d_o; pre-vane cross-sectional average velocity, u_o; pre-vane longitudinal slope, S; radius of curvature, r; pre-vane resistance parameter, m, determined as $\kappa u_o/\sqrt{gSd_o}$; pre-vane width–depth ratio, b/d_o; radius–width ratio, r/b; and the pre-vane sediment Froude number, $\mathbf{F}_D$, determined as $u_o/\sqrt{gD}$. The sediment Froude number is a measure of the mobility of the sediment.The general trend is that the vane-induced changes in bed level increase with increasing value of $\mathbf{F}_D$. An increase of the induced changes in bed level also occurs when vane height, angle of attack, and bed resistance increase. Results of sample calculations are presented in Figs. 2-7 and 2-8. The figures show depth and velocity distributions across curved and straight channels with and without vanes along one of the banks. Velocities and depths are normalized with their pre-vane values, u_o and d_o.

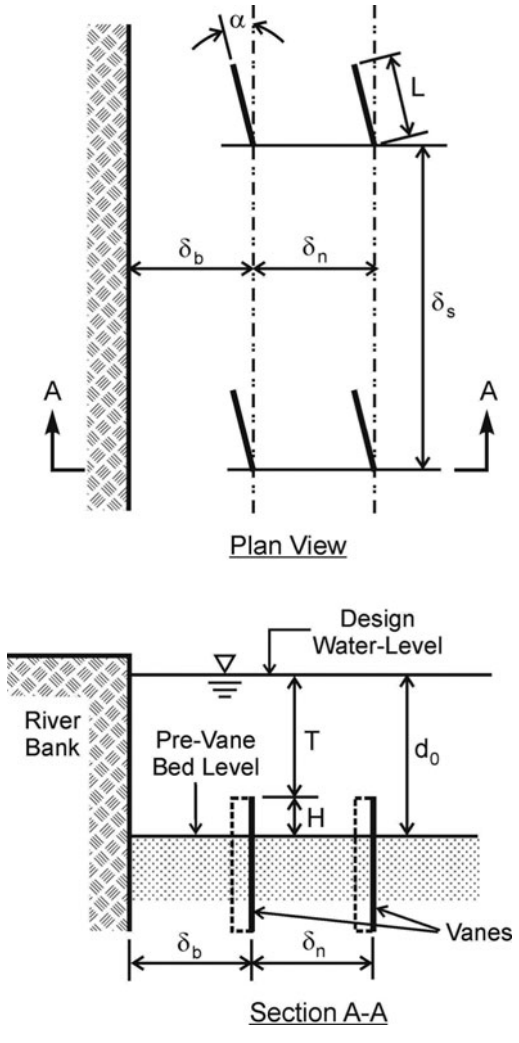

Figure 2-6. Vane design parameters.

2.3 Design Objectives

Most design objectives can be formulated in terms of a desired change in bed elevation at some point in the channel cross section. In the following section, typical situations will be described. The section concludes with a formulation of design objectives for installation of vanes to stabilize alignment of a meandering river channel.

2.3.1 Stabilization of River Bank

Most often, river banks are stabilized to prevent erosion. As indicated earlier, bank erosion generally occurs in curves of river channels, where the interaction

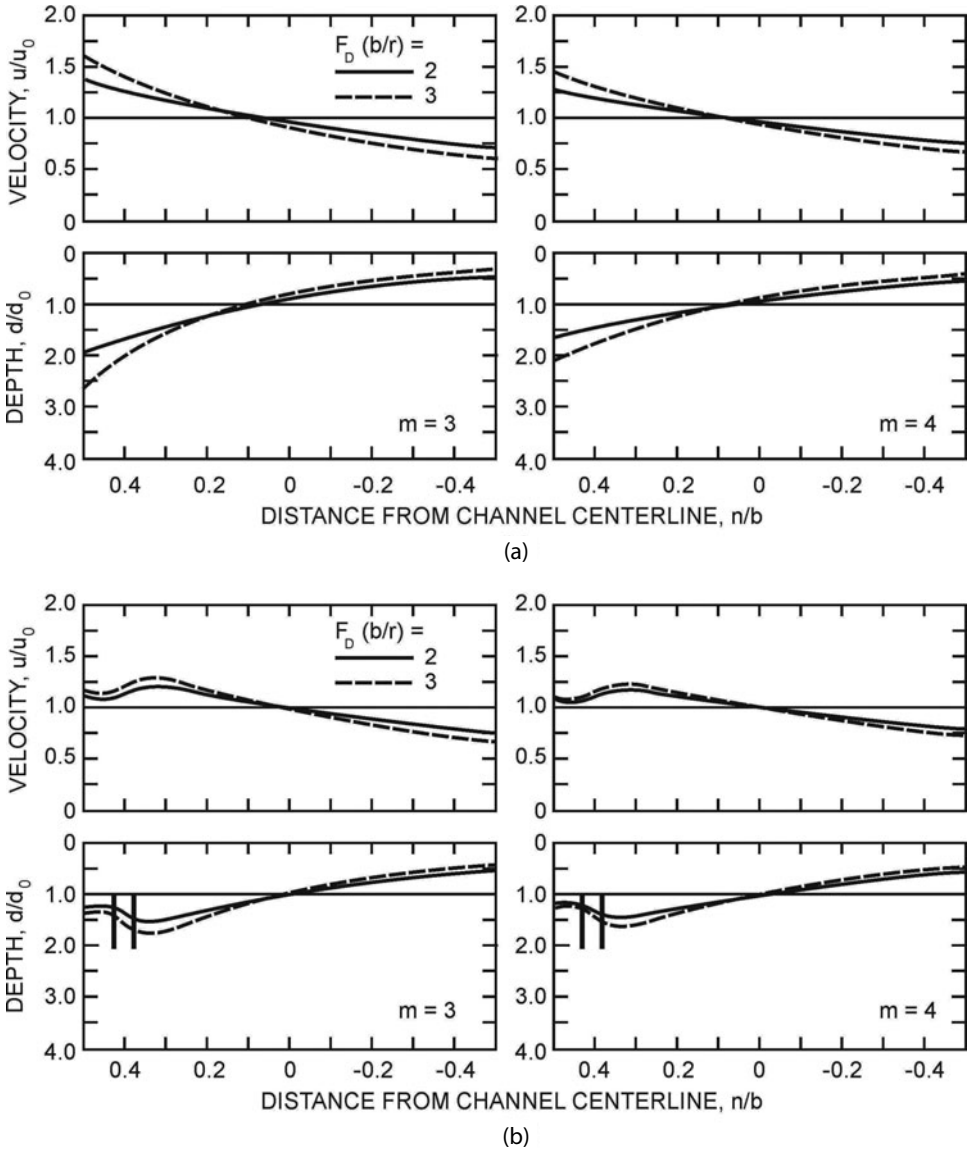

Figure 2-7. Calculations of depth and velocity distributions in river bend without vanes (a), and with vanes (b), with $T/d_o = 1.0$, $H/L = 0.3$, $\alpha = 25$ degrees (toward bank), $\delta_n = 3H$, $\delta_s = 15H$, $\delta_b = 1.5d_o$, and $d_o/b = 0.05$. *Source:* Odgaard and Wang (1991), ASCE.

between the vertical gradient of the velocity and the curvature of the flow generates a so-called secondary or spiraling flow. The secondary flow moves the high-velocity, near-surface current outward and the low-velocity, near-bed current inward, thereby producing larger depths and velocities near the outer banks. The deepening of the channel diminishes the toe support of the bank and the larger velocities attack it, setting the stage for bank erosion.

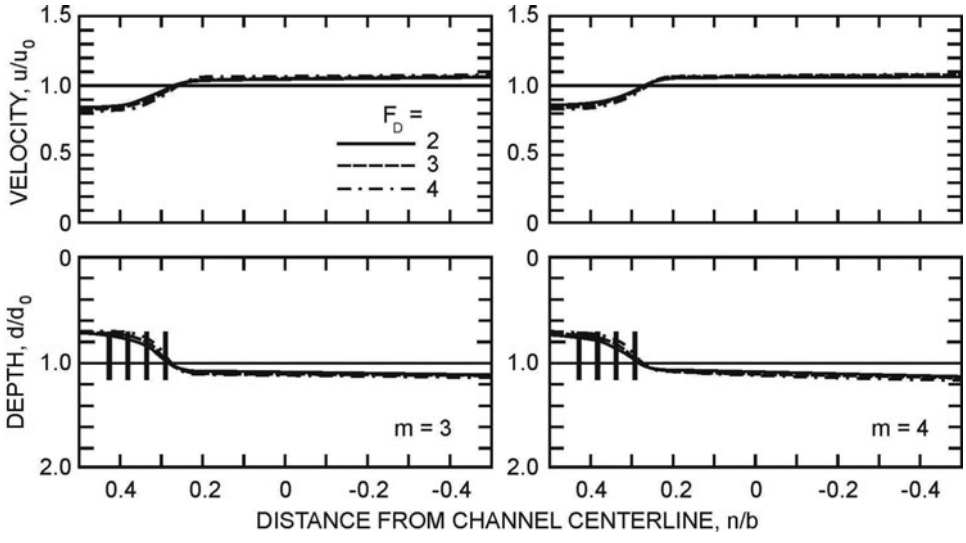

Figure 2-8. Calculations of depth and velocity distributions in straight channel with four-vane arrays, with $T/d_o = 0.7$, $H/L = 0.3$, $\alpha = 25$ degrees (toward bank), $\delta_n = 3H$, $\delta_s = 15H$, $\delta_b = 1.5d_o$, and $d_o/b = 0.05$. *Source:* Odgaard and Wang (1991), ASCE.

For design purposes, the variation of velocity and depth in fully developed bend-flow may be estimated using the following approximate relations (Odgaard 1989a)

$$\frac{u}{u_c} = \sqrt{\frac{d}{d_c}} \tag{2-25}$$

and

$$\frac{d}{d_c} = 1 + \frac{n}{d_c} S_{tc} \tag{2-26}$$

where u = velocity and d = depth at distance n outward from the centerline; S_{tc} = transverse bed slope at the centerline; and subscript c = the centerline values. Figure 2-9 shows the basic bend-flow variables. The transverse bed slope may be estimated from Eq. 2-23 taken at the centerline of the channel,

$$S_{tc} = 2cM\mathbf{F}_D \frac{d_c}{r_c} \tag{2-27}$$

This relation has been validated with data from several studies. Reference is made to Odgaard and Wang (1991). As discussed in Odgaard (1989a), the value of c may depend on sediment gradation and mobility; however, field data suggest that the variation is quite limited. For design, using a value of $c = 1.0$ provides a reason-

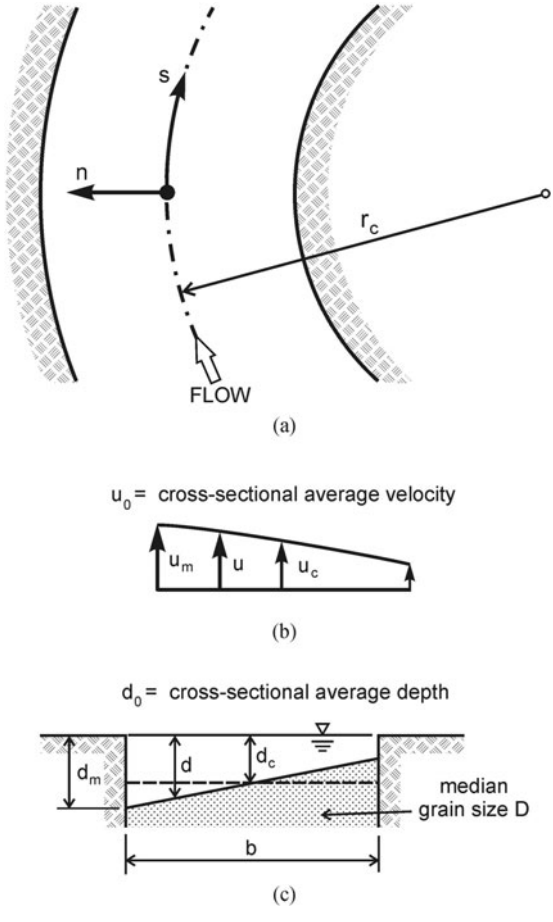

Figure 2-9. Bend-flow variables.

able measure of safety. If the width of the river channel is b, the maximum depth, d_m, and velocity, u_m, at the outer bank of the curve are given by

$$\frac{d_m}{d_c} = 1 + cM\mathbf{F}_D \frac{b}{r_c} \tag{2-28}$$

$$\frac{u_m}{u_c} = \sqrt{\frac{d_m}{d_c}} \tag{2-29}$$

The aforementioned relations apply to fully developed bend-flow only; they may be used for an estimate of maximum depth and velocity at the bank to be stabilized. Typically, design conditions range from medium flow to bank-full flow. Figure 2-10 is a graphical depiction of Eq. 2-28 using $c = 1$. It is seen that when $\mathbf{F}_D(b/r_c)$ is greater than about 3 and m less than 4, near-bank depth can be expected to be more than twice the average flow depth.

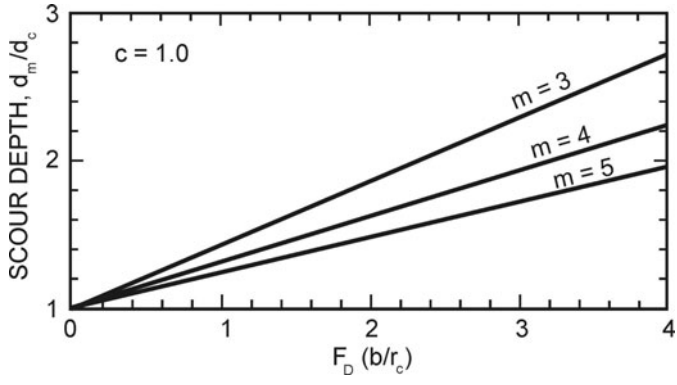

Figure 2-10. Scour depth at outer bank in river curve estimated using Eq. 2-28.

Figure 2-11 shows how vanes would be used to stabilize a river bank in a curved channel. As indicated in Fig. 2-11(a), the vanes would be installed at a relatively low stage when the velocities in the channel are low and the bed profile is only slightly warped. The low-flow bed profile would be either measured or calculated. Figure 2-11(b) shows the bed profile at design stage. Shown also in Fig. 2-11(b) is the bed profile that would have been if vanes had not been installed. The design objective is indicated by the linear distance between these two profiles at the bank, $d_m - d_v$, where d_v = vane-induced flow depth at the bank. Figure 2-11(c) shows the subsequent low-flow bed profile. The vanes ensure that the near-bank bed elevation obtained at design stage is maintained at all subsequent stages.

For developed bend flows, the design objective can also be formulated through a torque balance (Odgaard and Kennedy 1983). The bed warping and larger velocity near the concave bank are caused by the secondary current, which in turn is the result of flow torque due to the centrifugal force being distributed nonuniformly over the depth. The submerged vanes are installed to exert a torque on the flow that counters the centrifugally induced torque. The design relation for complete elimination of centrifugally induced torque in fully developed bend flow over a channel segment of length $r\theta$ (Odgaard and Mosconi 1986) is:

$$\frac{NLH}{r\theta b} = \frac{2}{c_L}\frac{d}{r}F \tag{2-30}$$

where N = number of independent vanes required, θ = included angle of channel segment, c_L = lift coefficient for the force exerted on the flow by each vane, given by Eq. 2-5, and

$$F = \left(\frac{d}{H}\right)^{2/m}\left[(m+1) - (m+2)\frac{H}{d}\right]^{-1} \tag{2-31}$$

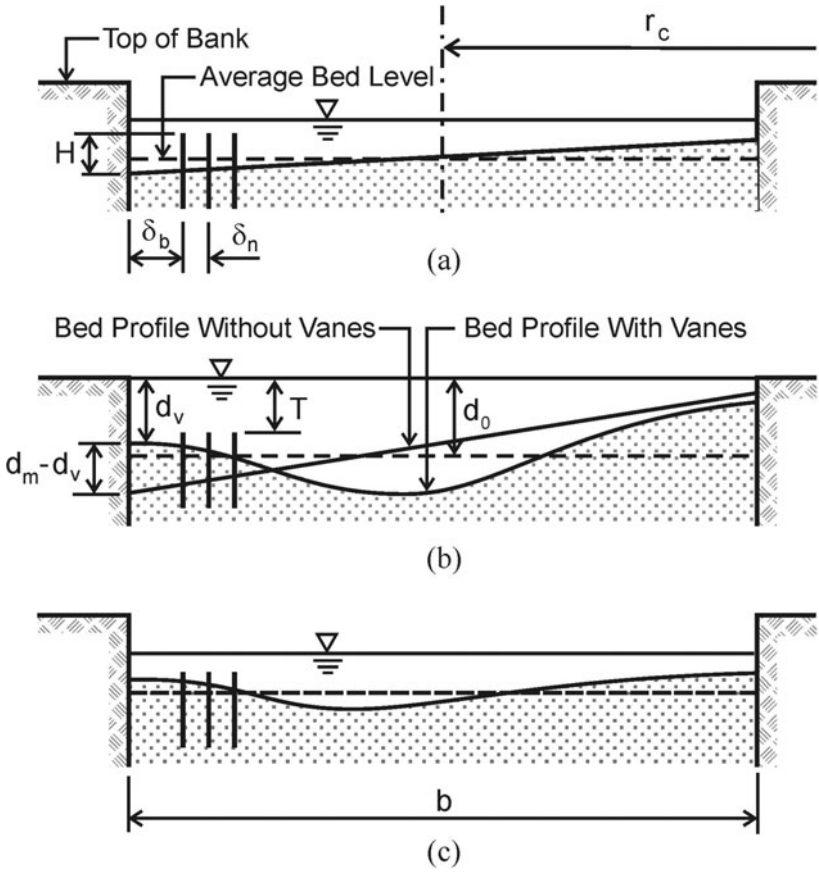

Figure 2-11. Stabilization of a riverbank in a curved channel. The schematic shows primary design variables and flow sections at (a) installation, (b) subsequent design flow, and (c) subsequent low flow.

Function F has its minimum with respect to H at $H/d = 2(m + 1)/(m + 2)^2$:

$$F_{min} = \frac{m+2}{m(m+1)}\left[\frac{2(m+1)}{(m+2)^2}\right]^{-2/m} \tag{2-32}$$

It is seen that F is relatively insensitive to variations of H/d over a fairly large range of H/d values. For example, for $m = 4$, F is within 20% of its minimum value when H/d is within the range $0.12 < H/d < 0.48$ (i.e., when the water depth is between two and eight times the vane height). In other words, the vanes function nearly

optimally over a wide range of river stages. It is also noted that discharge is not a primary design parameter. Discharge is used only for the determination of m.

Stabilization of a given river bank may not require complete elimination of the secondary current across the entire river cross section. By placing vanes only along the concave bank, as shown in Fig. 2-11, the vanes will not (and may not need to) eliminate the secondary current farther away from the bank.

2.3.2 Stabilization of River Bed

In Fig. 2-12 vanes are used to stabilize the bed topography in a straight river channel. The schematic shows how this could be accomplished by making the vanes develop and maintain a compound channel (i.e., a channel with berms along each bank). As indicated in Fig. 2-12(a), the vanes would be installed at a relatively low stage when the velocities in the channel are low. Figure 2-12(b) shows the bed profile at design stage. Shown also in Fig. 2-12(b) is the bed profile that would have

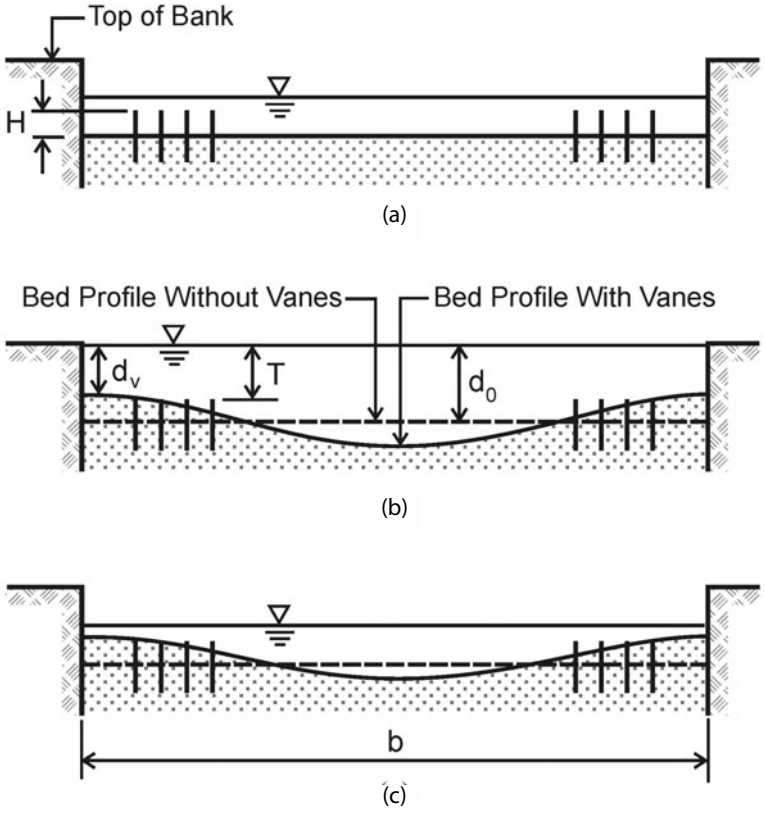

Figure 2-12. Stabilization of a riverbed. The schematic shows primary design variables and flow sections at (a) installation, (b) subsequent design flow, and (c) subsequent low flow.

been if vanes had not been installed. The design objective is indicated by the linear distance between these two profiles at the bank, $d_o - d_v$. Figure 2-12(c) shows the subsequent low-flow bed profile. The vanes ensure that the bed topography developed at the design stage is maintained at all subsequent stages.

2.3.3 Sediment Control at Water Intake or Diversion

When vanes are used at water intakes or diversions, their role is usually to prevent sediment from being drawn into the water intake or diversion. The sediment problem occurs because the withdrawal of water reduces the downstream flow velocity and, hence, downstream sediment-transport capacity at the intake. The bed level rises, typically along the downstream portion of the intake or diversion, and sediment is being drawn in along with the water. Occasionally, the bed level may rise to such a level that a portion of the intake is blocked. The design objective is formulated in terms of a desired increase in depth over a certain region in front of the intake. Figure 2-13 shows schematically the primary design variables. The desired increase in depth along the intake is obtained by designing the vane system such that it generates and maintains a transverse bed shear stress directed

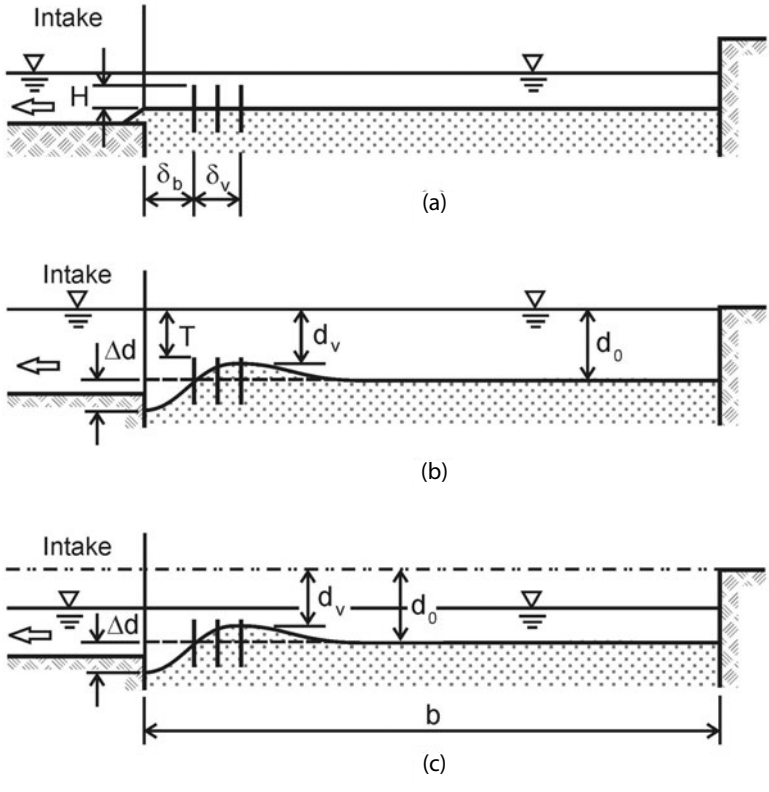

Figure 2-13. Schematic showing design variables for a vane system at a water intake or diversion.

away from the intake, causing the bed to deform as indicated in Fig. 2-13. The width of the vane field, δ_v, must be sufficient that the induced aggradation within the field, $d_o - d_v$, results in a channel along the intake of sufficient width, depth, and velocity to accommodate the flow into the intake as well as maintain a sufficiently high flow velocity past it.

For the vanes to effectively lower the bed elevation in front of the intake or diversion, δ_b should not be much larger than δ_v (see Fig. 2-13). For a two-vane array system, $\delta_v = \delta_n$; for a three-vane array system, $\delta_v = 2\delta_n$. Figure 2-14 shows alternate placements of vanes relative to the bank at the intake or diversion. The fig-

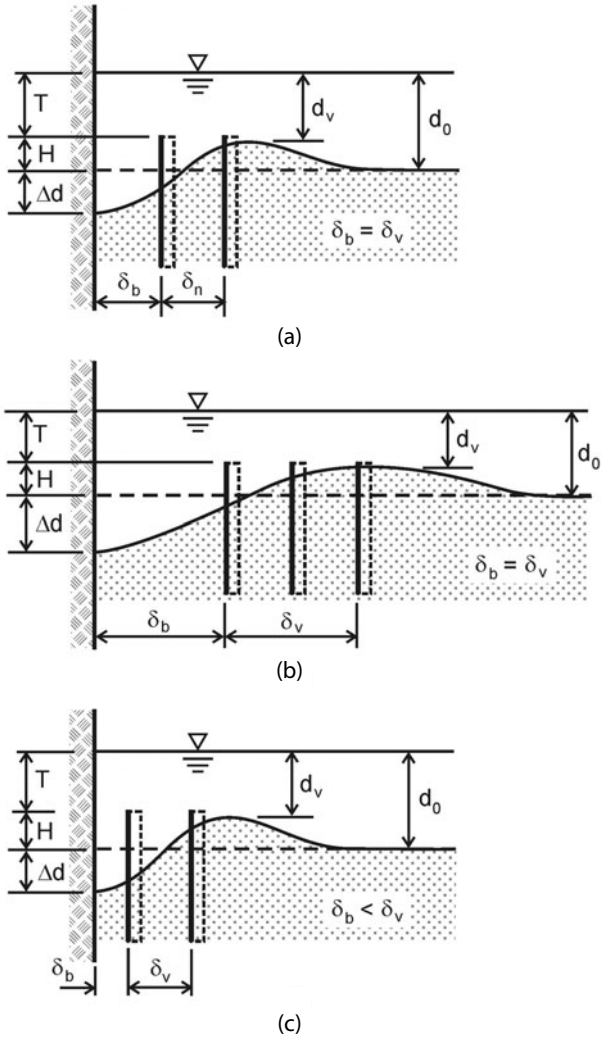

Figure 2-14. Schematic showing alternative placements of vanes relative to the bank at an intake or diversion.

ure also indicates the corresponding change in bed level as it would appear in a section immediately upstream from the intake or diversion. Ideally, δ_b should be large enough that the stream surface separating flow entering the intake from flow continuing downstream be located between the bankline and the innermost row of vanes, that is, within a distance of δ_b from the bankline (see Fig. 2-15). The average width b_s of the stream tube formed by the separating stream surface and the bankline is estimated by proportioning:

$$\frac{b_s}{b} = \frac{Q_i}{Q} \tag{2-33}$$

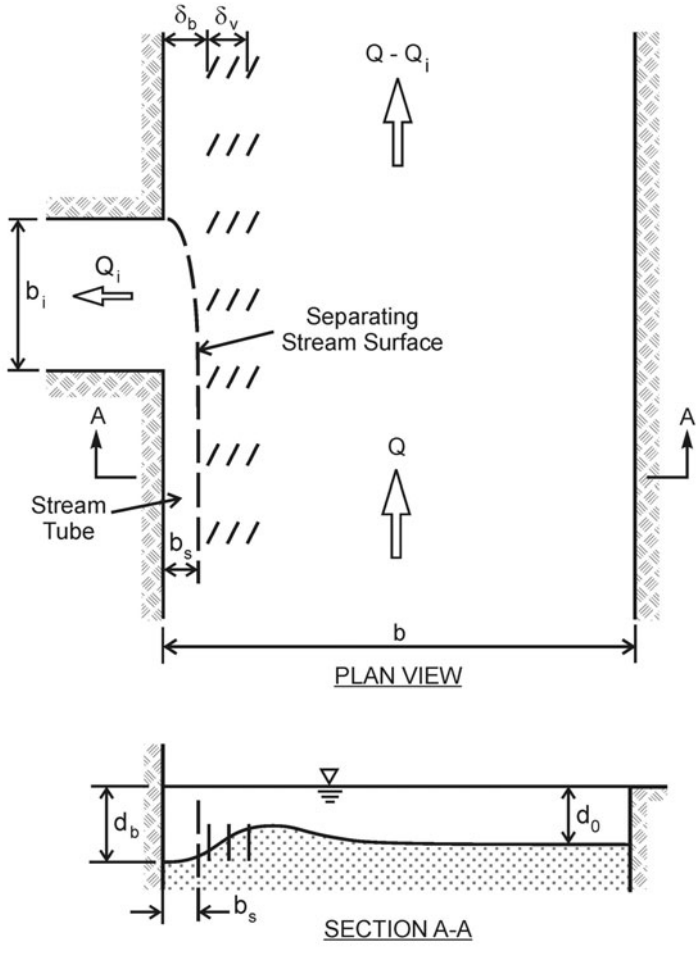

Figure 2-15. Sediment exclusion at an intake or diversion. The schematic shows the stream tube for flow entering the intake. The stream tube is bounded by the bankline and the separating stream surface, and is located between the vane field and the bankline.

where b = width of main channel, Q = discharge in main channel, and Q_i = discharge in diversion or intake. Ideally, this width (b_s) should be considerably less than the vane-to-bank distance δ_b. In this case, the flow in the channel between the vanes and the bank would be sufficiently large that it not only provides the necessary flow into the intake but also enough flow for transport of sediment past the intake. As the discharge in the near-shore channel decreases as the flow approaches the downstream end of the intake, the bed level in the channel will gradually increase. The increase will occur in step with the decrease in discharge in the near-shore channel. Assuming that all the sediment transport in the near-shore channel bypasses the intake (which is the desired situation and the reason for lowering the bed along the intake in the first place), conservation of water and sediment transport in the channel yield a bed-level increase at the downstream end of the intake of roughly

$$\Delta h = \frac{Q_i}{Q_b} d_b \tag{2-34}$$

where Q_b and d_b are discharge and depth, respectively, in the vane-generated, near-shore channel at the upstream end of intake. If Δh is large enough to increase the bed level to the sill of the intake, sediment ingestion may be expected at the downstream end of the intake.

Local considerations may limit the outward extent of the vane system. If this is the case, δ_b may have to be less than δ_v and perhaps even less than b_s. In this case, as indicated in Fig. 2-14(c), the design will still create a near-shore channel; however, because the inner row of vanes is now located within the stream tube, the flow in it will be more turbulent and may carry suspended bed material into the intake or diversion. Flow features associated with this configuration ($\delta_b < b_s$) were observed in the laboratory tests described in Chapter 3.

If intake velocity is relatively high, sediment ingestion may be unavoidable with any reasonable (or acceptable) vane design. In this case, consideration should be made to construct a sediment barrier or skimming wall parallel with and at a distance from the intake, and locating the vane field outside the wall (see Fig. 2-16). For it to be most effective, the skimming wall should be located such that the stream tube defined by the withdrawal rate lies completely within the channel formed by the skimming wall and the bankline. Thereby, overflow over the wall is minimized and inflow to the near-shore channel will occur primarily at the upstream flared section of the wall. However, local considerations may limit the outward extent of the skimming wall/vane system. If this is the case, the skimming wall may fall within the stream tube. In the extreme case, the skimming wall could be a mere increase in intake sill elevation.

2.3.4 Stabilization of River Channel Alignment (and Re-Meandering)

As indicated earlier, vanes can be used to stabilize a meandering river reach (Figs. 1-12 and 1-13). In this case, proper formulation of the design objective requires information about the channel's natural alignment characteristics. The vane sys-

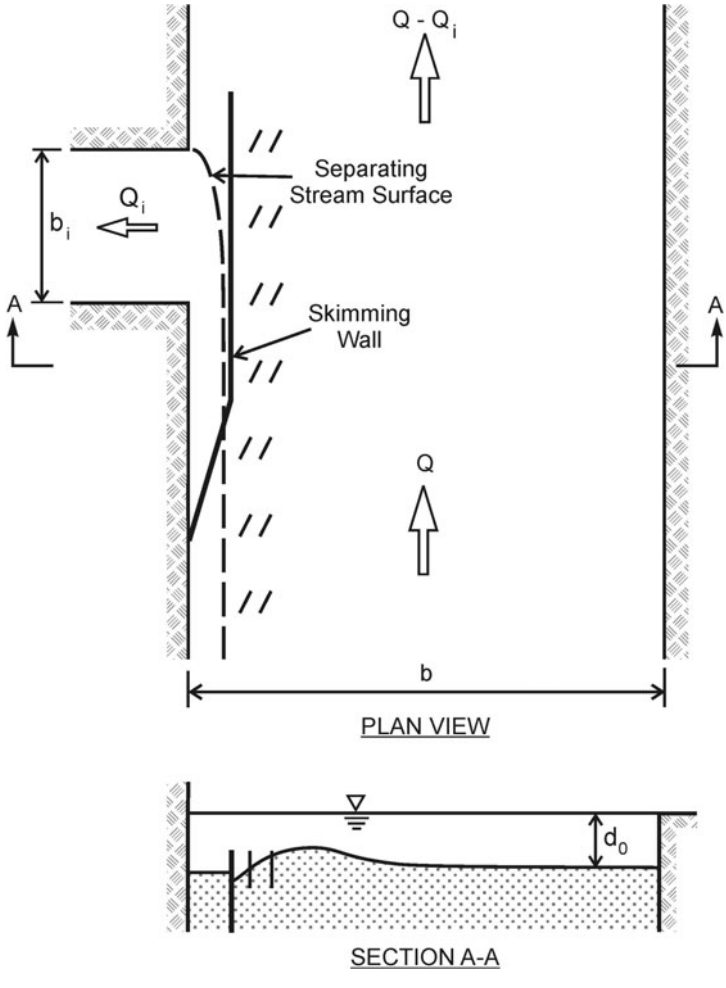

Figure 2-16. Sediment exclusion at an intake or diversion. The schematic shows the location of a skimming wall between the separating stream surface and the inner row of vanes.

tem must be designed to be consistent with the natural tendency of the river to attain and maintain a certain meander plan form.

The natural alignment of a river channel may not always be in the form of a meander plan form. For certain combinations of channel slope and bank-full or channel-forming discharge, the natural tendency will be to form a braided channel—a channel consisting of multiple branches separated by sand bars and small islands. Certain thresholds were identified by Lane (1957) and by Leopold and Wolman (1957). The discharge–slope relation obtained by Leopold and Wolman (see Fig. 2-17) for the threshold separating meandering and steeper braided stream is

$$S = 0.0125Q^{-0.44} \tag{2-35}$$

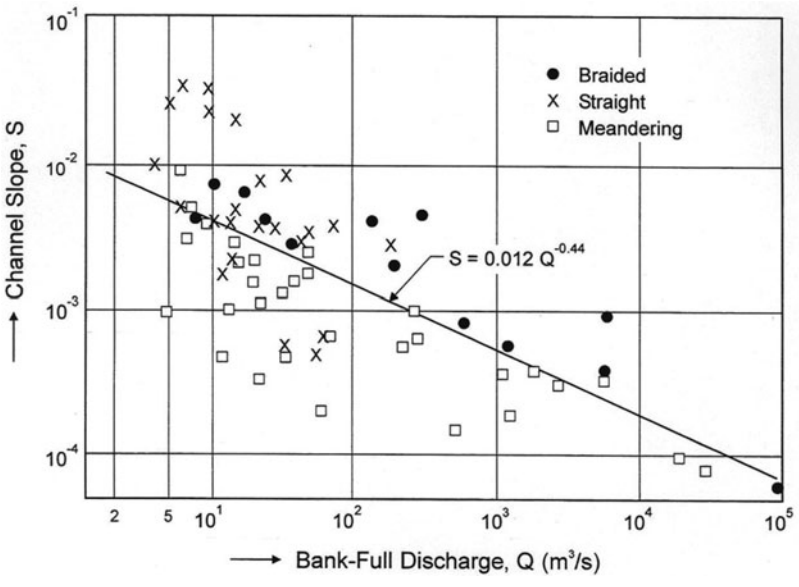

Figure 2-17. Discharge–slope relation for the threshold separating meandering and braided streams. *Source:* Adapted from Leopold and Wolman (1957).

where Q is the channel-forming discharge in m^3/s. This equation was obtained using data from sand-bed and gravel-bed streams. Henderson (1963) refined this equation by including the effect of bed-particle size and suggested the following equation for gravel-bed streams:

$$S = 0.0002 D^{1.15} Q^{-0.46} \tag{2-36}$$

where D is median particle size in millimeters. Consequently, if channel slope is close to this critical value, channel adjustments involving a small change in slope could lead to large changes in channel pattern. On the other hand, if the slope of a braided channel reach is close to the critical value, it may not take a major construction effort to transform the channel reach into a single-thread meandering channel.

Measurements of the dimensions of meander patterns suggest there are relations between certain plan-form characteristics that are relatively consistent for a large range of stream sizes. The plan-form characteristics, defined in Fig. 2-18, are meander length, ℓ; wavelength, λ; amplitude, a; channel width, b; and minimum centerline-radius of curvature, r_c. Many relationships have been suggested over the years, along with theories for explaining them. Reference is made to Chang (1988).

Most recently, considering that meandering is considered the result of channel instability, many researchers have used perturbation stability analysis to evaluate the stability of a given channel alignment. That is, if a given channel alignment has characteristics similar to those calculated by the stability analysis, the alignment is considered "relatively stable" or "minimally destructive" in terms of

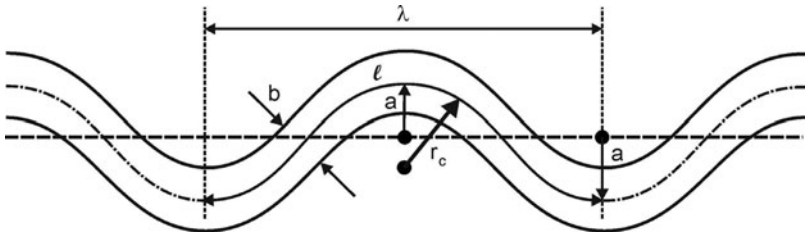

Figure 2-18. Meander-plan form characteristics.

bank erosion. An example of a stability analysis is given by Odgaard (1989a,b). The example is based on the equations for conservation of mass (water and sediment) and momentum, and a stability criterion for sediment particles on the stream bed. By order of magnitude considerations and linearization, these equations are reduced to those of a damped oscillating system. The stability of the system is examined by forcing upon it a traveling, small-amplitude alignment wave. The growth rate of the amplitude is determined by relating the alignment wave and the change in channel alignment through a bank-erosion model. The bank-erosion model is a relationship between rate of bank retreat and increase in near-bank scour depth. (Odgaard 1989a also tested a bank-erosion model that relates rate of bank retreat and increase in near-bank velocity.) The dominant wave length, λ, is calculated as the wave length at which the amplitude growth rate is optimum ($\partial^2 a/\partial t \partial k = 0$, k = wave number, and t = time).

The principal quantities and concepts are shown schematically in Fig. 2-19. The figure shows the path of maximum flow depth through two consecutive meander bends. As indicated, the depth distribution responds to the change in chan-

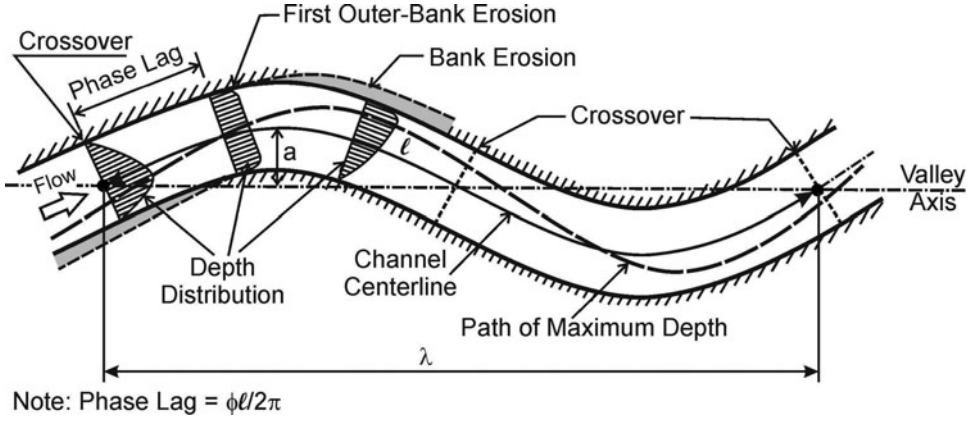

Figure 2-19. Schematic showing principal quantities and concepts associated with flow through a meander curve, including phase lag for maximum flow depth. *Source:* Odgaard and Wang (1991), ASCE.

nel curvature with a phase lag given by $\varphi\ell/2\pi$, where φ = the corresponding phase angle defined in Odgaard (1989a).

Figure 2-20 shows the result of a calculation of dominant wavelength, λ, and phase shift, φ, as a function of width–depth ratio, b/d_o, sediment Froude number, $\mathbf{F}_D$, and friction factor, m. The typical bank-full ranges of $\mathbf{F}_D$ and m are $5 \leq \mathbf{F}_D \leq 20$ and $3 \leq m \leq 5$. For width–depth ratios between 10 and 60 (the typical range), the dominant wavelength is between 9 and 24 times the width, which is in agreement with data presented by Zeller (1967) and Leopold and Wolman (1957; 1960). The results presented in Fig. 2-20 may be used for design.

The vane system should be designed and installed to preserve the dominant wavelength calculated by the stability analysis. The phase lag calculated would give the distance from the crossover point to the point where the first vane array should be installed (the point of "first outer-bank erosion occurrence").

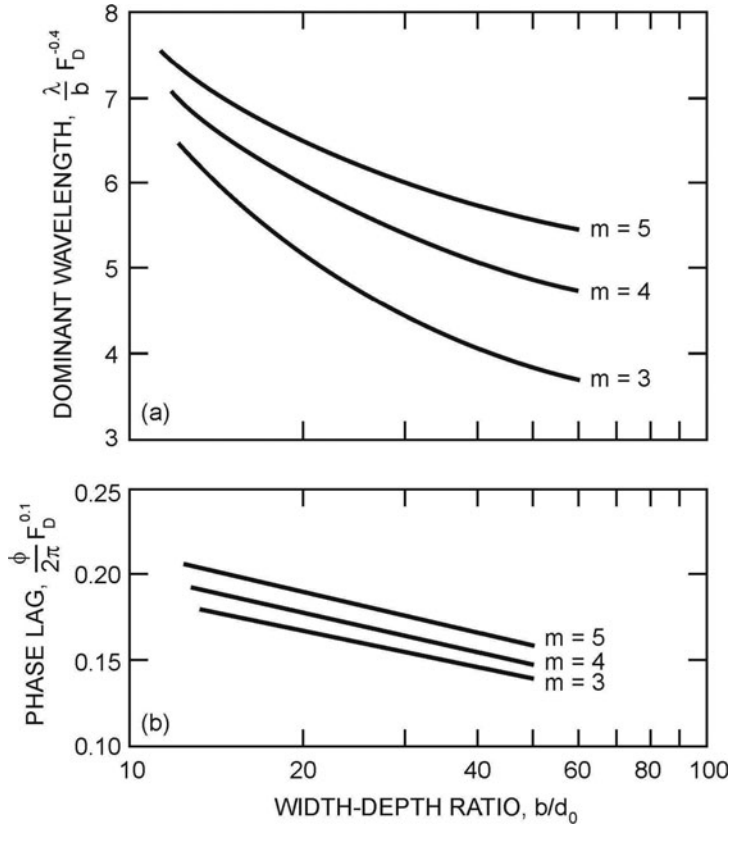

Figure 2-20. Dominant meander wavelength and phase lag for typical bank-full ranges of sediment Froude number, width–depth ratio, and friction factor.

2.4 Design Graphs

To facilitate design of submerged vane systems, graphs have been prepared (Figs. 2-21, 2-22, and 2-23), showing calculated changes in maximum flow depth as a function of flow, sediment, and vane parameters. The calculations are made using Eqs. 2-22 and 2-23, and are for a section midway between two vane arrays. Results are shown for arrays with two and three vanes, relative vane submergences of $T/d_o = 0.5$, 0.7, and 1.0, Froude numbers of $\mathbf{F}_D = 5$, 15, and 25, aspect ratio of $H/L = 0.3$, angle of incidence of $\alpha = 20$ degrees, and resistance parameter of $m = 3$ and 4. Calculations are shown for vane spacings of $\delta_n = 3H$ and $\delta_s = 15H$ and $30H$, and for channels with a depth–width ratio of 0.03. The values of $(d_m - d_v)/d_m$ increase or decrease by about 3% for every degree that α increases above or decreases below 20 degrees.

Equation 2-28 and Fig. 2-10 suggest that when $\mathbf{F}_D b/r_c$ is greater than about 3 and m less than 4, near-bank depth can be expected to be at least twice the depth at the centerline of the channel, d_c. With an assumed linear variation of depth across the channel, centerline depth d_c will be equal to cross-sectional average depth d_o. If $\mathbf{F}_D = 15$, $b/r_c = 0.2$, and $m = 4$, Eq. 2-28 (with $c = 1$) and Fig. 2-10 yield a scour depth of $d_m = 1.9d_c = 1.9d_o$. The graphs in Fig. 2-21 show that, to

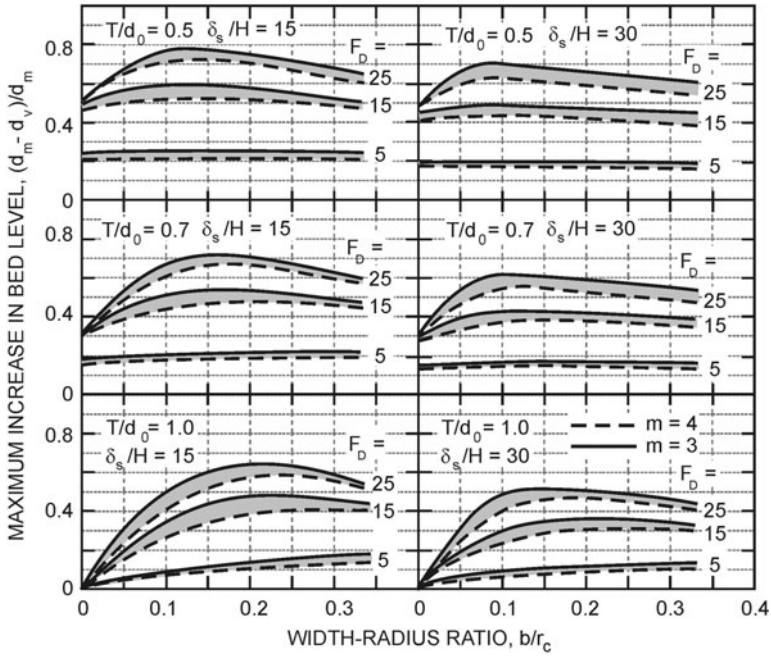

Figure 2-21. Computed vane-induced maximum increase in bed level along a bank with three vanes per array. Depth–width ratio $d_o/b = 0.03$, vane–aspect ratio $H/L = 0.3$, vane angle $\alpha = 20$ degrees, and vane spacings $\delta_n = 3H$ and $\delta_b = 1.5d_o$. *Source:* Odgaard and Wang (1991), ASCE.

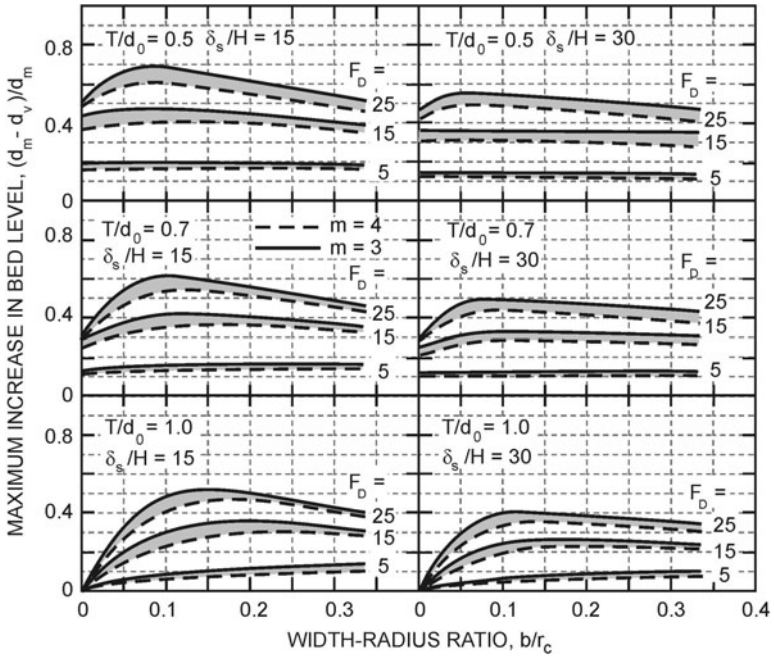

Figure 2-22. Computed vane-induced maximum increase in bed level along a bank with two vanes per array. Depth–width ratio $d_o/b = 0.03$, vane–aspect ratio $H/L = 0.3$, vane angle $\alpha = 20$ degrees, and vane spacings $\delta_n = 3H$ and $\delta_b = 1.5d_o$. *Source:* Odgaard and Wang (1991), ASCE.

prevent such a scour hole from forming and to maintain a near-bank bed level at or near the cross-sectional average level, there must be at least three vanes in each array. If $T/d_o = 0.7$, $H/L = 0.3$, $\alpha = 20$ degrees, $\delta_n = 3H$, $\delta_s = 15H$, and $d_o/b = 0.03$, a vane system with three vanes in each array yields $(d_m - d_v)/d_m = 0.48$. With $d_m = 1.9d_o$, the vane-induced depth at the bank is $0.99d_o$, or just about the cross-sectional average depth d_o. Figure 2-11(b) is a schematic illustration of what the new bed profile will look like (with $d_v = d_o$). If T/d_o is increased to 1.0 (i.e., the top of the vanes are set at average bed level), then a vane system with three vanes in each array yields $(d_m - d_v)/d_m = 0.39$. With $d_m = 1.9d_o$, the vane-induced depth at the bank is now $d_v = 1.16d_o$, or 16% larger than average depth. Increasing the near-bank bed level to the average bed level using three-vane arrays with the top of vanes set at average bed level (i.e. $T/d_o = 1.0$) could be accomplished by increasing vane angle. To achieve a 16% increase in bed level, the vane angle will have to be increased to a little more than 25 degrees. By increasing vane angle from 20 degrees to 25 degrees, the value of $(d_m - d_v)/d_m$ increases to 0.45, yielding $d_v = 1.04d_o$ (i.e., a decrease in near-bank depth to within 4% of average depth).

Figure 2-21 shows that in a straight channel ($b/r_c = 0$), three vanes per array will, in most cases, bring the near-bank bed level to the top of the vanes, provided

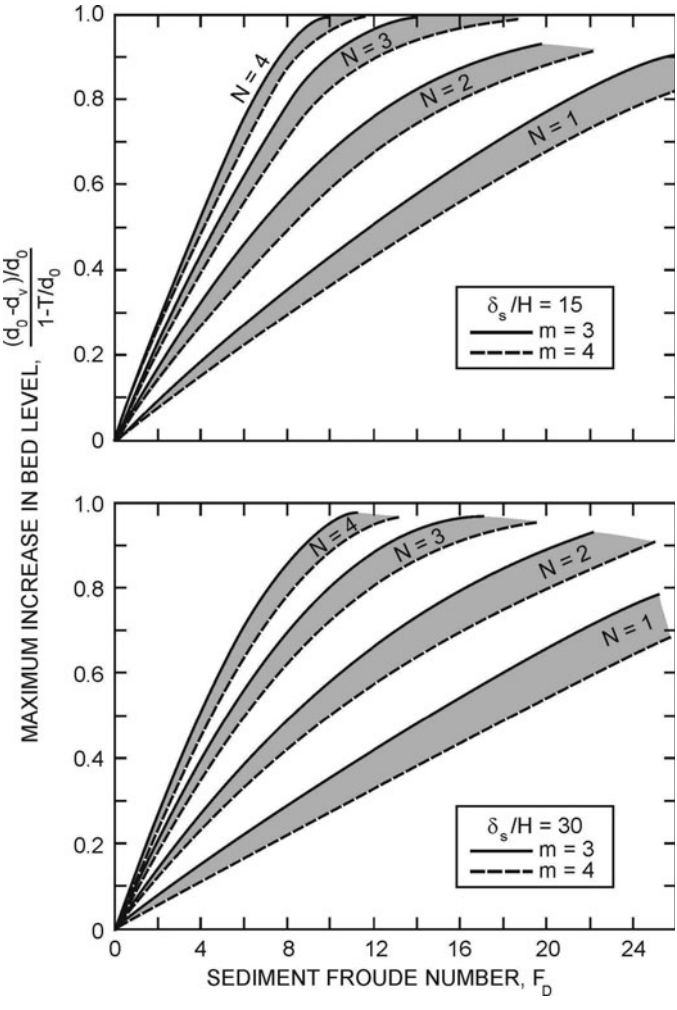

Figure 2-23. Computed vane-induced maximum increase in bed level with one, two, three, and four vanes per array ($N = 1$, 2, 3, and 4), longitudinal spacing $\delta_s = 15H$ and $30H$, and resistance parameter $m = 3$ and 4. Depth–width ratio $d_o/b = 0.03$, vane–aspect ratio $H/L = 0.3$, vane angle $\alpha = 20$ degrees, and vane spacings $\delta_n = 3H$ and $\delta_b = 1.5d_o$.

that $\mathbf{F}_D$ is greater than about 15 and $\delta_s \leq 30H$. Figure 2-21 also shows that the induced changes in the bed level decay relatively slowly in the downstream direction. By increasing the spacing δ_s from $15H$ to $30H$ in a system with three vanes per array, the induced change in bed level is reduced by only about 10% to 20%, depending on the value of b/r_c.

Finally, it should be noted that, for these vane arrays, the vane-induced increases in bed level are essentially independent of the channel's depth–width ratio, d_o/b, when this ratio is less than about 0.05. The depth–width ratio enters the

calculations through the boundary condition (continuity equation), and when the width of the channel is large compared with the width of the vane field, the distance from the vane field to the far bank has essentially no effect on the bed level changes within the vane field.

The graphs in Fig. 2-23 apply to straight channels (i.e., channels with $b/r_c = 0$). The graphs are based on the same calculations that produced the graphs in Figs. 2-21 and 2-22. However, in Figs. 2-21 and 2-22 the values of $(d_m - d_v)/d_m$ are difficult to read at $b/r_c = 0$. In Fig. 2-23, the values of $(d_m - d_v)/d_m$, which in a straight channel are equal to $(d_o - d_v)/d_o$, are plotted as a function of $\mathbf{F}_D$ and m. Furthermore, in Fig. 2-23, vane submergence, T, is incorporated into the ordinate, and results for four-vane array systems are included. For example, if $\mathbf{F}_D = 10$ and $m = 4$, a three-vane array system with array spacing $\delta_s = 15H$ will produce a maximum increase in bed level given by

$$\frac{\dfrac{(d_o - d_v)}{d_o}}{1 - \dfrac{T}{d_o}} = 0.83$$

A four-vane array system with same array spacing will produce a maximum increase in bed level given by

$$\frac{\dfrac{(d_o - d_v)}{d_o}}{1 - \dfrac{T}{d_o}} = 0.97$$

If initial vane submergence is $T/d_o = 0.7$, these vane arrays will cause the flow depth in the vane field to decrease from d_o to $0.75d_o$ and $0.71d_o$, respectively (i.e., the bed will rise to just about the top of the vanes). The vane-induced bed change is approximately as shown in Fig. 2-8.

CHAPTER 3

Laboratory Validation Tests

A series of laboratory tests was conducted to validate the theory described in the previous chapter (Wang 1989; Odgaard and Wang 1991; Wang and Odgaard 1993; Barkdoll et al. 1999). Three of the test series are described below. One series is proof-of-concept tests conducted in a rigid-bed channel to demonstrate and quantify the flow features that are unique to the theory (without having the bed deformed by sediment movement). The rest of the tests are conducted in movable-bed channels. The chapter includes a summary of tests conducted by Voisin and Townsend (2002) with vanes in a sharply curved channel (Section 3.3).

3.1 Rigid-Bed Channel (Proof-of-Concept)

The proof-of-concept tests were conducted in a long, 0.91-m-wide channel with a bed consisting of 4-mm sand (large enough to be immobile at the test flow rates). Water was recirculated through the channel and return circuits by centrifugal pumps and the flow rate was measured with calibrated orifice meters. Velocities were measured with a two-dimensional miniature electromagnetic current meter that was calibrated and periodically checked with a laser Doppler anemometer to maintain accuracy better than 2%. Water surface elevations were measured with static tubes that could be read with an error of less than 0.3 mm. The water-surface elevations were used to determine water surface slope S and Darcy-Weisbach friction factor $f = 8gRS/u_o^2$, where u_o = undisturbed (pre-vane) cross-sectional-averaged velocity. In all tests, $u_o = 0.24$ m/s. The vanes were made of 0.75-mm-thick sheet metal. They were rectangular in shape, with height $H = 0.5d$, and length $L = 2H$. In all tests, the vanes were placed at an angle of attack of 20 degrees with the channel centerline.

In the tests with a single vane, vane height and length were 0.076 m and 0.152 m, respectively. Water depth was 0.152 m. Pre-vane water-surface slope and friction factor were 1.74×10^{-4} and 0.026, respectively.

Figure 3-1 shows transverse and streamwise velocity components as measured at three sections downstream from the vane. The opposite directions of transverse

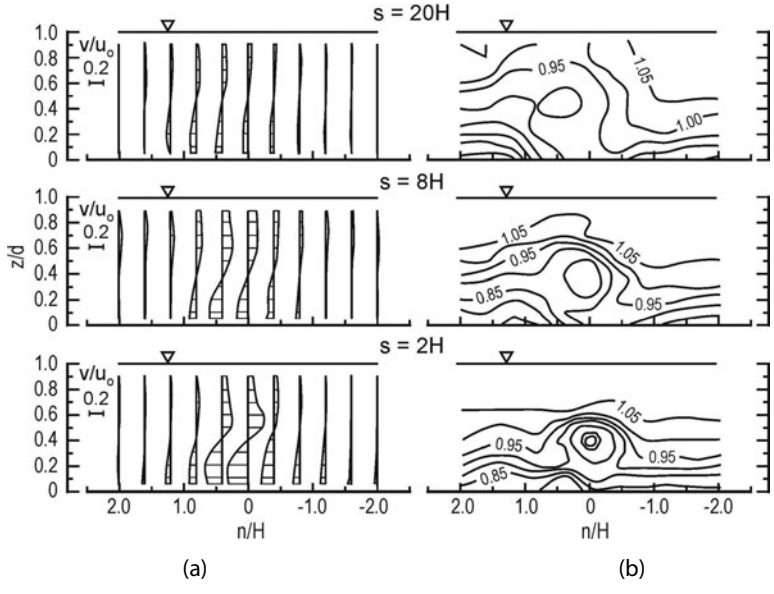

Figure 3-1. Velocity distribution downstream from single vane. (a) Transverse (v/u_o), and (b) streamwise (u/u_o) component. *Source:* Wang and Odgaard (1993), with permission of IAHR.

velocity in the upper and lower part of the flow section indicate the presence of the tip vortex. The distributions show that the vortex persisted a considerable distance downstream from the vane. At a distance of $s = 20H$, the maximum value of v was still about 35% of that immediately downstream from the vane at $s = 2H$. This low rate of decay was due to the transverse bed shear stresses being very small. The formation and development of the vane-induced tip vortex is also seen on the contour plots of streamwise velocity. The location of the vortex is indicated by the depressed core in the plots. As the vortex is carried downstream, its strength decays and the depression of u becomes less pronounced. The figure shows that the flow is "lifted up" on the pressure side of the vane (left side) and "pressed down" on the suction side. The 1.0-velocity contour, which without a vane in the channel would have been at an elevation of about $0.4d$, is closer to the water surface on the pressure side and farther away on the suction side. This feature occurs as a result of the vortex motion. On the pressure side, the vertical velocity component of the vortex is upward and it brings the low velocity fluid up. On the suction side, the higher velocities are brought down toward the bed because the vertical velocities are there directed down toward the bed. Due to these modifications of the velocity distribution, the streamwise bed shear stresses are higher on the suction side than on the pressure side. Such a trend was confirmed, by direct measurements of skin friction, by Eibeck and Eaton (1987), and Pauley and Eaton (1987) in their wind-tunnel experiments with vortex generators. On a movable bed, the larger shear stresses on the suction side will augment the motion

of sediments in that region, whereas reduction in sediment movement will occur on the pressure side where bed shear stresses are reduced.

The velocity-contour plots (Fig. 3-1) also indicate that there is a significant net transport of volume flux from the pressure side to the suction side. Due to the nonuniform distribution of streamwise velocity in the vertical direction, a net transport of momentum occurs in the transverse direction. This transport is described by the term $\partial(uv)/\partial n$ in the streamwise component of the momentum equation.

Tests with smaller H/d ratios were also conducted. These are described by Wang (1989). A notable observation in these tests is that the vortex, as it travels downstream, tends to center itself with its axis at mid-depth and with the transverse velocity near the water surface, becoming nearly equal in magnitude to the velocity near the bed. This feature is associated with the relatively large viscous dissipation occurring near the bed, which causes the transverse velocity near the bed to decay at a somewhat higher rate than elsewhere over the depth.

Figure 3-2 shows that Eq. 2-2 provides a reasonably good description of the distribution of vane-induced transverse velocity. The calculation in Fig. 3-2 is made using six images.

As mentioned earlier, to generate a larger, coherent vortex that affects the flow pattern over a wider area of the channel cross section, several vanes must be employed. Figures 3-3 and 3-4 show results with two vanes placed side-by-side at the channel centerline.

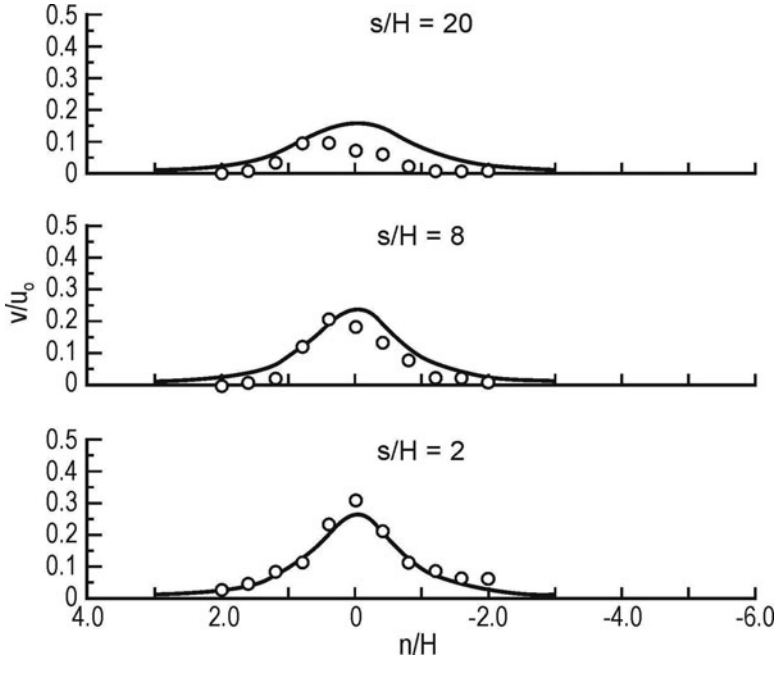

Figure 3-2. Calculated (solid line) and measured near-bed ($z/d = 0.05$) transverse velocities downstream from single vane. *Source:* Wang and Odgaard (1993), with permission of IAHR.

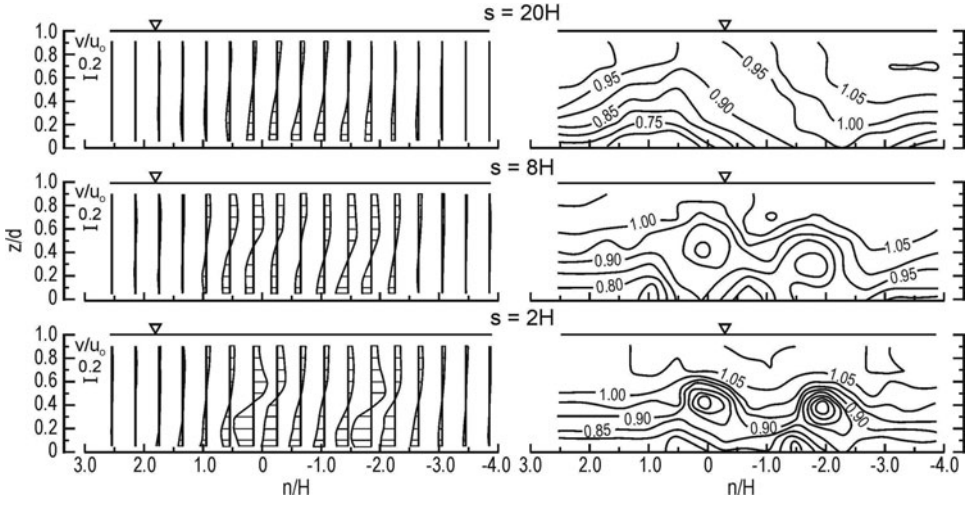

Figure 3-3. Velocity distribution downstream from vane pair. (a) Transverse (v/u_o), and (b) streamwise (u/u_o) component. Vane spacing $= 2H$.
Source: Wang and Odgaard (1993), with permission of IAHR.

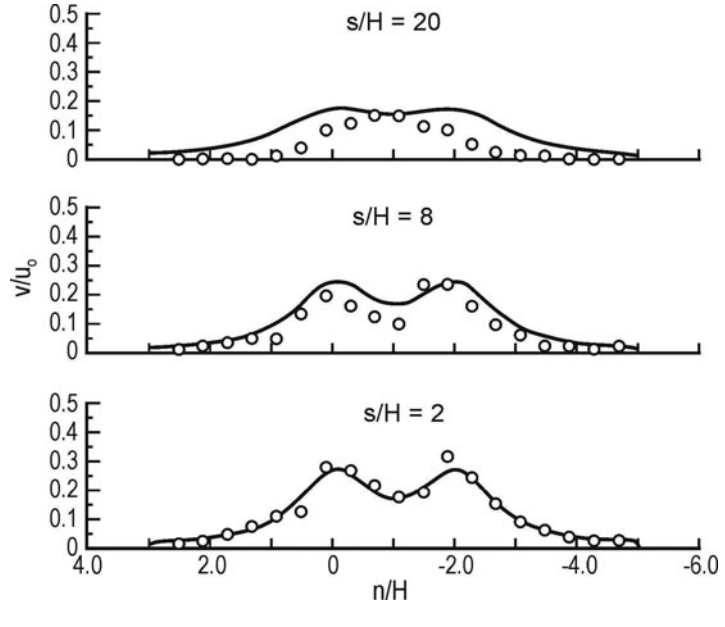

Figure 3-4. Calculated (solid line) and measured near-bed ($z/d = 0.05$) transverse velocity downstream from vane pair. Vane spacing $= 2.67H$.
Source: Wang and Odgaard (1993), with permission of IAHR.

The results in Fig. 3-3 are with a vane spacing of $2H$. In Fig. 3-4, the vane spacing is $2.67H$. [Results of other vane spacings are presented in Wang (1989)]. In these tests, vane height and length, flow depth, water-surface slope, and friction factor are the same as in the single-vane tests. As seen, the area of channel cross section over which the flow is affected by the two vanes is larger than that affected by a single vane. In both cases, the vane pair generates a single, coherent vortex. However, the transverse velocity in the region between the vanes decreases as vane spacing increases. The u-contour plots define the location of the vortex cores and show the merging of the vortices downstream. The distance downstream for complete merging increases with increasing vane spacing. The contour plots also show how the contour lines are "lifted up" on the pressure side and "pressed down" on the suction side, indicating that the vortices together produce a net transport of momentum from one side of the channel to the other. It is noted that the maximum transverse velocity is nearly the same in all cases, despite the difference in vane spacing. Obviously, the resulting distribution of v and, hence, induced transverse bed shear stress are not obtained by simple superposition of those associated with individual, isolated vanes. As mentioned earlier, the lower measured values are due to interference of vortices, which reduces the circulation per vane. Figure 3-4 shows that the transverse velocity calculated using an interaction coefficient based on biplane theory (as discussed in Chapter 2) is in good agreement with the experimental data at $s = 2H$ and $s = 8H$. At $s = 20H$ the calculated values are somewhat larger than the measured, which could be because the calculation does not account for vane-generated eddy viscosity.

The experiments confirm what the calculations indicate, that a vane spacing of two to three times the vane height is appropriate for the vortices induced by a vane pair to merge into a distinct, common vortex with relatively large transverse velocity in the region between the vane axes, and not too large a reduction of circulation per vane due to vortex interference.

Figure 3-5 shows the layout that was used to test the performance of a larger vane field. In this test, the flume was tilted to a slope of 2.5×10^{-4}, which yielded uniform flow (constant depth) in the channel without vanes. Water depth and friction factor were 0.102 m and 0.028, respectively (without vanes). The total number of vanes was 60. Each vane was 0.051 m tall and 0.102 m long. With vanes installed, the water surface slope increased to 3.6×10^{-4} and caused the water depth to increase by about 1% at the upstream end of the vane system. (In a natural river channel such a large change in water-surface slope would normally not be acceptable, nor would such a large number of vanes in a relatively narrow channel). Figure 3-6 shows the induced distributions of transverse and streamwise velocity components at three sections. The data were taken midway between two vane arrays, as indicated in Fig. 3-5. As seen, the vane system generated a coherent vortex in the vane-covered area throughout the channel. Outside the vane-covered area, no noticeable vortex was observed. The vane-induced adjustments of the streamwise velocity were considerable both within and outside the vane field. The depth-averaged velocity was reduced by about 18% within the vane field and was increased

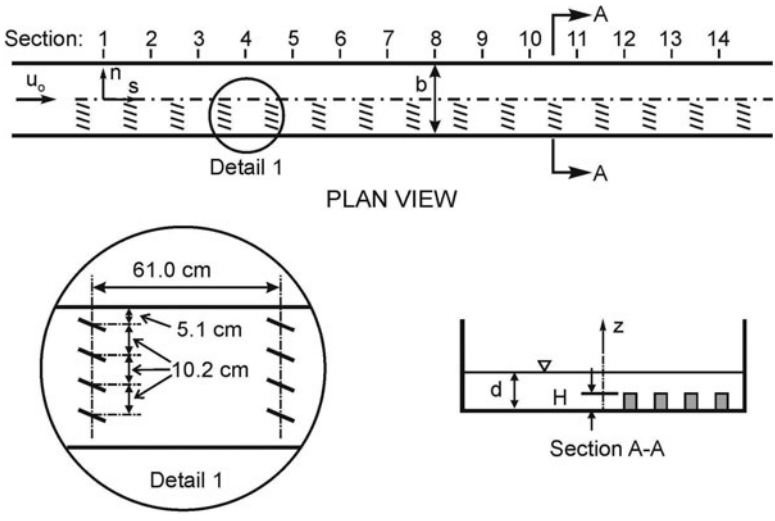

Figure 3-5. Layout of vane arrays in a rigid-bed channel. *Source:* Wang and Odgaard (1993), with permission of IAHR.

by about 18% outside. Obviously, the vane system generated a considerable net transport of momentum across the channel.

Figure 3-7 shows depth-averaged velocities measured in two sections of the channel flow. The data are normalized with the velocity in the vane-free part of the cross section and far from the vane field,

$$u_\infty = \frac{m}{\kappa}\sqrt{gSd} \tag{3-1}$$

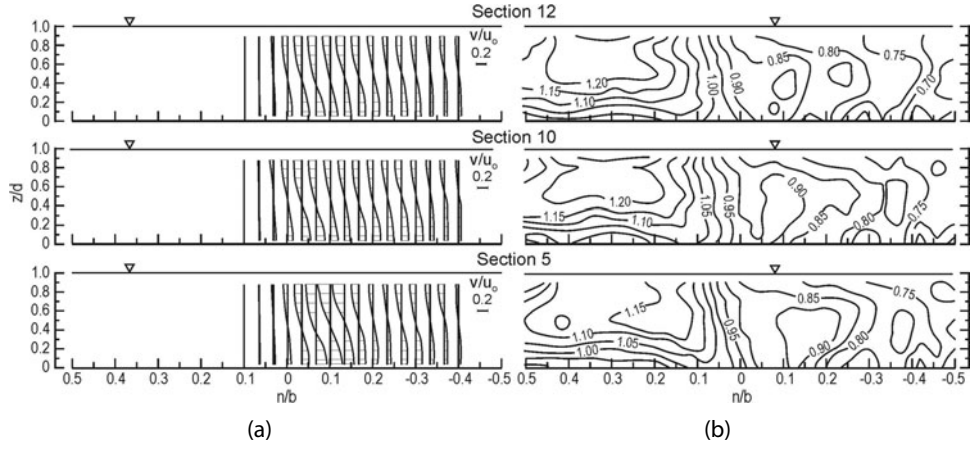

Figure 3-6. Velocity distribution within and outside a vane field. (a) Transverse (v/u_o), and (b) streamwise (u/u_o) component. *Source:* Wang and Odgaard (1993), with permission of IAHR.

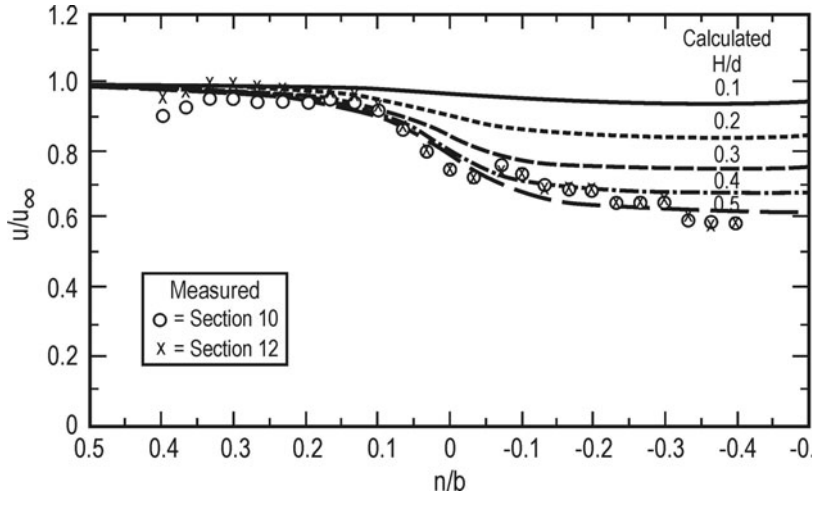

Figure 3-7. Depth-averaged velocity distributions calculated for different vane heights. *Source:* Wang and Odgaard (1993), with permission of IAHR.

The figure also shows calculated velocities both for $H/d = 0.5$ and for vane heights other than $H/d = 0.5$. Obviously, vane height is a critical parameter. At $H/d = 0.5$, the velocity in the vane-covered area is reduced to nearly 60% of the maximum velocity outside the vane-covered area, which, as seen, is in good agreement with the calculation.

A simple calculation will illustrate the use of the theoretical relations in Chapter 2: By normalizing the depth-averaged velocity u with u_∞, Eq. 2-22 reads

$$\frac{u}{u_\infty} = \sqrt{1 - \frac{\tau_{vs}}{\rho g S d}} \tag{3-2}$$

The term $\tau_{vs}/(\rho g S d)$ is calculated based on Eq. 2-13, which relates τ_{vs} and vane-induced drag force F_D, and Eq. 2-10 relating drag force and dynamic pressure. The following values are used: $\lambda = 0.88$ (from Fig. 2-5), $\beta_s = 0.9$, $c_D = 0.17$ (from Eq. 2-11), $u = 0.20$ m/s (18% less than u_o), $H = 0.052$ m, $L = 0.102$ m, $\delta_n = 0.102$ m, $\delta_s = 0.61$ m, $d = 0.102$ m, $S = 0.00036$, and $g = 9.81$ m/s^2. Hence,

$$\frac{\tau_{vs}}{\rho g S d} = \frac{(0.88)(0.9)(0.5)(0.17)(0.051)(0.102)(0.2)^2}{(9.81)(0.00036)(0.102)(0.102)(0.61)} = 0.63$$

Substituting this value into Eq. 3-2 yields $u/u_\infty = 0.60$, in good agreement with measurements. Estimating vane-induced increase in water-surface slope by Eq. 2-14 yields

$$\Delta S = (0.88)(0.9)\frac{(60)(0.5)(0.17)(0.051)(0.102)(0.24)^2}{(0.91)(15)(0.61)(9.81)(0.102)} = 0.00015$$

which gives a water surface slope of 0.00024 + 0.00015 = 0.00039, in reasonable agreement with the slope measured directly (0.00036). It is useful to note that in

all tests, the maximum value of v/u_o is within a relatively narrow range of 0.2 to 0.3, probably because the vane angle of attack in all tests was fixed at 20 degrees.

In summary, the rigid-bed proof-of-concept-tests show that, despite obvious shortcomings, the simple airfoil analogy described in Chapter 2 is a reasonable basis for design of vane systems.

3.2 Movable-Bed Curved and Straight Channels

The curved channel was a 1.94-m-wide (at top), 0.6-m-deep, 12.9-m-radius bend with a 20-m straight approach section [Fig. 3-8(a)]. The outer bank of the curve was vertical. The inner bank was on a 2:3 slope (2 vertical, 3 horizontal). The straight channel was 2.44 m wide (at top), 0.6 m deep, and 16.2 m long [Fig. 3-8(b)]. In both channels, the bottom consisted of an approximately 14-cm-thick layer of sand with a median diameter of 0.41 mm and a geometric standard deviation of 1.45. Both the water and the sediment it transported were recirculated throughout the channels and their return circuits by a centrifugal pump. The discharge was controlled by means of a butterfly valve and measured with an orifice meter. A drop gate and a weir at the downstream end of the channels were adjusted to

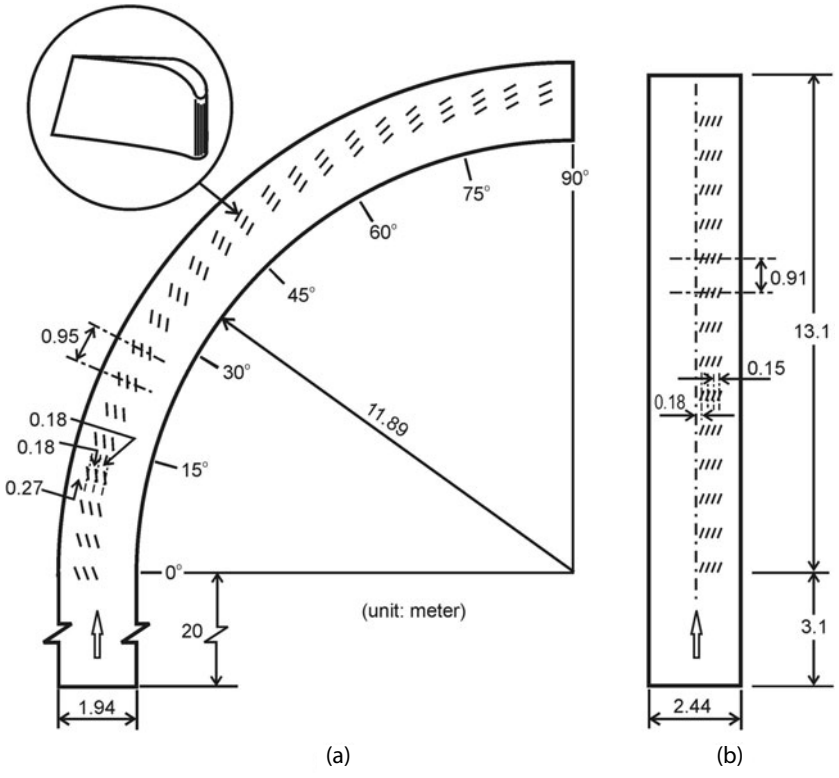

Figure 3-8. Layout of vane system in (a) curved, and (b) straight, recirculating laboratory channels. *Source:* Odgaard and Wang (1991), ASCE.

produce uniform flow in the channels. Velocities were measured with a two-component electromagnetic meter, depths with a sonic sounder, and water-surface elevations with a static tube. The current meter, sounder, and tube were mounted on a movable instrument carriage, which rode on rails atop the channel walls, on a traversing mechanism which enabled them to be positioned at any desired location in the channels. Positioning and data sampling were controlled from a computer on the carriage.

In the curved flume, the vanes were double-curved foils with a slight twist [Fig. 3-8(a)]. These vanes were 7.4 cm tall (initially) and 15.2 cm long. They were installed in arrays with two or three vanes in each array, angled 15 to 20 degrees toward the bank. The tests were conducted at discharges ranging from 0.11 m^3/s to 0.15 m^3/s. In the straight channel, the vanes were 0.8-mm-thick sheet metal plates, 7.4 cm tall (initially) and 15.2 cm long. These were installed in arrays with four vanes in each array, angled 20 degrees toward the bank [Fig. 3-8(b)]. In this case, tests were conducted at discharges ranging from 0.088 m^3/s to 0.15 m^3/s. The tests are described in detail by Wang (1989).

Figure 3-9(a) shows measured velocity and depth distributions in the curved flume, with and without vanes, in tests with discharge = 0.136 m^3/s. The data points are average values in four sections at approximately 45 degrees, 60 degrees, 75 degrees, and 90 degrees into the bend. It is seen that both a two-vane array system and a three-vane array system are effective in eliminating the bed scour along the outer bank. The photos in Fig. 3-10 were taken after one of the tests after draining most of the water from the flume. Figure 3-10(a) shows the bed topography prior to vane installation, and Fig. 3-10(b) shows the bed topography after vane installation. It is evident that the vane system caused a considerable redistribution of sediment. By creating a wide berm along the bank, the vanes effectively moved the thalweg to the center of the channel. As seen in Odgaard and Wang (1991), the measured distributions of depth and velocity are in good agreement with those calculated using Eqs. 2-22 and 2-23.

A simple calculation will illustrate the use of the design graphs in Figs. 2-21 and 2-22. In the curved-flume test without vanes, the steady-state average depth, velocity, resistance factor, and water-surface slope were $d_o = 0.174$ m, $u_o = 0.43$ m/s, $m = 4.7$, and $S = 0.00078$, respectively. These values yield effective width $b = 1.82$ m, centerline-radius of curvature $r_c = 12.9$ m, and sediment Froude number $\mathbf{F}_D = 6.8$. Maximum depth and velocity as calculated by Eqs. 2-28 and 2-29,

$$\frac{d_m}{d_c} = 1.25$$

$$\frac{u_m}{u_c} = 1.12$$

are in agreement with measurements. These values are obtained using a value of $c = 1.0$.

In the curved-flume tests with vanes, the steady-state average depth, velocity, resistance factor, and water-surface slope were $d_o = 0.180$ m, $u_o = 0.424$ m/s, $m = 4.4$,

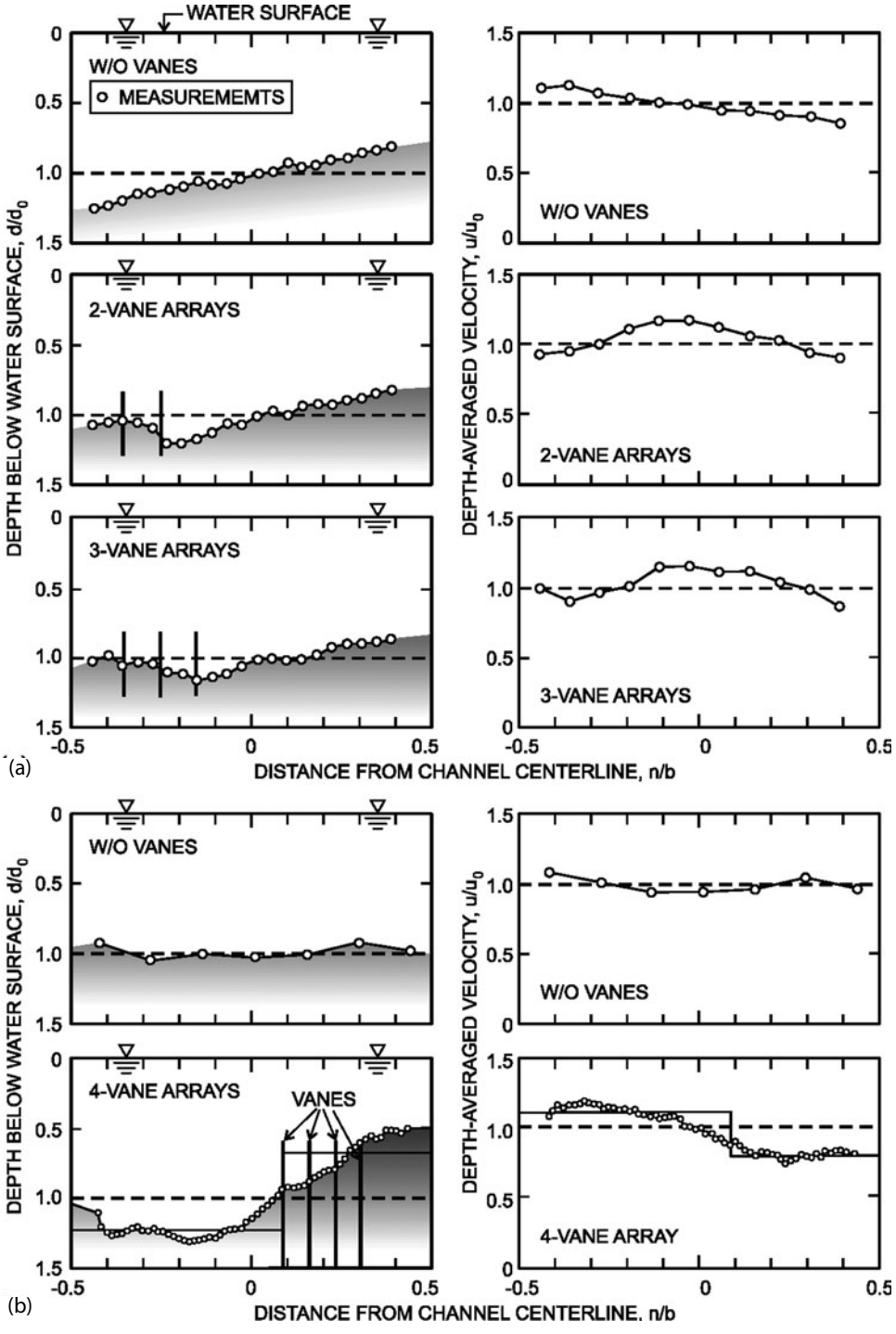

Figure 3-9. Velocity and depth distributions without and with vanes (a) in curved channel, and (b) in straight channel. *Source:* Odgaard and Wang (1991), ASCE.

(a)

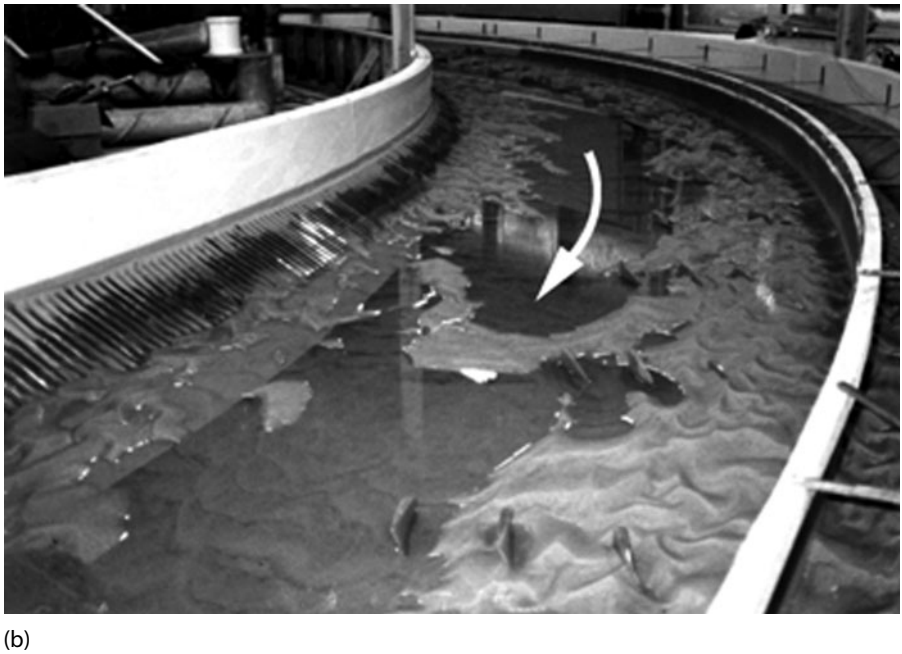

(b)

Figure 3-10. Upstream view of nearly drained channel bend without vanes (top) and with vanes (bottom). *Source:* Odgaard and Wang (1991), ASCE.

and $S = 0.00083$, respectively. These values yield effective width $b = 1.78$ m, centerline-radius of curvature $r_c = 12.9$ m, and sediment Froude number $\mathbf{F}_D = 6.7$. Entering Figs. 2-21 and 2-22 with these values yield for the three-vane array system

$$\frac{d_v}{d_o} = 1.0$$

and for the two-vane array system

$$\frac{d_v}{d_o} = 1.1$$

both of which are in agreement with measurements. The tests show that unlike the three-vane array system [Fig. 3-9(a)], the two-vane array system is not quite able to eliminate the bed scour at the bank.

Figure 3-9(b) shows measured velocity and depth distributions in the straight flume in a test with discharge = 0.154 m^3/s. Average flow depth was $d_o = 18.2$ cm, and the slope of the water surface was $S = 0.00064$. The data points are average values in four sections in the downstream half of the flume. The vanes reduced the depth near the right bank by about 50%. This caused the depth near the left bank to increase by 20% to 30%. Figure 3-11 is a view of the bed topography after draining most of the water from the flume. It shows the sediment accumulation in the vane field and the associated degradation of the channel outside the field. As shown in Odgaard and Wang (1991), these distributions of vane-induced depth and velocity are also in good agreement with those calculated with Eqs. 2-22 and 2-23.

The utility of the design graphs in Fig. 2-23 is illustrated using the data from the aforementioned straight-channel test: The vane system consisted of 14 arrays of vanes with four vanes in each array. Vane spacings were $\delta_n = 0.152$ m laterally and $\delta_s = 0.914$ m longitudinally. With average flow depth $d_o = 0.183$ m, average flow velocity $u_o = 0.396$ m/s, and vane submergence $T = 0.101$ m, average vane height was $H = 0.183 - 0.101 = 0.082$ m, effective channel width $b = Q/(u_o d_o) = 2.13$ m, relative vane submergence $T/d_o = 0.55$, and streamwise spacing $\delta_s = 11.2H$. The channel's resistance parameter was

$$m = \frac{\kappa u_o}{\sqrt{gSd_o}} = \frac{(0.4)(0.396)}{\sqrt{(9.81)(0.00064)(0.183)}} = 4.7$$

and the sediment Froude number was

$$\mathbf{F}_D = \frac{u_o}{\sqrt{gD}} = \frac{(0.396)}{\sqrt{(9.81)(0.4\times10^{-3})}} = 6.3$$

With these values, Fig. 2-23 yields for a four-array vane system ($N = 4$)

$$\frac{\dfrac{(d_o - d_v)}{d_o}}{1 - \dfrac{T}{d_o}} \approx 0.7$$

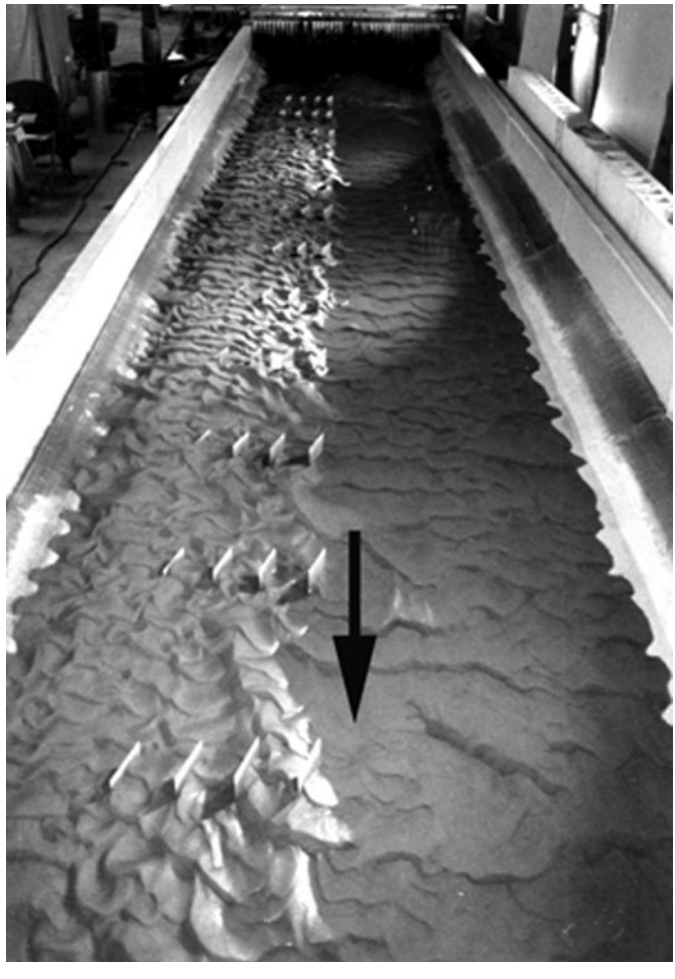

Figure 3-11. Upstream view of nearly drained, straight channel with vanes. *Source:* Odgaard and Wang (1991), ASCE.

from which

$$\frac{d_o - d_v}{d_o} = (0.7)\left(1 - \frac{T}{d_o}\right) = 0.32$$

$$\frac{d_v}{d_o} = 0.68 \qquad \text{or} \qquad d_v = 0.124 \text{ m}$$

The calculated depth, $d_v/d_o = 0.68$, is seen to be about the average flow depth over the vane-covered part of the cross section from the first vane in the array to the bank (i.e., over width $\delta_v = 0.884$ m). As seen in Fig. 3-9(b), this is approximately the flow depth measured near the fourth vane in the vane array. The flow depth in the flume is seen to decrease even further closer to the bank, which undoubtedly is due to the proximity of the bank and bank resistance.

The average depth over the part of the cross section outside the vane field (of width δ_b = 1.25 m) is readily estimated by assuming conservation of conveyance (and constant slope and resistance). Referring to the schematic in Fig. 3-12, and applying Manning's equation, conservation of conveyance yields

$$A_b R_b^{2/3} + A_v R_v^{2/3} = A_o R_o^{2/3} \tag{3-3}$$

where A = area, R = hydraulic radius, and subscript o refers to the total cross section prior to vane installation, and subscripts b and v refer to the left and right parts of the cross section after vane installation, respectively. Using the notation indicated in Fig. 3-12, Eq. 3-3 yields

$$\delta_b \frac{(d_o + \Delta d)^{5/3}}{\left[1 + \frac{2(d_o + \Delta d)}{\delta_b} - \frac{d_v}{\delta_b}\right]^{2/3}} + \delta_v \frac{d_v^{5/3}}{\left(1 + \frac{d_v}{\delta_v}\right)^{2/3}} = \frac{(\delta_b + \delta_v)^{5/3} d_o^{5/3}}{(\delta_v + \delta_b + 2d_o)^{2/3}} \tag{3-4}$$

Substituting δ_b = 1.25 m, δ_v = 0.884 m, d_o = 0.183 m, and d_v = 0.124 m yields Δd = 0.041 m, or d/d_o = 1.22 for the outer part of the cross section. As seen in Fig. 3-9, this estimate is in perfect agreement with measurements.

The average velocities in the two parts of the cross section are estimated to be

$$\frac{u_v}{u_o} \cong \left(\frac{R_v}{R_o}\right)^{2/3} = \left(\frac{0.180}{0.156}\right)^{2/3} = 1.10$$

$$\frac{u_b}{u_o} \cong \left(\frac{R_b}{R_o}\right)^{2/3} = \left(\frac{0.109}{0.156}\right)^{2/3} = 0.79$$

As seen in Fig. 3-9, these estimates are also in good agreement with measurements.

The above simplified calculations demonstrate the utility and expediency of the design graphs. Although it is an approximation only, Eq. 3-4 is a convenient tool for estimating the bed level in the channel outside the vane field. Obviously,

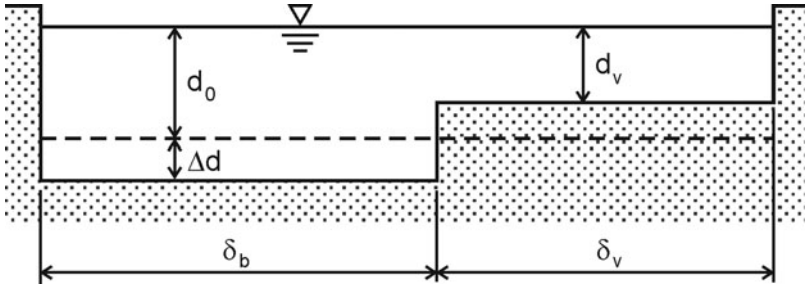

Figure 3-12. Straight-channel cross section (simplified) maintained by vanes over width δ_v along right bank.

the calculations are only applicable when the velocity differences between the two parts of the channel are relatively small.

One of the most important observations made in the tests in both the curved and straight flume is that the vane-induced changes occurred without causing significant changes in the area of the cross sections and of the longitudinal slope of the water surface. The changes in slope were less than 8%. This observation is important because it implies that the vanes will not cause any changes of the stream's sediment-transport capacity upstream and downstream from the vane field and, therefore, should not alter the overall characteristics of the stream.

Another notable observation is that the vane-induced redistribution of sediment within a cross section is an irreversible process in the sense that a reduction of discharge does not lead to recovery of original distributions. A reduction in discharge does not result in a reduction in the volume of sediment accumulated in the vane field because, at the lower discharge, the sediment-transport capacity in the vane field is too low to remove the sediment that accumulated at the higher discharge.

Finally, it must be recognized that the relatively good agreement between theory and data might be somewhat deceptive. The theory of vanes is developed for nonseparated flow around the vanes. The magnitude of the induced circulation is calculated by assuming that the rear stagnation point on the low-pressure side is shifted to the trailing edge of the vane. In reality, some flow separation occurs, and induced circulation and bed shear stresses are probably somewhat different from those calculated. The probable reason for the relatively good agreement between theory and experiments is that, whereas it reduces the transverse component of the induced bed shear stress, flow separation increases the streamwise component by a comparable amount. In this case, the difference between theory and data is not in the total amount of aggradation but in the transverse slope of the aggraded bed, which obviously is difficult to measure.

3.3 Movable-Bed Sharply Curved Channel

In the aforementioned tests, the radius–width ratio was about 7. Many natural river bends have a minimum radius width ratio considerably lower. Leopold and Wolman (1960) found that many bends have a minimum radius–width ratio of the order 3. In view of that, Voisin and Townsend (2002) performed a series of tests exploring vane performance in a laboratory bend with this radius–width ratio. The width–depth ratio of their tests was also about 3; the width–depth ratio of the tests described in Section 3.2 was greater than 10. Voisin's and Townsend's experimental channel is representative of small, migrating rivers, which generally have width–depth ratio less than 10 and typically have a minimum radius–width ratio of about 3.

The test channel was rectangular in cross section, 0.305 m wide and 0.150 m deep. It consisted of three sections: a straight entrance section, a bend section, and a straight exit section. Two bend test sections were used, a 90-degree and a 135-degree section. Both bend test sections had inner and outer radii of 0.748 m and 1.053 m, respectively. The bed sediment was quartz sand with a median diameter

of 0.7 mm and a geometric standard deviation of 1.3. Channel-bed slope and starting-flow depth throughout the test section were $S = 0.00065$ and $d_o = 0.10$ m, respectively. Critical velocity for initiation of sand movement was 0.28 m/s. At this depth and mean flow velocity, channel discharge was 0.0085 m^3/s.

The vanes were constructed of 0.5-mm-thick galvanized sheet metal. A total of 13 different sizes were tested. Vane height, H, ranged from 15 mm to 65 mm and vane length, L, from 50 mm to 150 mm with aspect ratio H/L ranging from 0.15 to 1.30. Vane angle with the bankline varied within the range -4 degrees $\leq \alpha \leq 16$ degrees. Because of the small width–depth ratio, the tests were with only a single array of vanes (a system with one vane per array). Transverse distance from the channel's outer bank to the vane centerline was $\delta_b = 80$ mm. Streamwise spacing between the vanes varied in the range 10 mm $\leq \delta_s \leq 40$ mm.

Five criteria were used to evaluate the effectiveness of the various vane configurations tests:

1. Reduction in average scour depth at the outer bank
2. Generation of a positive transverse bed slope at the outer bank
3. Reduction in general erosion throughout the bend
4. Avoidance of excessive local scouring in the vicinity of the vanes
5. Practicality of vane size and spacing (relative to channel width and depth).

The tests resulted in the optimum design configurations listed in Table 3-1.

The reason for the relatively small vane angle is that the secondary current in this strongly curved channel causes the near-bed velocity vector to have a relatively large skew angle toward the inside of the bend, so the effective angle of attack on the vane is considerably larger than 2 degrees. Obviously, the optimum value of α will increase with increasing value of radius–width ratio. The tests described in Section 3.2 suggest that as radius tends toward infinity (straight channel), the optimum value of α is greater than 10 degrees.

3.4 Movable-Bed Straight Channel with Diversion

As mentioned earlier, field installations have shown that, strategically placed, submerged vanes can be effective in preventing bed-load transport from entering

Table 3-1. Optimum design configuration for vanes in sharply curved channel.

Design variable	*Value*
Vane length, L/b	0.33
Vane height, H/d_o	0.35
Angle to main flow direction, α	2 degrees
Streamwise spacing, δ_s/b	0.70
Transverse spacing from outer bank to vane centerline, δ_b/b	0.24

diversions and water intakes (Wang et al. 1996). Figures 1-15 and 2-13 are schematics of the layout for this application. The tests described below were aimed at defining the relationship between vane design parameters and effectiveness in terms of reduction in sediment ingestion for select vane layouts (Barkdoll et al. 1999).

The laboratory channel was 24 m long and 1.5 m wide. It was filled with a 15.2-cm-deep layer of uniform, 0.9-mm-diameter sand. The diversion channel, which was located 15.5 m downstream from the flume inlet, was 2.44 m long and 0.61 m wide. The floor of the diversion was level with the bed in the flume. Flow in the flume was kept constant at $Q = 0.104$ m^3/s and had a uniform depth of $d_o = 0.152$ m upstream of the diversion. Thus, average velocity, unit discharge, and sediment Froude number were $u_o = 0.456$ m/s, $q = 0.069$ m^2/s, and $\mathbf{F}_D = 4.9$, respectively.

The sand bed in the flume was in a dune regime, with sand moving as bed load. The mean velocity of flow in the main channel was 1.6 times that required for incipient movement of the sand bed, as estimated using the Shields diagram (ASCE 1975). It was assumed that this main-channel flow and bed condition was sufficiently representative for determining proportionate rates of bed-sediment movement (g_r) into a lateral diversion adjoining an alluvial channel. Variable g_r represents the ratio of bed-load transport into the diversion per unit width, g_i, to the bed-load transport in the main channel per unit width. The corresponding ratio of unit discharge of water in the diversion, q_i, to unit discharge of water in the main channel, q, is denoted q_r (i.e., $q_r = q_i/q$). The assumption made in these tests was that the ratio g_r depends predominantly on q_r. Higher or lower intensities of bed-sediment movement in the main channel were not expected to alter the relationship between g_r and q_r. The floor of the diversion/intake channel was smooth and fixed (to replicate a concrete intake floor) and turbulence from the flow contraction in the entrance area actively kept sediment moving, except within the entrance eddy, where sediment became entrapped.

Flow velocities were measured using an acoustic Doppler velocimeter. Bed elevations were measured using a Delft Bed Profiler, which senses bed elevation by means of electromagnetic signals. Dye was used to identify the main flow features at the diversion. For example, it was used together with velocity measurements to determine the near-bed location of the stream surface between the flume flow and flow into the diversion.

To measure the rate of sediment transport into the diversion, a sediment-collection trap was positioned below the diversion outlet pipe. The trap was composed of a strainer mesh with holes smaller than the sediment grain size to enable water to pass through to the tail box of the flume. Sediment was collected for a two-hour period, then removed from the strainer and weighed; a two-hour period corresponded to about the time required for a dune to pass the face of the diversion. To measure the rate of sediment transport in the flume upstream of the diversion, the height and wavelength of a representative dune were measured using the Delft Bed Profiler. The average volume of bed sediment per unit length of channel width was estimated as half the average dune-crest height multiplied by the average wavelength. Average dune celerity was measured using a stopwatch

and a distance scale. Values of the ratio of diversion to flume sediment transport rate, g_r, and the volume fraction of diversion occupied by settled sediment, V, were determined for a range of discharge ratios, q_r.

Each set of experiments began with a level sand bed in the flume. Water flow and sediment movement were left to develop a condition of equilibrium bathymetry, which was judged to have occurred when the following quantities were time-invariant: dune height, length, and migration velocity in the flume, and plan form and height of a sediment bar in the entrance to the diversion channel. After equilibrium was achieved, g_r and V were measured. Flow patterns were observed using neutrally buoyant dye injected at various locations by means of a dye wand.

The vane experiments were performed under the same conditions of flume flow and sediment movement used for the experiments without vanes. The performance of various schemes of vane arrays was investigated. The two most promising schemes were:

1. Submerged vanes placed at the diversion entrance to scour bed-load sediment away from the diversion (Fig. 3-13)

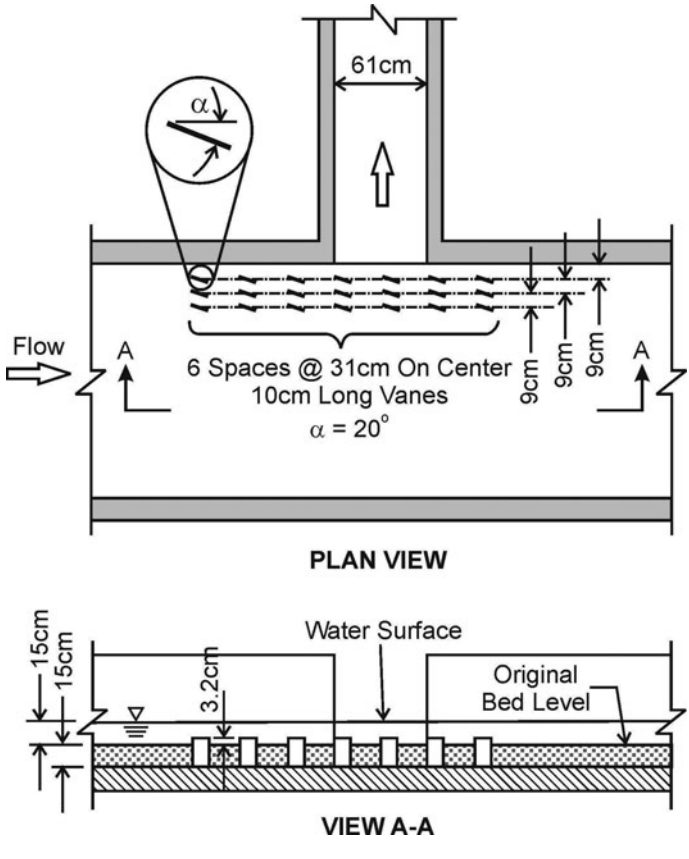

Figure 3-13. Vanes at a diversion entrance. *Source:* Barkdoll et al. (1999), ASCE.

2. Submerged vanes placed as a guide upstream of the diversion to deflect bedload sediment away from the diversion site (Fig. 3-14).

Observations of flow and sediment movement at the laboratory-scale diversion led to the following set of assessment criteria for effective sediment control:

1. *Minimum sediment transport rate into the diversion*. This is the most important guideline because it gives a direct measure of sediment ingestion into the diversion and is of prime concern at plant intakes, for example, to minimize intake dredging and plant (power station or water supply) shutdowns.
2. *Minimum volume of sediment accumulation in the diversion*. This guideline has implications for the asymmetry of the flow in the diversion channel. Flow asymmetry has implications for pump vibrations in intakes, for example.
3. *Acceptable localized scour of the bed near the diversion*. Sufficient scour below the diversion sill elevation reduces sediment ingestion.

Both layouts of vane systems (Figs. 3-13 and 3-14) reduced the rate of sediment movement into the diversion. Figure 3-15 shows the extents to which the rates were

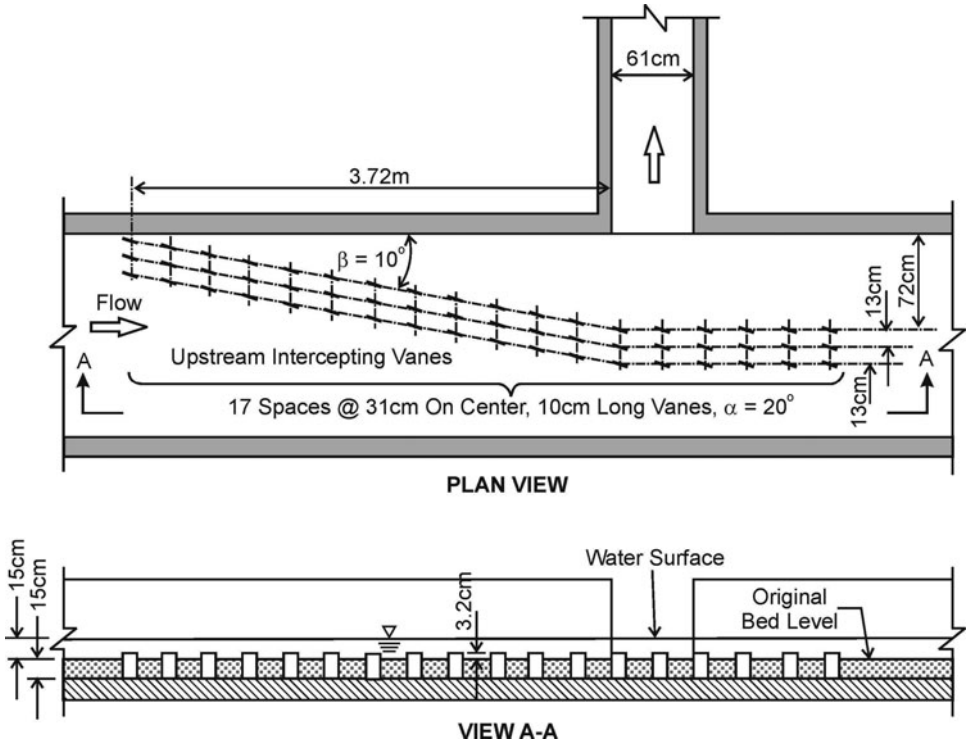

Figure 3-14. Upstream interception layout of vanes. *Source:* Barkdoll et al. (1999), ASCE.

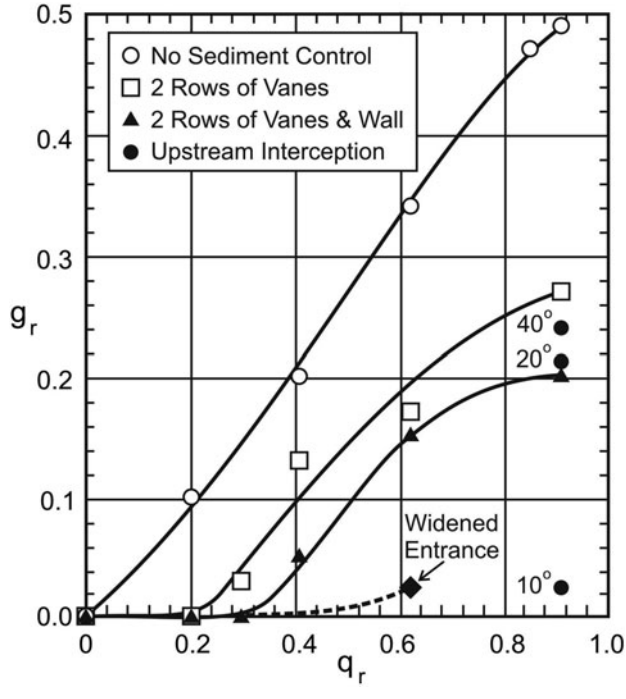

Figure 3-15. Rate of bed-sediment entry into a diversion. *Source:* Adapted from Barkdoll et al. (1999), ASCE.

reduced. For both vane layouts, two rows of vanes were found to be nearly as effective for sediment control as three rows.

The vane systems prevented sediment movement into the diversion for values of q_r up to about 0.2. Beyond this value, the vane system reduced the rate of sediment entering but did not eliminate it. This observation is consistent with the previously discussed design objective for this application. In order for the near-shore stream tube for the intake flow (see Fig. 2-15) to be limited to the channel between bank and innermost row of vanes, the intake flow rate must be limited to

$$Q_i \approx u_o \delta_b (d_o + \Delta d) \tag{3-5}$$

where Δd = increase in depth in the near-shore channel. The value of Δd is estimated by first determining minimum depth generated by the vanes, d_v. With $\mathbf{F}_D = 4.9$ and resistance parameter of the order of $m = 4$, Fig. 2-23 yields for a three-vane array system

$$\frac{d_o - d_v}{d_o} = 0.48\left(1 - \frac{T}{d_o}\right)$$

With $T = 0.128$ m and $d_o = 0.152$ m, this relationship yields $d_v = 0.140$ m. Substituting this value and $\delta_v = 0.18$ m into Eq. 3-4 yields $\Delta d = 0.05$ m. Hence,

$$Q_i \approx (0.456)(0.09)(0.152 + 0.05) = 0.0083 \text{ m}^3/s$$

$$q_i = \frac{0.0083}{0.61} = 0.0136 \text{ m}^2/s$$

and

$$q_r = \frac{q_i}{q} = \frac{0.0136}{0.069} = 0.20$$

For an intake flow rate larger than this limiting value ($Q_i \geq 0.0083$ m^3/s, and $q_r \geq 0.2$), the innermost row of vanes will be inside the stream tube. As indicated before, in this case the flow in the stream tube will be more turbulent and more likely to stir up bed material and carry it into the intake. Indeed, in the tests, intermittent wake vortices were seen to be shed from several vanes near the center of the diversion axis and from the sill of the diversion entrance. These vortices were seen to lift sediment into the diversion.

Another unsteady vortex formed by flow reversing upstream after striking the flume wall downstream of the entrance to the diversion. The flow deflected upstream merged with the flow moving downstream a short distance away from the diversion to form the vortex. This second vortex also lifted sediment up and into the diversion.

Upstream interception of approaching bed sediment and guidance of it away from the diversion proved to be effective when the vane array extended at about 10 degrees ($\beta = 10$ degrees) from the upstream bank, as indicated in Fig. 3-14. This configuration worked well, moving bed sediment from one vane downstream to the next and leading it away from the flow region between the dividing stream-plane and the diversion entrance. A reduction in the number of vanes used, coupled with an increase in angle $\beta = 20$ degrees and 40 degrees, proved less effective, due to the decreased efficiency with which the vanes could pass sediment at the greater angle.

Upstream interception of bed-load sediment is potentially expensive because of the number of vanes involved and because the vanes may overly intrude into a river channel. Therefore, it may not be suitable for many channels, especially those used for navigation. The vane array at the diversion entrance requires much fewer vanes and therefore is likely to be more appealing economically.

Two enhancements to vane performance were also tested:

1. Sill level of diversion entrance effectively raised by means of a skimming wall to block sediment (Fig. 3-16).
2. Diversion entrance widened so that q_r at the entrance is within the limit for vane effectiveness (Fig. 3-17).

As mentioned in Section 2.3.3, when intake velocity is relatively high, sediment ingestion may be unavoidable with any reasonable (or acceptable) vane design. In

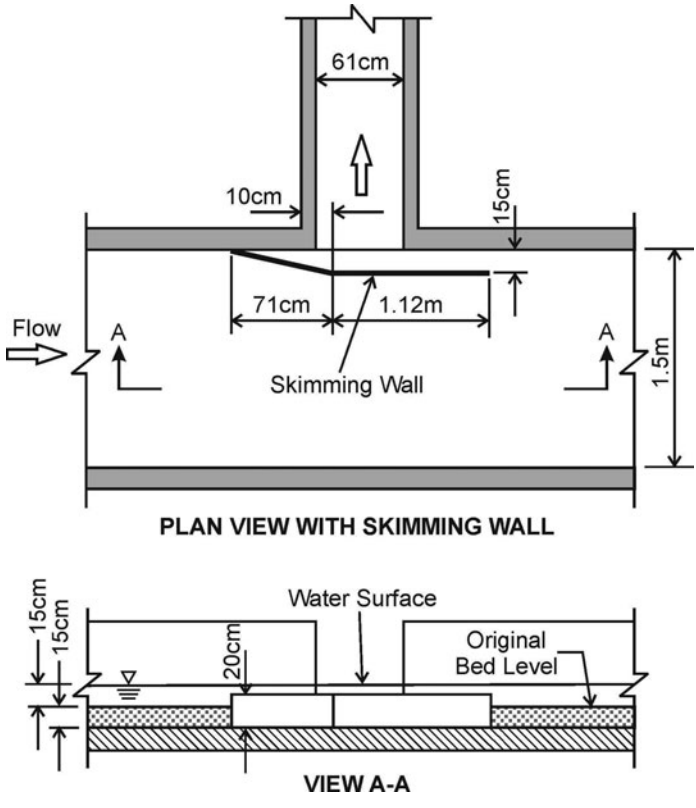

Figure 3-16. Layout of a skimming wall. *Source:* Barkdoll et al. (1999), ASCE.

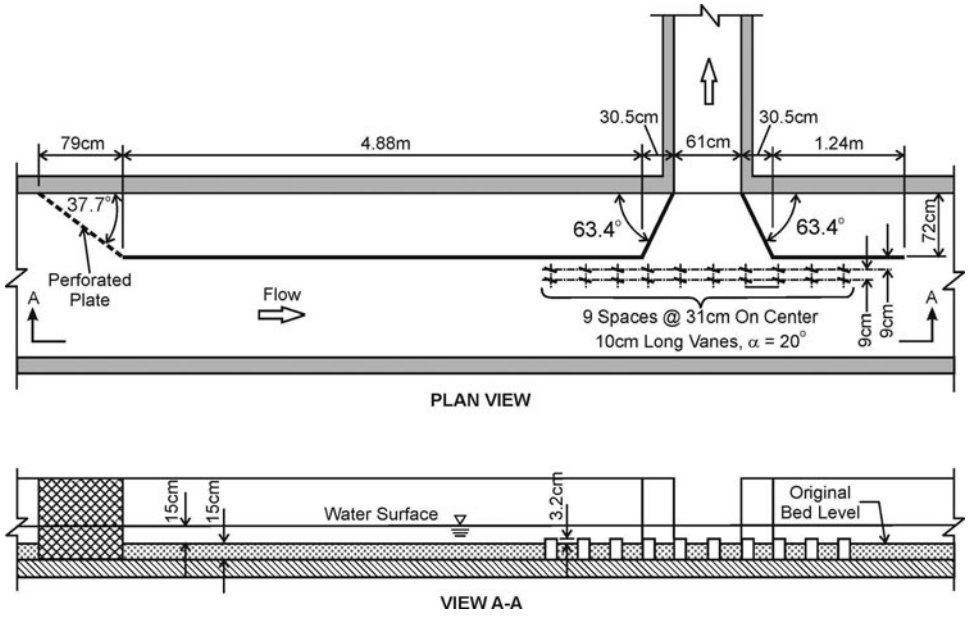

Figure 3-17. Diversion entrance flared wider. *Source:* Barkdoll et al. (1999), ASCE.

this case, consideration should be made to construct a sediment-skimming wall. Tests were conducted with a wall located as shown in Fig. 3-16. The wall was located 0.15 m away from the face of the intake. At this distance, the stream tube would remain inside the wall for q_r values up to about 0.25. The height of the wall was 0.2 m. At this height, the top elevation of the wall was about one-third of the flow depth (or 0.048 m) above the floor of the intake. Decreasing the height would enable sediment to flow over the wall at lower diversion discharges and thereby reduce the effectiveness of the wall. Increasing the wall height would cause undesirable hydraulics in the diversion, possibly leading to a hydraulic jump.

The main concern with use of a skimming wall alone is that a large bed form at the diversion entrance could still overwhelm the wall. It was found that with only a skimming wall skirting the diversion, sediment entered the diversion in two places. Some sediment came over the wall at a location just downstream of the diversion. Sediment then was carried in suspension into the diversion. In addition, sediment went around the downstream end of the wall and was moved upstream, where it collected between the wall and the diversion. From this location, an unsteady vortex carried the sediment by bursts up and into the diversion.

Vanes used in concert with the wall kept the bed level scoured well below the top of the wall. With the wall 0.15 m from the face of the intake, wall plus vanes worked well for values of q_r up to about 0.3, as seen in Fig. 3-15. For higher values of q_r, sediment started to overtop the wall. This observation is consistent with the previously discussed design objective for this application. For q_r values larger than 0.3, the wall and some of the vanes were located within the stream tube, causing the flow in it to be more turbulent and carrying more suspended bed material into the intake. The main flow feature feeding sediment into the diversion was a vertical, unsteady vortex located just outside the wall. The sudden increase of transport rate at a flow slightly above that for wall overtopping occurred because the vortex became strong enough to move sediment over the wall.

For further details about these laboratory tests, readers are referred to Barkdoll et al. (1999).

This page intentionally left blank

CHAPTER 4

Design Calculations

4.1 Design Steps

The following steps are typical in design calculations:

1. Determine design-flow conditions. The design-flow conditions depend on the application, and each requires unique considerations.
   A. *Bank protection*. If the objective is to prevent bank erosion, the vane system must create near-bank velocities that are low enough that bank material stays in place and is not moved by the current at any stage. This means that the composition of the bank material needs to be analyzed and a limiting velocity determined. The vane system should be designed so that near-bank velocity is reduced from a maximum that typically occurs at bank-full flow to the limiting velocity. Vane height must be selected such that the system can accomplish this also at less than bank-full flow. For vanes to function optimally, their height should be less than half the water depth. They typically perform within 20% of optimum when H/d is within the range $0.12 < H/d < 0.48$ (i.e., when the water depth is between two and eight times the vane height). Their height should be selected such that when the water depth is less than twice the vane height, near-bank velocity is well below the limiting velocity.
   B. *Maintenance of compound, navigation, and/or flood-flow conveyance channel*. In this case, vane height and layout must be selected based on the desired increase in flow depth over a given width of the channel. This increase in flow depth is accomplished by the vane system creating and maintaining sediment deposition elsewhere in the channel cross section, usually within the vane field. Vane height is selected based on the amount of sediment that needs to be permanently relocated. Typically, vanes can maintain a sediment deposit to a level close to the top of the vanes. In this objective it is important to perform a channel stability analysis prior to design. The compound channel segment created by the vanes must maintain and possibly enhance the natural stability of the channel.

C. *Sediment control at water intake or diversion*. If the objective is to prevent bed load from entering a diversion or intake, vanes are typically located such that they create large enough flow depth and velocity along the intake or diversion that bed load cannot enter. Vane height is selected such that the channel is maintained at all flow rates with velocity large enough to move bed-load material.

D. *Stabilization of channel alignment*. Whether stabilization is in the context of a river restoration project or it is a re-meandering of a previously straightened river reach, the design flow rate should be the channel-forming discharge. If the design is a single-thread meandering channel, the plan form should be selected such that it is consistent with that of a stable meander plan form—a plan form obtained either from analysis of upstream or downstream stable reaches of the same river or from a formal stability analysis, or from both. The wavelength of the plan form should be the so-called dominant meander wavelength, and the amplitude should be determined such that the water surface slope is, as much as possible, constant through the reach and equal to the slope in the reaches immediately upstream and downstream of the reach. The channel-forming discharge will often be the same as bank-full discharge; however, there are cases where a more comprehensive analysis is required. Reference is made to Doyle et al. (2007).

2. Determine design-flow variables for range of conditions determined in Step 1. For each condition, determine:
   A. Average width, b
   B. Average depth, d_o
   C. Average velocity, u_o
   D. Longitudinal slope, S
   E. Centerline radius of curvature, r_c
   F. Median grain diameter of bed material, D
   G. Depth variation across channel
   H. Velocity variation across channel
   I. Maximum depth without vanes, d_m
      a. In straight channel, $d_m = d_o$
      b. In curved channel, d_m = near-bank (scour) depth
   J. Desired (corresponding) depth with vanes, d_v
   K. Maximum velocity without vanes, u_m
   L. Desired (corresponding) velocity with vanes
3. For design-flow variables in Step 2, calculate:
   A. Friction parameter, $m = \kappa u_o/\sqrt{(gSd_o)}$
   B. Sediment Froude number, $\mathbf{F}_D = u_o/\sqrt{(gD)}$
   C. Depth–width ratio, d_o/b
   D. Width–radius ratio, b/r_c
   E. Desired maximum change of depth to be achieved, $d_m - d_v$
   F. Desired maximum change of velocity to be achieved

4. Select vane dimensions:
   A. Height, H ($0.12 < H/d_o < 0.48$)
   B. Length, $L(\approx 3H)$
   C. Angle of attack, $\alpha(10° < \alpha < 20°)$
   D. Submergence, T
5. Calculate:
   A. Relative vane submergence, T/d_o
   B. Vane height–length ratio, H/L
6. Enter appropriate graph and determine (read) the number of vanes per array and longitudinal spacing, δ_s, required to obtain the desired value of $(d_m - d_v)$. Note that the objective can often be met with different combinations of array spacing, δ_s, and the number of vanes per array. If necessary, solve Eqs. 2-22 and 2-23 using given boundary conditions.
7. Select other vane dimensions (for example, a different angle of attack, α) and enter the appropriate graphs or perform the appropriate numerical calculation to determine whether the objective can be met with more favorable designs and layouts.
8. Conduct a final channel stability analysis and/or estimate the vane system's impact on the longitudinal slope of the water surface. This step is important because, as a sustainable design, the vane system must not have undesirable impact on the river channel upstream or downstream of the site. Preferably, the vane system will improve channel stability and enhance the river environment.

The following numerical examples illustrate the procedure. The calculations in these examples are performed for just one set of design-flow variables. As mentioned above, in reality, a range of design-flow rates must often be calculated.

4.2 Stabilization of River Bank

A system of submerged vanes is to be designed to stabilize an eroding river bank. The bank is located on the outside of a river curve. At design flow, average width, depth, and slope are $b = 100$ m, $d_o = 4$ m, and $S = 0.0009$, respectively. Design discharge is $Q = 760$ m^3/s. Radius of curvature is $r_c = 800$ m. The bed material is sand with a median grain diameter of $D = 0.6$ mm. (In reality, a range of design-flow rates would be calculated). Figure 1-12 shows a schematic of the flow situation. Design objective and variables are described in Section 2.3.1.

The preliminary design consists of determining appropriate values of vane height, H; vane length, L; angle of incidence, α; distance from design water level (often top of bank) to top of vanes, T; longitudinal and lateral spacings, δ_s and δ_n; and vane-to-bank distance, δ_b.

Average velocity at design flow is:

$$u_o = \frac{Q}{bd_o} = \frac{(760)}{(100)(4)} = 1.9 \text{ m/s}$$

The channel's resistance parameter is:

$$m = \frac{\kappa u_o}{\sqrt{gSd_o}} = \frac{(0.4)(1.9)}{\sqrt{(9.81)(0.0009)(4)}} = 4.0$$

This m-value corresponds to a Darcy-Weisbach friction factor of $f = 8\kappa^2/m^2 = 0.08$ and a Manning's number of $n = 0.040$.

The sediment Froude number is

$$\mathbf{F}_D = \frac{u_o}{\sqrt{gD}} = \frac{(1.9)}{\sqrt{(9.81)(0.6 \times 10^{-3})}} = 24.8$$

and the channel's width–radius ratio is:

$$\frac{b}{r_c} = 0.12$$

The scour depth along the outer bank at design flow is estimated using Eq. 2-28 with $c = 1.0$:

$$\frac{d_m}{d_o} = 1 + (1.0)(0.304)(24.8)(0.12) = 1.9$$

or

$$d_m = 1.9d_o = 7.6 \text{ m}$$

Erosion of the bank can be prevented by designing a vane system that, at all stages, maintains a flow depth along the bank equal to or less than the average flow depth, d_o, in the channel (i.e., $d_v \leq d_o$). This implies that the system at design flow must generate a reduction of near-bank flow depth of at least

$$d_m - d_v = d_m - d_o = 7.6 - 4.0 = 3.6 \text{ m}$$

or

$$\frac{d_m - d_v}{d_m} = 0.47$$

The channel's depth–width ratio is $d_o/b = (4)/(100) = 0.04$, which is small enough that this parameter does not play a role in the solution.

The graphs in Figs. 2-21 and 2-22 show that the objective is met with the combinations of variables listed in Table 4-1. The most feasible alternatives (Alternatives 1–5) are indicated and are further detailed in Table 4-2. Vane systems with submergence lower than $0.7d_o$ (see Table 4-1) are less attractive because they may become ineffective at lower stages.

Table 4-1. Design limitations.

Number of vanes in each array	*Vane angle of attack (degrees)*	*Vane submergence T/d_o for $\delta_s/H = 15$*	*Vane submergence T/d_o for $\delta_s/H = 30$*
3	20	≤1.0 (Alternative 1)	≤0.9 (Alternative 2)
3	25	≤1.0	≤1.0 (Alternative 3)
2	20	≤0.9 (Alternative 4)	≤0.6
2	25	≤1.0 (Alternative 5)	≤0.7

Note: $\delta_b/d_o \leq 1.5$; $\delta_n/H \leq 3$.

In Alternatives 1, 3, and 5, vane submergence is $T = d_o$. In these alternatives, the top of the vanes are at the level of the average channel bed. In Alternatives 2 and 4, the top of the vanes are 0.4 m above the level of the average channel bed.

Results from field tests show that to create and maintain a reasonably uniform bed level within the vane field, vane angle of attack should not exceed about 20 to 25 degrees. The finer the bed material, the lower should be the ideal angle of attack. Uniformity may also be compromised if longitudinal spacing becomes too large. The calculations shown in Figs. 2-21 and 2-22 are for the midpoint between vane arrays; with a large spacing between arrays, because of the decay of vane circulation, there may be a considerable stretch between the arrays where near-bank bed level is below average bed level. Finally, tests indicate that a three-vane array system often produces a more uniform bed level within the vane field than does a two-vane array system. In view of these considerations, Alternative 1 is the most attractive solution. This design is shown Fig. 4-1.

The aforementioned design alternatives are for fully developed bend flow (i.e., the stretch of bend where near-bank depth is a maximum). Upstream of this stretch, near-bank depth is less and fewer vanes may be needed. However, in locating the vane arrays, it should be considered that it takes two to three vane arrays to fully develop the vane circulation and bed topography within the vane field. As a rule of thumb, there should be at least three vane arrays upstream of the eroding section of the bend.

Table 4-2. Specifications for design alternatives 1, 2, 3, 4, and 5.

Item	*Alt 1*	*Alt 2*	*Alt 3*	*Alt 4*	*Alt 5*
Number of vanes per array	3	3	3	2	2
Vane angle of attack, α (degrees)	20	20	25	20	25
Vane submergence, T (m)	4.0	3.6	4.0	3.6	4.0
Vane height, H (m)	3.6	4.0	3.6	4.0	3.6
Lateral vane spacing, δ_n (m)	7.2	8.0	7.2	8.0	7.2
Longitudinal vane spacing, δ_s (m)	54	120	108	60	54
Vane-to-bank distance, δ_b (m)	6.0	6.0	6.0	6.0	6.0

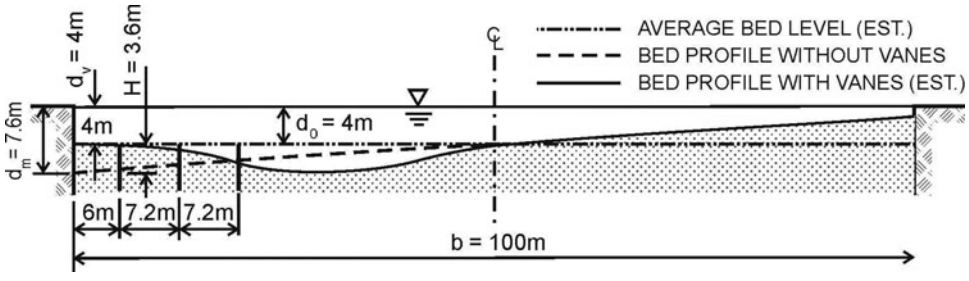

Figure 4-1. Alternative 1 design showing vane-induced change in the channel cross section.

In locating the vane arrays it is also important to ensure that overall channel stability is maintained. The example in Section 4.6 illustrates how a stability analysis may be used to determine the most appropriate vane layout in a stable river meander.

As part of the stability analysis, energy slope must be evaluated. The change in energy slope, ΔS, as a result of a vane system consisting of N vanes would be estimated using Eq. 2-14.

4.3 Stabilization of River Bed

A system of submerged vanes is to be designed to stabilize bed topography in a straight river channel. The problem could be undesirable shoaling in a bridge waterway (e.g., sand bars that block a portion of the bridge opening and cause the main channel to move toward and undermine the abutments). The objective would then be to design a vane system that can modify the flow field and create and maintain a depth distribution that permits the flow to pass the bridge without endangering the abutments. Figure 1-14 shows a schematic of the flow situation. Design objective and variables are described in Section 2.3.2.

Assume that at design flow the average width, depth, and slope are $b = 50$ m, $d_o = 2$ m, and $S = 0.00075$, respectively. Design discharge is $Q = 120$ m^3/s. The bed material is sand with a median grain diameter of $D = 0.6$ mm. These values are typical of many moderate-sized rivers in the midwest of the United States.

Average velocity at design flow is:

$$u_o = \frac{Q}{bd_o} = \frac{(120)}{(50)(2)} = 1.2 \text{ m/s}$$

The channel's resistance parameter is:

$$m = \frac{\kappa u_o}{\sqrt{gSd_o}} = \frac{(0.4)(1.2)}{\sqrt{(9.81)(0.00075)(2)}} = 4.0$$

This m-value corresponds to a Darcy-Weisbach friction factor of $f = 8\kappa^2/m^2 = 0.08$ and a Manning's number of $n = 0.036$.

The sediment Froude number is:

$$\mathbf{F}_D = \frac{u_o}{\sqrt{gD}} = \frac{(1.2)}{\sqrt{(9.81)(0.6\times10^{-3})}} = 15.6$$

and the channel's width–radius ratio $b/r = 0.0$.

The channel's depth–width ratio is $d_o/b = (2)/(50) = 0.04$, which is small enough that this parameter does not play a role.

One way to stabilize the cross section is to design a system of vanes such that they promote deposition of sediment on berms along the sides of the channel. The berms must be tall enough so the bed level in the central portion of the channel at all stages remains below the average bed level. To ensure that this is accomplished, the flow depth on the berms, d_v, must, at all stages, be less than the average flow depth in the channel, d_o.

The relationship between width and height of the berms and the increase in depth in the central portion of the channel is obtained by assuming conservation of conveyance (and constant slope and resistance). Assuming that the two berms will have the same width, δ_v, and same top elevation, $d_o - d_v$, above average bed level, and applying Manning's equation, conservation of conveyance yields

$$2A_vR_v^{2/3} + A_cR_c^{2/3} = A_oR_o^{2/3}$$

in which subscript c refers to the central portion of the channel. From this relationship, the average depth in the central portion is obtained as

$$d_c \approx \left(\frac{b}{\delta_c}d_o^{5/3} - \frac{2\delta_v}{\delta_c}d_v^{5/3}\right)^{3/5}$$

in which δ_c is the width of the central portion of the channel ($\delta_c = b - 2\delta_v$).

A reasonable height of the berm will be 0.2 to −0.3 times flow depth and the width of the berm 10% to 20% of channel width at design stage. By creating an 0.6-m-tall, 8-m-wide berm along each side of the channel, the depth of the central portion will be

$$d_c \approx \left[\frac{(50)}{(34)}(2)^{5/3} - \frac{(2)(8)}{(34)}(1.4)^{5/3}\right]^{3/5} = 2.3 \text{ m}$$

This should be sufficient to ensure that the river maintains a central approach to the bridge.

Vane height must be at least the height of the berm (i.e., 0.2 to 0.3 times flow depth). Two designs are discussed subsequently.

Design 1:

If the vane height is selected to be $H = 0.3d_o = 0.6$ m, the lateral spacing between the vanes should be of the order of $\delta_n = 3H = 1.8$ m or less. With $\delta_n = 1.8$ m, each array must contain four vanes. The vane-to-bank distance will then be $\delta_b = (8) - (3)(1.8) = 2.6$ m, which is acceptable. This distance should not exceed about $4H$.

Vane length and angle of attack are selected to be $L = 2$ m (so that $H/L = 0.3$) and 20 degrees, to enable use of graphs. With a 0.6-m-tall vane, the distance from design water level to top of vane will be

$$T = 2 - 0.6 = 1.4 \text{ m}$$

yielding a relative submergence of

$$\frac{T}{d_o} = \frac{1.4}{2} = 0.7$$

Entering Fig. 2-23 with $\mathbf{F}_D = 15.6$, $m = 4$, $T/d_o = 0.7$, and $b/r = 0$ yields for a four-vane array a maximum increase in bed level given by

$$\frac{d_o - d_v}{d_o} = 0.3$$

$$d_o - d_v = (0.3)(2) = 0.6 \text{ m}$$

Hence, at the bank the berms will be as high as the vanes. As seen in Fig. 2-23, this result is obtained for a streamwise spacing of the vane arrays of $\delta_s = 30H = 18$ m. The design is shown in Fig. 4-2.

Design 2:

If vane size is increased to $H = 1$ m and $L = 3$ m so that $T/d_o = 0.5$ and $H/L = 0.3$, and $\alpha = 20$ degrees as before, then it is sufficient to use only two vanes per array. The lateral spacing would be $\delta_n = 3H = 3$ m, and the vane-to-bank distance $\delta_b = (8) - (2)(3) = 2$ m.

Entering Fig. 2-23 with $\mathbf{F}_D = 15.6$, $m = 4$, $T/d_o = 0.5$, and $b/r = 0$ yields a maximum increase in bed level given by

$$\frac{d_o - d_v}{d_o} = 0.32$$

$$d_o - d_v = (0.32)(2) = 0.64 \text{ m}$$

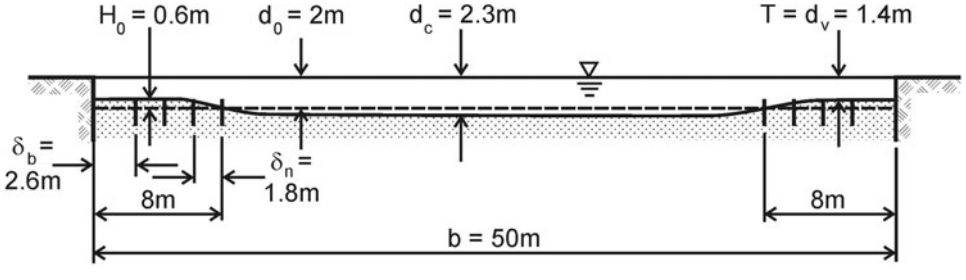

Figure 4-2. Design 1 for stabilizing the river bed.

Table 4-3. Specifications for design alternatives 1 and 2.

Item	*Alternative 1*	*Alternative 2*
Vane height, H (m)	0.6	1.0
Vane length, L (m)	2.0	3.0
Vane angle of attack, α (degrees)	20	20
Number of vanes per array, N	4	2
Vane submergence, T (m)	1.4	1.0
Lateral vane spacing, δ_n (m)	1.8	3.0
Longitudinal vane spacing, δ_s (m)	18	30
Vane-to-bank distance, δ_b (m)	2.6	2.0
Height of berms, $d_o - d_v$ (m)	0.6	0.64

As seen in Fig. 2-23, this result is obtained with a longitudinal spacing of the vane arrays of $\delta_s = 30H = 30$ m.

Hence, in Design 2, at the bank the berms will now be about two-thirds the height of the vanes. The larger vanes will create slightly higher berms and fewer vanes will be needed. The two design alternatives are summarized in Table 4-3.

To obtain a fully developed berm at the bridge crossing, there must be at least three vane arrays on each side of the channel upstream from the bridge. The distance upstream from the bridge to the most downstream array should not exceed about $30H$.

Final step is the estimate of the impact on overall channel stability. Best indicator is the vane-induced increase in water-surface slope, estimated with Eq. 2-14.

4.4 Stabilization of Compound Channel

A vane system is to be designed to maintain a compound channel to enable navigation and/or flood-flow conveyance. Assume that the channel is 200 m wide. At low flow, the average depth is 3 m; however, large dunes cause the depth to be reduced locally to 2 m, which is insufficient for navigation and for efficient flood-flow conveyance. The vane system is to be designed to create and maintain a low-flow depth of 4 m over a 100-m-wide central portion of the channel.

At design flow, the average depth and slope are $d_o = 4$ m and $S = 0.00038$. Design discharge is $Q = 960$ m^3/s. The bed material is sand with a median grain diameter of $D = 0.6$ mm.

Average velocity at design flow is:

$$u_o = \frac{Q}{bd_o} = \frac{(960)}{(200)(4)} = 1.2 \text{ m/s}$$

The channel's resistance parameter is:

$$m = \frac{\kappa u_o}{\sqrt{gSd_o}} = \frac{(0.4)(1.2)}{\sqrt{(9.81)(0.00038)(4)}} = 4.0$$

This m-value corresponds to a Darcy-Weisbach friction factor of $f = 8\kappa^2/m^2 = 0.08$ and a Manning's number of $n = 0.040$.

The sediment Froude number is:

$$\mathbf{F}_D = \frac{u_o}{\sqrt{gD}} = \frac{(1.2)}{\sqrt{(9.81)(0.6\times10^{-3})}} = 15.6$$

and the channel's width–radius ratio $b/r = 0.0$.

The channel's depth–width ratio is $d_o/b = (4)/(200) = 0.02$, which is small enough that this parameter does not play a role.

The height of berm required to achieve a 4-m-deep, 100-m-wide low-flow channel is estimated using the equation for conservation of convergence (same equation as in previous example):

$$2A_v R_v^{2/3} + A_c R_c^{2/3} = A_o R_o^{2/3}$$

which yields

$$d_v \approx \left(\frac{b}{2\delta_v} d_o^{5/3} - \frac{\delta_c}{2\delta_v} d_c^{5/3} \right)^{3/5}$$

Substituting $b = 200$ m, $\delta_v = (200 - 100)/2 = 50$ m, $d_c = 5$ m, and $d_o = 4$ m yields

$$d_v \approx \left[\frac{(200)}{(100)}(4)^{5/3} - \frac{(100)}{(100)}(5)^{5/3} \right]^{3/5} = 2.8 \text{ m}$$

That is, a 1.2-m-tall, 50-m-wide berm along each side of the channel will achieve the goal.

By selecting a vane height of $H = 1.2$ m, the distance from design water level to top of vane will be $T = 4 - 1.2 = 2.8$ m, and relative submergence $T/d_o = 2.8/4 = 0.7$. Figure 2-23 shows that when $\mathbf{F}_D = 15.6$, $m = 4$, and $N \geq 4$, maximum increase in bed level will be given by

$$\frac{d_o - d_v}{d_o} = 1.0\left(1 - \frac{T}{d_o}\right)$$

$$d_v = 2.8 \text{ m}$$

That is, the berms will be as high as the vanes, as desired.

This result is obtained with a lateral and longitudinal spacing of the vanes of $\delta_n = 3H = 3.6$ m and $\delta_s = 30H = 36$ m, and with $\alpha = 20$ degrees, and arrays of four or more vanes. Hence, the goal is achieved with a vane system consisting of 50-m-long arrays on each side of the channel with 1.2-m-tall, 3.6-m-long vanes in each array, and a longitudinal distance between the arrays of no more than 36 m. The design is shown in Fig. 4-3.

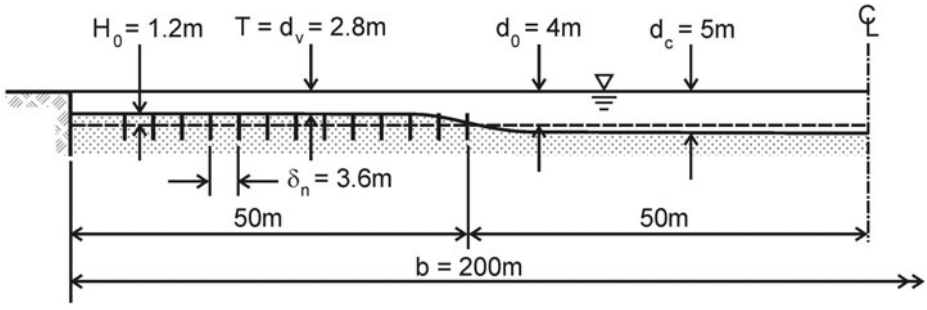

Figure 4-3. Design for stabilizing a compound channel.

In the design and maintenance of a compound channel of this magnitude, it is important that channel stability be maintained. This requires (a) an estimate of the vane systems' impact on the water-surface slope (Eq. 2-14); (b) an analysis of upstream and downstream channel characteristics, including plan form; and (c) construction of stable transition sections upstream and downstream of the stabilized reach.

4.5 Sediment Control at Diversion/Water Intake

A system of submerged vanes is to be designed to prevent or reduce sediment entrainment into a water intake located on the bank of a straight 200-m-wide alluvial channel. Due to aggradation over a period of time, the channel bed in front of the intake is now, on average, at the sill elevation of the intake, and bed sediment is being entrained on a regular basis.

Figure 1-15 shows a schematic of the flow situation. The design objective and variables are described in Section 2.3.3.

The intake opening is 20 m wide and the face of the intake is aligned with the bank of the river. The intake sill is at elevation 95 m. Intake discharge is 10 m^3/s. At the intake, the river discharge varies between 720 m^3/s at low flow and 1,600 m^3/s at high flow. The corresponding variation in water level is from elevation 98 m to 100 m. The slope of the river is 0.00050. The bed material is sand with a median grain diameter of $D = 0.5$ mm.

The solution strategy consists of (a) defining the flow and channel characteristics; (b) determining the effectiveness of alternative submerged vane designs; and (c) evaluating whether a skimming wall is necessary and/or feasible.

Average velocity in the river at low flow and high flow, respectively, is:

$$u_o = \frac{Q}{bd_o} = \frac{(720)}{(200)(3)} = 1.2 \text{ m/s}$$

$$u_o = \frac{Q}{bd_o} = \frac{(1{,}600)}{(200)(5)} = 1.6 \text{ m/s}$$

The channel's resistance parameter at low flow and high flow, respectively, is:

$$m = \frac{\kappa u_o}{\sqrt{gSd_o}} = \frac{(0.4)(1.2)}{\sqrt{(9.81)(0.0005)(3)}} = 4.0$$

$$m = \frac{\kappa u_o}{\sqrt{gSd_o}} = \frac{(0.4)(1.6)}{\sqrt{(9.81)(0.0005)(5)}} = 4.1$$

These values correspond to a Manning number of about 0.038.

The sediment Froude numbers are:

$$\mathbf{F}_D = \frac{u_o}{\sqrt{gD}} = \frac{(1.2)}{\sqrt{(9.81)(0.5\times10^{-3})}} = 17.1$$

$$\mathbf{F}_D = \frac{u_o}{\sqrt{gD}} = \frac{(1.6)}{\sqrt{(9.81)(0.5\times10^{-3})}} = 22.8$$

and the channel's width-radius ratio is:

$$\frac{b}{r} = 0.0$$

The channel's depth–width ratio ranges from d_o/b = (3)/(200) = 0.015 to d_o/b = (5)/(200) = 0.025, both of which are small enough that this parameter does not play a role.

The location of the stream surface that separates the flow into the intake from the flow continuing downstream is determined by Eq. 2-33, at low flow:

$$b_s = b\frac{Q_i}{Q} = (200)\left(\frac{10}{720}\right) = 2.78 \text{ m}$$

and at high flow:

$$b_s = b\frac{Q_i}{Q} = (200)\left(\frac{10}{1600}\right) = 1.25 \text{ m}$$

The vanes should be located well beyond this stream surface to ensure that the flow in the near-shore channel can not only provide the necessary flow into the intake but can also transport the sediment in the channel past the intake.

The vane height should be selected such that the vanes are effective over the entire range of water depths (i.e., for water depths ranging from 3 m to 5 m). The range of feasible vane heights is (see the idealization in Fig. 4-4):

$$1.00 \text{ m} \le H \le 1.50 \text{ m}$$

For H = 1 m, the T/d_o range is:

$$0.67 \le \frac{T}{d_o} \le 0.80$$

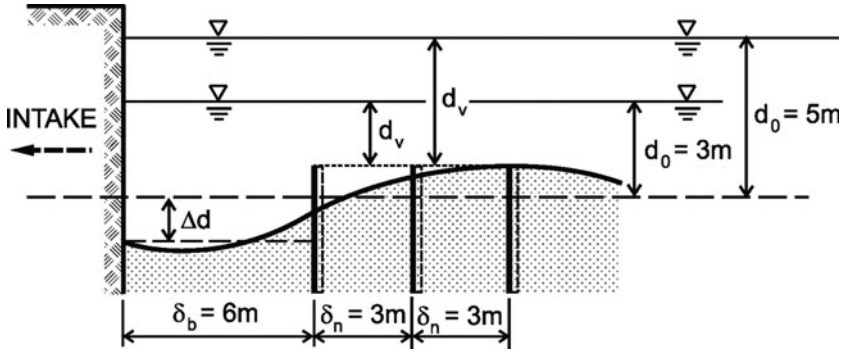

Figure 4-4. Schematic showing vane-induced bed-level changes just upstream of the intake.

For $H = 1.5$ m, the T/d_o range is:

$$0.50 \le \frac{T}{d_o} \le 0.70$$

Figure 2-23 shows that with these T/d_o values, and with $m = 4$ and $\mathbf{F}_D \ge 17$, a three-vane array system with $\delta_n = 3$ m, $\delta_s = 15$ m, and $\delta_b = 6$ m can create a local increase in bed level by as much as the vane height:

$$\frac{d_o - d_v}{d_o} = 1 - \frac{T}{d_o} = \frac{H}{d_o}$$

Hence, if a 1.5-m tall-vane is selected, the bed level in the vane field will increase by up to 1.5 m; if a 1-m-tall vane is selected, the bed level in the vane field will increase by up to 1 m. The bed change will take the form shown schematically in Fig. 4-4.

Table 4-4 shows the estimated maximum bed-level changes that the two alternative vane systems can create at the sill along the face of the intake. The estimates are made using Eq. 3-4 and the idealization shown in Fig. 4-4.

The corresponding flow rates in the near-shore channel are estimated using Manning's equation and the idealized section in Fig. 4-4. At low flow, with a three-vane array system of 1-m-tall vanes, the estimate is:

$$Q_b = \frac{1}{n_b} A_b R_b^{2/3} S^{1/2} = \frac{1}{0.038}(6)(4.3)\left[\frac{(6)(4.3)}{6 + 4.3 + 2.3}\right]^{2/3}(0.0005)^{1/2} = 24.5 \text{ m}^3/\text{s}$$

Table 4-4. Estimated maximum depth increase in near-shore channel just upstream of intake, Δd.

	H = 1.0 m	*H = 1.5 m*
Low flow (d_o = 3 m)	1.3 m	1.8 m
High flow (d_o = 5 m)	1.5 m	2.3 m

Table 4-5. Estimated discharge in near-shore channel just upstream of intake, Q_b.

	H = 1.0 m	*H = 1.5 m*
Low flow (d_o = 3 m)	24.5 m^3/s	27.3 m^3/s
High flow (d_o = 5 m)	43.5 m^3/s	48.3 m^3/s

Values for all flow and vane combinations are shown in Table 4-5.

The flow in the near-shore channel decreases along the face of the intake because of the withdrawal into the intake. At the downstream end of the intake, the flow rate in the near-shore channel is reduced by Q_i = 10 m^3/s. At low flow, with a three-vane array system of 1-m-tall vanes, the bed level at this point in the channel is increased by an estimated

$$\Delta h = \frac{Q_i}{Q_b} d_b = \frac{10}{24.5} \times 4.3 = 1.8 \text{ m}$$

Values for all flow and vane combinations are listed in Table 4-6.

By comparing Tables 4-4 and 4-6, it is seen that a three-vane array system with 1-m-tall vanes is not expected to prevent sediment from being drawn into the intake. At low flow, the vanes can lower the bed elevation by about 1.3 m upstream before the intake. However, due to the withdrawal, the bed elevation at the downstream end of the intake opening will likely rise above the sill elevation (Δh = 1.8 m, which is greater than Δd = 1.3 m).

At high flow, the 1-m-tall vanes may lower the bed elevation about 1.5 m just upstream of the intake, but the bed level is expected to rise 1.5 m by the downstream end of the intake.

The three-vane array system with 1.5-m-tall vanes is expected to prevent sediment withdrawal at all river stages, although barely at low flow.

Thus, if vane height is limited to 1 m (for example, due to navigation considerations), the vane system should be supplemented with a skimming wall. Otherwise, the vanes in the vane system would have to be 1.5 m tall. With 1.5-m-tall vanes, a skimming wall would not be necessary.

If the skimming wall solution is selected, the height of the skimming wall should be the same as the vane height (i.e., 1 m as measured from the average bed

Table 4-6. Estimated rise in bed elevation in near-shore channel at downstream end of intake, Δh

	H = 1.0 m	*H = 1.5 m*
Low flow (d_o = 3 m)	1.8 m	1.8 m
High flow (d_o = 5 m)	1.5 m	1.5 m

level). In this case, the main function of the vanes, located outside the skimming wall, is to prevent sediment from overflowing the wall. In this case, a two-vane array system will suffice.

Note that the skimming wall should not be so tall that it causes undesirable hydraulics in the intake, such as excessive vorticity and/or hydraulic jumps.

4.6 Stabilization of River Channel Alignment

Figure 4-5 shows a river reach that has braiding tendencies. The objective is to stabilize the reach as a single-thread channel. It is assumed that this objective is also environmentally acceptable and that it will not have negative ecological consequences.

The strategy consists of (a) determining the most stable channel alignment; (b) estimating scour depths where appropriate; and (c) selecting the most appropriate combination of channel-stabilization measures (vanes, dikes, etc.).

A relatively stable reach immediately upstream has the following bank-full (channel-forming) channel characteristics: average width, $b = 75$ m; average depth, $d_o = 3$ m; slope $S = 0.0009$; friction factor $f = 0.06$; and grain size $D = 0.6$ mm.

The channel classification is checked by comparing with Leopold's and Wolman's (1957) data presented in Fig. 2-17. Bank-full velocity is:

$$u_o = \sqrt{\frac{8gSd_o}{f}} = \sqrt{\frac{(8)(9.81)(0.0009)(3)}{0.06}} = 1.88 \text{ m/s}$$

which yields a bank-full (channel forming) discharge of:

$$Q = u_o b d_o = (1.88)(75)(3) = 423 \text{ m}^3/\text{s}$$

According to Fig. 2-17, these values of Q and S place this channel reach at the transition between a braided channel and a meandering channel.

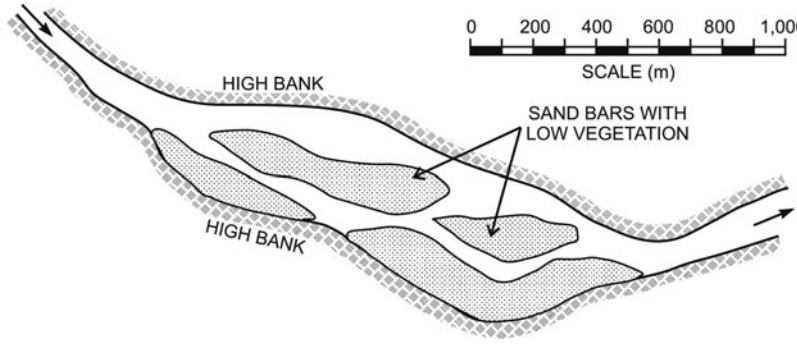

Figure 4-5. Channel reach to be stabilized.

Figure 2-20 is used for estimating the dominant meander-wavelength, λ. Values of $\mathbf{F}_D$, m, and b/d_o are:

$$\mathbf{F}_D = \frac{u_o}{\sqrt{gD}} = \frac{(1.88)}{\sqrt{(9.81)(0.0006)}} = 24.5$$

$$m = \kappa\sqrt{\frac{8}{f}} = (0.4)\sqrt{\frac{8}{0.06}} = 4.6$$

$$\frac{b}{d_o} = \frac{75}{3} = 25$$

Entering Fig. 2-20 with these values yields:

$$\frac{\lambda}{b}\mathbf{F}_D^{-0.4} = 5.9$$

$$\lambda = (5.9)(75)(24.5^{0.4}) = 1{,}591 \text{ m}$$

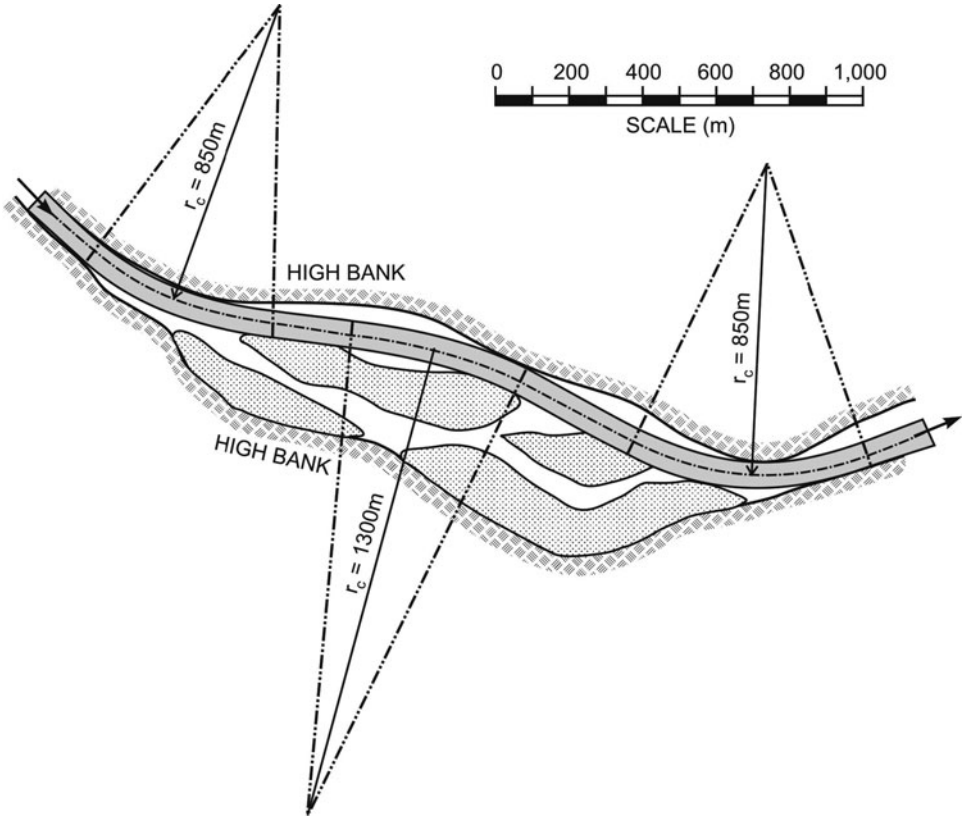

Figure 4-6. Most stable channel alignment through the reach.

Based on this wavelength and considering the surrounding topography, it is reasonable to select a channel alignment as delineated in Fig. 4-6. The new channel consists of three circular arcs of radii, 850 m, 1,300 m, and 850 m, respectively, connected with straight-channel segments.

Maximum scour depth, d_m, and velocity, u_m, are estimated using Eqs. 2-20, 2-28, and 2-29:

$$M = \frac{(2m+1)(m+1)}{m(m+1+2m^2)} = \frac{(10.2)(5.6)}{(4.6)(47.9)} = 0.259$$

$$\frac{d_m}{d_c} = 1 + cM\mathbf{F}_D \frac{b}{r_c} = 1 + (0.8)(0.259)(24.5)\left(\frac{75}{850}\right) = 1.45$$

$$d_m = 4.34 \text{ m}$$

$$\frac{u_m}{u_c} = \sqrt{\frac{d_m}{d_c}} = 1.20$$

$$u_m = 2.26 \text{ m/s}$$

Figure 2-21 shows that a system of 1.34-m-tall vanes (H = 1.34 m) placed in arrays of three and spaced longitudinally a distance of 15H will increase the bed elevation along the outer bank to approximately the elevation of the average bed. The first vane array of each system would be installed at the point of estimated "first outer-bank erosion occurrence," which is determined by calculating the phase shift, φ. Entering Fig. 2-20 yields:

$$\frac{\varphi}{2\pi}\mathbf{F}_D^{0.1} = 0.17$$

$$\frac{\varphi}{2\pi} = 24.5^{-0.1} \times 0.17 = 0.123$$

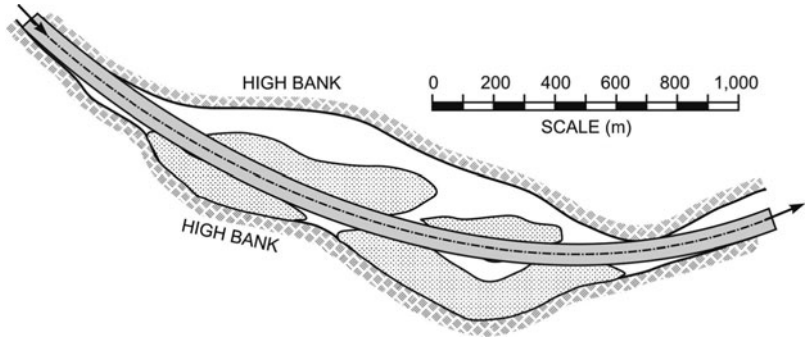

Figure 4-7. Intuitive channel alignment but not consistent with given data.

Thus, the first vane array should be installed at the halfway point between the beginning of the bend and the bend apex (at the apex, $\varphi/2\pi = 0.25$).

The steps of the vane design procedure are similar to those described in Section 4.2.

As mentioned above, the selection of channel alignment must be, to some extent, based on existing high-bank alignment. When the calculated wavelength differs from that fitting in naturally with the existing high-bank alignment, the selected wavelength should obviously be adapted to fit the existing high-bank alignment as much as possible. The alignment shown is the most appropriate for the given high-bank alignment and the calculated wavelength. Had the calculated wavelength been twice that calculated above (if, say, channel width and grain size had had different values), a more appropriate channel alignment fitting with the given high-bank alignment could have been the one shown in Fig. 4-7. In either case, systems of submerged vanes can be used to effectively stabilize and confine the river channel to a single-thread channel.

CHAPTER 5

Field Installations

As mentioned earlier, vanes have been and are being installed in several rivers throughout the world. In the following, select installations are reviewed. Tables 5-1 and 5-2 summarize design objectives and flow conditions at these installations. The basic design parameters are summarized in Table 5-3.

5.1 Stabilization of River Bank

This section describes three installations in sand-bed rivers and one in a gravel-bed river. Four different vane designs are represented.

The first installation described is the East Nishnabotna River (Iowa) installation, which was the first field test conducted with vanes in the United States. This test was conducted prior to or parallel with similar laboratory tests. Although it did not fully benefit from the results of the laboratory tests, the East Nishnabotna field test provided valuable data for the development of the design guidelines. Next, the section describes subsequent field installations in Wapsipinicon River (Iowa) and North Fish Creek (Wisconsin). All three installations are in sand-bed rivers. The section concludes with a description of an installation in a gravel-bed river in Taiwan, China.

5.1.1 Sand-Bed Rivers

East Nishnabotna River, United States

The first vane installation in the United States for stabilizing a river bank was in a bend of the East Nishnabotna River, Iowa. Design, construction, and performance evaluation were described earlier by Odgaard and Mosconi (1987), and parallel laboratory tests by Odgaard and Lee (1984). Figure 5-1 shows three aerial photos of this bend taken in 1972, 1977, and 1982. The bend was approaching U.S. Highway 34 at a rate of 6 to 9 m/year. Figure 1-1 shows bank erosion occurring at 70% of bank-full discharge. The objectives were to (a) design the vane system to stop or reduce the migration of the bend; and (b) obtain field experience for future projects.

Table 5-1. Design objectives for installations reviewed in this chapter.

Objective	*River*	*Sediment size (mm)*
Stabilization of river bank	East Nishnabotna	0.4
	Wapsipinicon	0.5
	North Fish Creek	Broadly mixed
	Feng-Shan Creek	21.2
Stabilization of river bed	West Fork Cedar	0.5
Sediment control at water intake	Cedar, Rock	0.3–0.5
	Waikato	0.5–0.7
	Muskingum	1.5
	Missouri	0.5*
	Kosi	30.0
Channel alignment stabilization	Des Moines	0.7

*Average for the Missouri River reach investigated (four installations).

East Nishnabotna runs through a flood plain consisting of a 1.5- to 4.5-m-thick layer of loess-derived alluvium with about 14% clay, 63% silt, and 23% sand, underlain by Pennsylvanian shale. The drainage area above the bend is 2,314 km^2, and the average discharge and suspended load through the bend 10.6 m^3/s and 862,000 metric tons/yr, respectively.

Cross sections of the river bend were surveyed October 6–7, 1983, and April 30–May 2, 1984 to define the channel geometry at two different times for two different flow rates. Also, detailed velocity measurements and bed material samples were taken. In the first survey (October), the flow rate was about 3.3 m^3/s; in the second, about 100 to 120 m^3/s (60%–70% of bank-full discharge). A report of the

Table 5-2. Design flow conditions for installations reviewed.

River	*Discharge (m^3/s)*	*Width (m)*	*Depth (m)*	*Velocity (m/s)*	*Channel slope*
East Nishnabotna	180	60	2.4	1.3	0.00065–0.00070
Wapsipinicon	400	80–100	3.5	1.1–1.4	0.00053
North Fish Creek	26	15	1.4	1.2	0.0070
Feng-Shan Creek	1,500	180	3.7	2.3	0.0015
West Fork Cedar	100	30–40	1.9–2.1	1.2–1.8	0.00049
Cedar	190	100–110	2.2	0.8	0.00050
Rock	230	210	2.7	0.4	0.00011
Waikato	400–970	220	3.4–5.4	0.5–0.8	0.00012
Muskingum	273*	73	6.0	0.6	0.00038
Missouri	600–1,500	200–300	4.6	0.8–1.1	0.0002
Kosi	2,000–8,000	370	2.7–5.0	2.0–4.3	0.0013–0.0025
Des Moines	900	176	4.8	1.1	0.00041

*Average discharge November through May.

Table 5-3. Design parameters for installations reviewed.

River	*Resistance parameter, m*	*Sediment Froude number,* $\mathbf{F}_D$	*Number of vanes (N)*	*Submergence of vanes,* T/d_o	*Height of vanes, H(m)*	*Length of vanes, L(m)*
East Nishnabotna	4	20	77	1.0	0.9	3.7
Wapsipinicon	3–4	16–20	28	0.7	0.9	2.7
North Fish Creek	1.5	—	45****	0.6	0.4	0.9
Feng-Shan Creek	4.5	5.0	16	0.4–0.6	1.6–2.6	3.2–5.2
West Fork Cedar	4	13	12	0.7	0.6	3.7
Cedar	3	15	9	0.6	0.9	3.1
Rock	3	7.4	40	0.7	0.9***	2.7
Waikato	3.2–4.0	6.5–11	26	0.7–0.8	1.0–1.5**	7.0
Muskingum	2	5.1	13	0.5	5.0–5.3	3.0
Missouri	3.4–4.6	11–16	58*****	0.7–0.8	1.0–2.1	0.9–3.0
Kosi	4.3–5.0	3.7–7.9	35	0.5–0.8	1.2–1.5	6.0
Des Moines	3.1	10.1	8*			

*Recommended.
**Physical height of vane = 2.0 m.
***Physical height of vane = 1.8 m.
****At each of two sites.
*****Total at four sites.

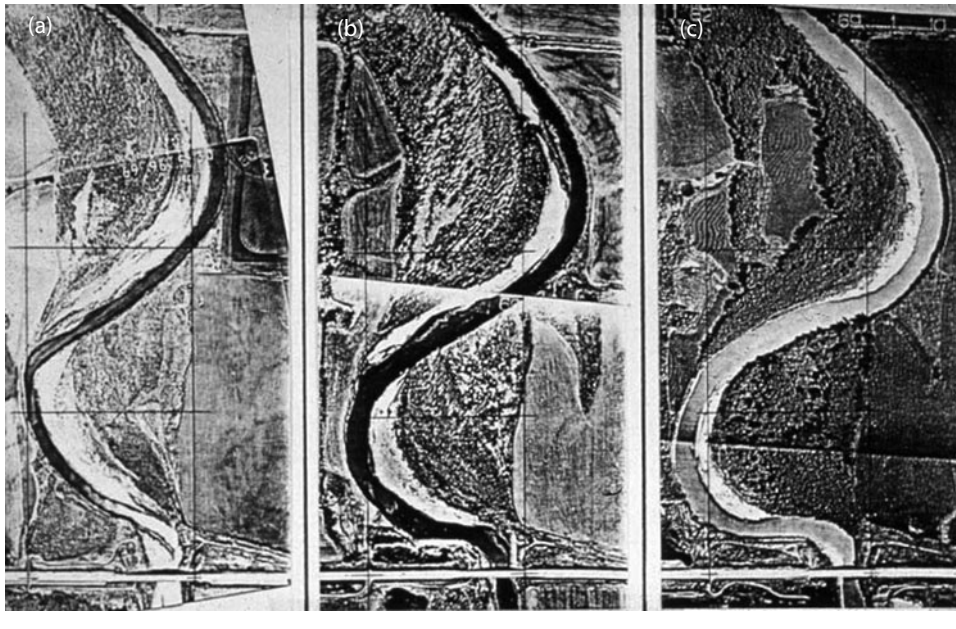

Figure 5-1. Aerial photos of East Nishabotna River, Iowa. (a) 1972; (b) 1977; (c) 1982. *Source:* Odgaard and Mosconi (1987), ASCE.

data was given by Odgaard and Lee (1984). Longitudinal slope of the water surface through the bend was measured to be $S = 0.00065–0.00070$. Median grain diameter and geometric standard deviation of the bed material were 0.45 mm and 2.0, respectively.

Design calculations were based on a torque balance (i.e., Eqs. 2-30 and 2-31). For details, readers are referred to Odgaard and Mosconi (1987). A critical design parameter, vane height, H, was selected based on the following considerations: For vanes to function optimally, H must be less than about half the water depth at the flow rates at which bank erosion occurs. In the East Nishnabotna bend, bank erosion occurs when the flow rate is greater than about 60 m^3/s. [Also, at 60 m^3/s, the maximum (near-bank) velocity exceeds 1.1 m/s, which is the limiting velocity recommended by the U.S. Bureau of Reclamation for the design of a stable, firm loam channel carrying water with colloidal silts.] Because the 60-m^3/s average water depth is 1.3 to 1.5 m, the vane height should not exceed 0.7 to −0.8 m. On the other hand, the vanes must perform nearly optimally at bank-full stage, at which the average depth is up to 3 m at some sections, thus requiring a vane height of about 1 m. As a compromise, a vane height of 0.91 m was selected. The low-flow (3.3 m^3/s) survey showed the bed level along the outer bank to be, on the average, 0.65 m below the low-flow water level; therefore, being 0.91 m high and resting on the bed 0.65 m below the surface, the top edge of the vane should be 0.25 m above the low-flow water level.

According to the guidelines that were being established in the laboratory studies at the time, the vane should be about four times as long as it is high. A 0.91-m-high vane should then be 3.66 m long. The laboratory studies indicated that vanes longer than four times their height tend to generate two (or more) secondary flow cells downstream rather than one, and thus are less effective. The laboratory tests also indicated that the optimum angle of attack, α, is generally about 20 degrees. In view of these considerations, the design was for a 0.91-m-high, 3.66-m-long vane at $\alpha = 20$ degrees.

Figure 5-2 shows the layout of the vane system and details of the vane design. Each vane consists of three creosoted planks, 7.6 cm × 30.5 cm × 3.66 m, held together in a vertical position by two HP 8 × 36 steel bearing piles driven into the streambed (about 1.5 m into a shale layer underlying a 2- to 4-m layer of sand). The planks were fastened to the piles by straps (135 cm × 15 cm × 1 cm bent plates) and were prevented from floating by anchor plates on the flanges of the H-piles.

The vane system was installed at low flow between July 26 and September 4, 1985. Except for three to four days, the water depth throughout was less than 0.5 m during this period. The piles were driven starting at the upstream end of the bend. In each array, the upstream piles were driven at the given distances from the bankline. The downstream piles in each array were driven 4.22 m from the upstream piles and 0.9 m closer to the bank, yielding an angle with the mean flow direction of 12.2 degrees. Accounting for the skew of the velocity profile due to the centrifugal acceleration, this angle would make the near-bed flow approach the vane at about 20 degrees. The direction of the mean flow was determined by

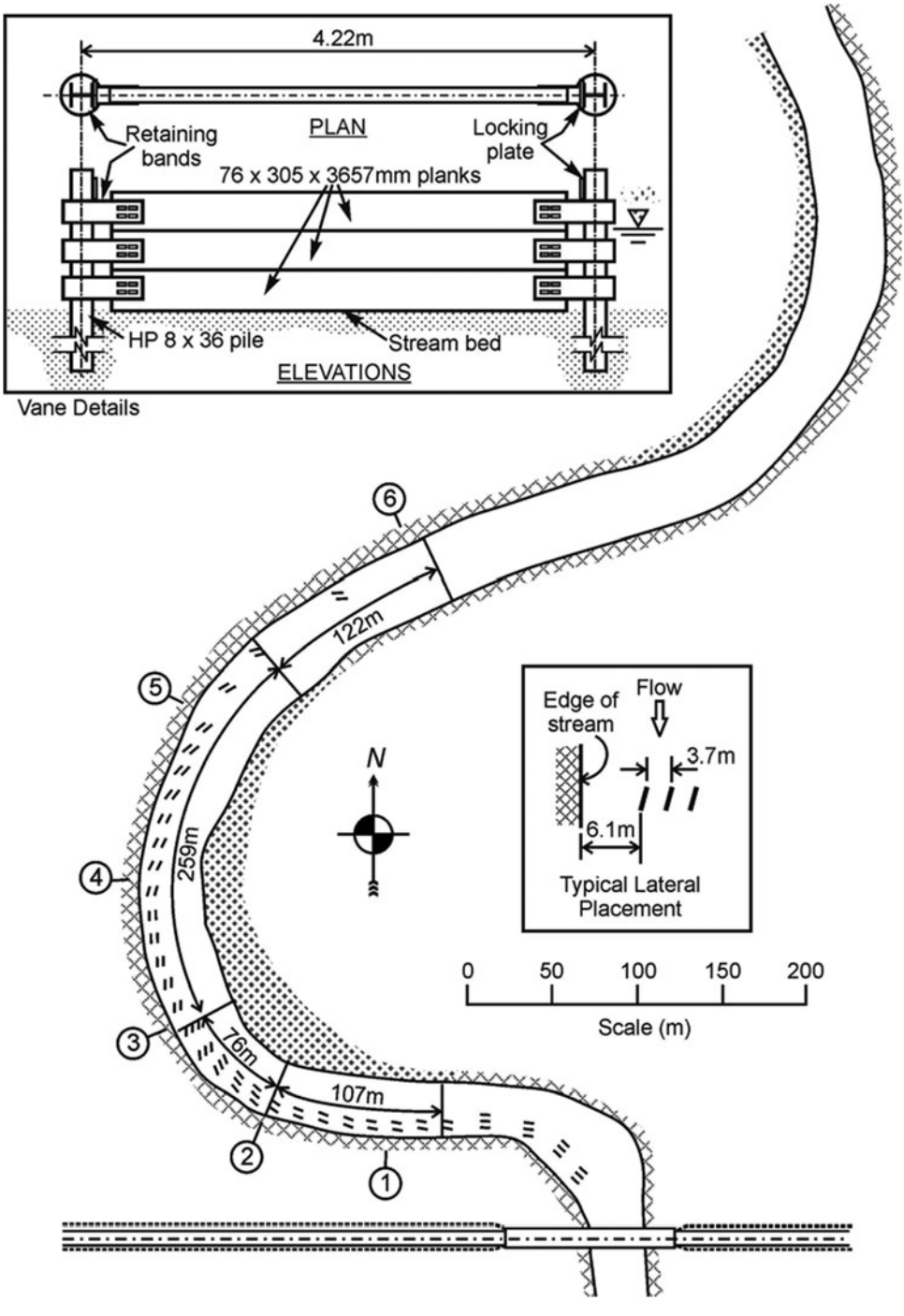

Figure 5-2. Layout of vane system in the East Nishnabotna River bend.
Source: Odgaard and Mosconi (1987), ASCE.

surface floats. In each array, the pile nearest the bank was driven 6.1 m, or twice the bank-full flow depth, from the low-flow edge of the water. This vane-to-bank distance was chosen because it scales the vane-to-bank distance used in most of the laboratory tests. (In retrospect, the vane-to-bank distance should probably have been somewhat less than 6.1 m along part of the bank, as discussed later.) After completion of the pile-driving on August 22, the planks were provided with straps and lowered in place between the piles (Fig. 5-3). The system was provided with five can buoys (float collar cans with internal ballast) and marked with the "restricted area" symbol.

The cost of the installation per meter of bank was about half the cost of a rock riprap structure along a comparable reach of the nearby Raccoon River, by Highway 90 [Iowa Department of Transportation Project number FN-90-1(6)-21-25). The Raccoon River riprap embankment was completed just prior to the vane installation in East Nishnabotna.

The vane system was subjected to its first test in the spring of 1986, which was among the wettest on record. From February to June, there were about 22 days in which the daily average discharge exceeded 60 m^3/s (a record exceeded only twice since 1973). The river was ice-covered from mid-December to mid-February, during which period the top of the vanes were exposed. All buoys disappeared during snow melt in February and March, and had to be replaced.

Cross sections were surveyed March 20–21 and May 12–13, 1986, when the discharge was 18% and 58% to 100% of bank-full discharge, respectively. Measurements were taken of stage, flow depth and velocity, surface flow paths, bank retreat, and water surface slope. A detailed report was given by Odgaard and Mosconi (1987). Figure 5-4 shows the velocity and depth distributions at Section 4

Figure 5-3. Plank with straps being lowered in place between piles.

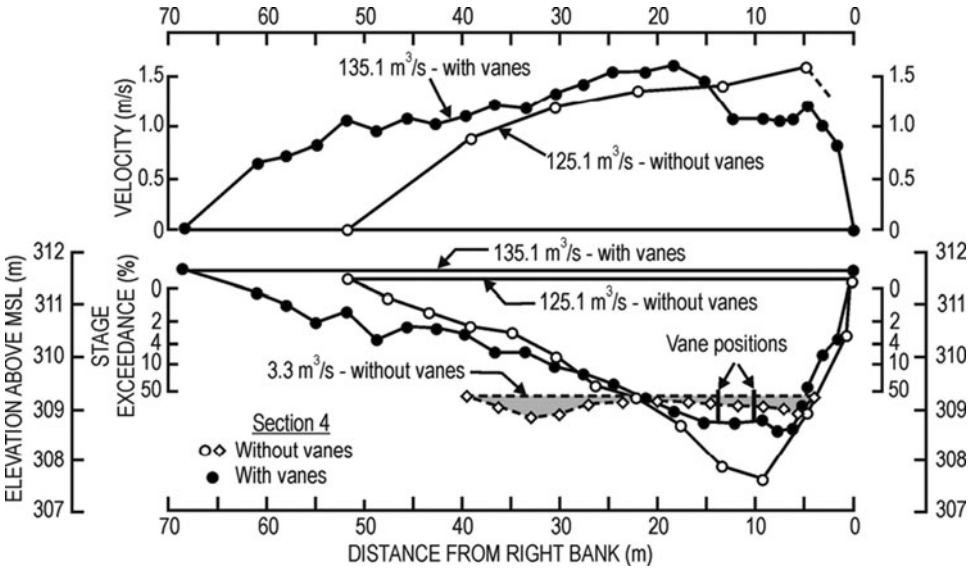

Figure 5-4. Section 4 measured before, at $Q = 3.3$ m^3/s and $Q = 125.1$ m^3/s, and after installation of vanes, at $Q = 135.1$ m^3/s. *Source:* Odgaard and Mosconi (1987), ASCE.

(at midbend) measured during the high-flow event (May 13) when the discharge was about 135 m^3/s. The pre-vane cross sections are superimposed for comparison, one cross section at 124 m^3/s (about 70% of bank-full discharge), the other at about 3.3 m^3/s. The pre-vane high flow bed profiles in this bend were, essentially, a tilting of the low-flow profile about the high-flow channel centerline. The vane system was installed at low flow in the outer part of the low-flow channel to maintain the low-flow bed elevation there at all stages. In other words, the vanes were to move the high-flow scour holes away from the bank, toward the center of the channel (without changing the cross-sectional area and channel slope). As seen, the vanes were able to accomplish this. Along the outer bank, the vanes were able to maintain the bed at its low-flow elevation and prevent the near-bank scour typical of the pre-vane cross section. Instead of scouring along the outer bank, the flow widened its channel by removing sand from the inside point bar. As seen in Fig. 5-4, there was also a notable improvement in the velocity distributions, which, of course, corresponds with the reduction of the transverse bed slope. The reduction in near-bank velocity was significant. The maximum velocity, which in the pre-vane cross sections generally occurred within a distance of 6 m from the bank, was moved at least 18 m away from the bank at most sections.

In order to directly test the vanes' efficiency in eliminating the secondary flow component, float studies were performed. By releasing 500 plastic balls at Section 3 at distances of 3.3, 6.1, 9.1, 12.1, and 15.2 m from the outer bank, and recording their lateral position at Section 2, 76 m downstream from Section 3, the overall average deflection angle was measured to be less than zero. The floats generally

moved away from the bank. Without vanes, the deflection angle would have been greater than 10 degrees toward the bank. Figure 1-6 (in the Introduction) is a downstream view of the installation at extreme low flow.

As reported in Odgaard and Mosconi (1987), there was no indication that the vane system changed the energy slope, either through the bend or in the channel downstream from the bridge. However, as mentioned in Odgaard and Mosconi, the bend immediately upstream continued to migrate downstream at a rate of 6 to 9 m/year, causing (a) a change in the approach angle to the uppermost vanes in the system, and (b) a reduction of the radius of curvature of the bend and thus a change in the design basis. (This problem was foreseen, and a stabilization of the upstream bend was, in fact, recommended as part of the original design.)

Because of the sensitivity of the design to the approach-flow conditions, the channel segment upstream from the first vanes should have been stabilized to ensure that the approach-flow angle remains constant. This would have been possible in the East Nishnabotna bend because the upstream bend is preceded by a long, straight reach. To ensure that an adverse flanking does not occur, the uppermost vanes in the system should have been installed closer to the bank, and their density should have been greater than the theoretical. The near-bank vanes in the uppermost array could possibly connect with the bank. Today (2008) the uppermost arrays are no longer providing bank protection. The downstream vanes continue to provide protection of the bank along the highway and at the bridge.

Wapsipinicon River, United States

The Wapsipinicon River meanders across northeastern Iowa to the Mississippi River. One particular bend in Jones County was moving at an average rate of 3 m per year toward a county road, and ultimately endangering a bridge structure. The bend is in the upper left corner of the aerial photo in Fig. 5-5. Figure 5-6 is a downstream view of the eroding bank. The bank height is 3.5 m and bank-full flow is about 400 m^3/s. The county decided to protect only the upstream third of the bend, which was the critical section relative to the road. The county's intent was to continue the stabilization, if required, in the future, thereby minimizing the initial cost.

A system of 28 vanes was installed along approximately 100 m of the bend in May, 1988 (Odgaard and DeWitt 1989; DeWitt and Odgaard 1991). The vanes were fabricated of reinforced concrete (Fig. 5-7) and each mounted on a single H-pile, which was driven approximately 4.6 m into the streambed (Fig. 5-8). The vanes were oriented at approximately 20 degrees with the direction of flow at bank-full flow. They were installed at low flow (1 m or less water depth) by county crews (Figs. 5-8, 5-9, and 5-10).

The connection arrangement between piling and vanes on this project involved bolting the vane to plates welded to the H-pile. Although this is an effective connection, it is time-consuming in that the pile has to be carefully oriented with the stream flow and some or all of the bolts are placed by feel under water (Fig. 5-10). In other than shallow water, this type of connection must be made by divers. Experience with this and subsequent projects resulted in development of a

Figure 5-5. 1988 aerial view of Wapsipinicon River, Iowa. Courtesy of Robert DeWitt, River Engineering International.

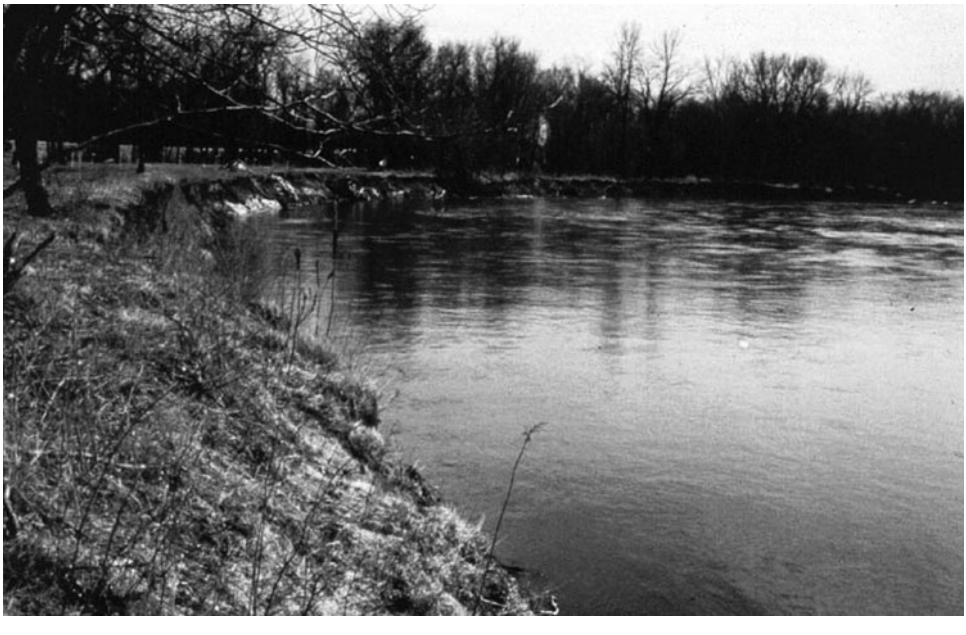

Figure 5-6. View downstream in the Wapsipinicon River, showing bank erosion along left bank. Courtesy of Robert DeWitt, River Engineering International.

Figure 5-7. Delivery of vanes to the Wapsipinicon site, summer, 1988. Courtesy of Robert DeWitt, River Engineering International.

Figure 5-8. Driving of H-piles, summer, 1988. Courtesy of Robert DeWitt, River Engineering International.

Figure 5-9. Vane is lowered in place on top of pile, summer, 1988.
Source: Odgaard and Abad (2007), ASCE.

Figure 5-10. Vane is connected to pile, summer, 1988. Courtesy of Robert DeWitt, River Engineering International.

connection detail consisting of a pipe section at the top of the pile and a sleeved vane. The piling is driven to the design elevation, and the vane is slipped over the pipe connection and locked into the proper orientation. Utilizing guides that extend from the top of the pile to above water surface, this arrangement has been used for installation in up to 3 m of water.

The years 1988 and 1989 were dry years with no threats of further erosion. 1990 was a very wet year with significant flooding on the Wapsipinicon. The portion of the bend protected with vanes showed no movement and, in fact, exhibited evidence of aggradation at the toe of the outer bank (Fig. 5-11).

The portion of bank that was unprotected receded as much as 13 m during the 1990 heavy flows, as indicated in Fig. 5-12. Top of bank movement actually started in the last 12 m of the protected portion. It appeared that movement in this section resulted from the substantial movement of the bank farther downstream and the associated weakening of the adjacent bank. Subsequently, the county installed additional vanes downstream to protect the entire bankline through the apex of the curve. During the 1993 flood, the flood plain was under water for about two months. Figure 5-13, taken shortly after the 1993 flood, shows that the vane system kept the bank in place. The county has since installed vanes to protect banks of the Maquoketa River. Both installations are still (2007) performing satisfactorily.

North Fish Creek, United States

A unique field test was conducted in North Fish Creek, Wisconsin from 2000 to 2003 in a joint venture between the Wisconsin Department of Natural Resources,

Figure 5-11. Wapsipinicon River bend at low flow, May 10, 1990, about two years after installation of vanes. *Source:* Odgaard and Abad (2007), ASCE.

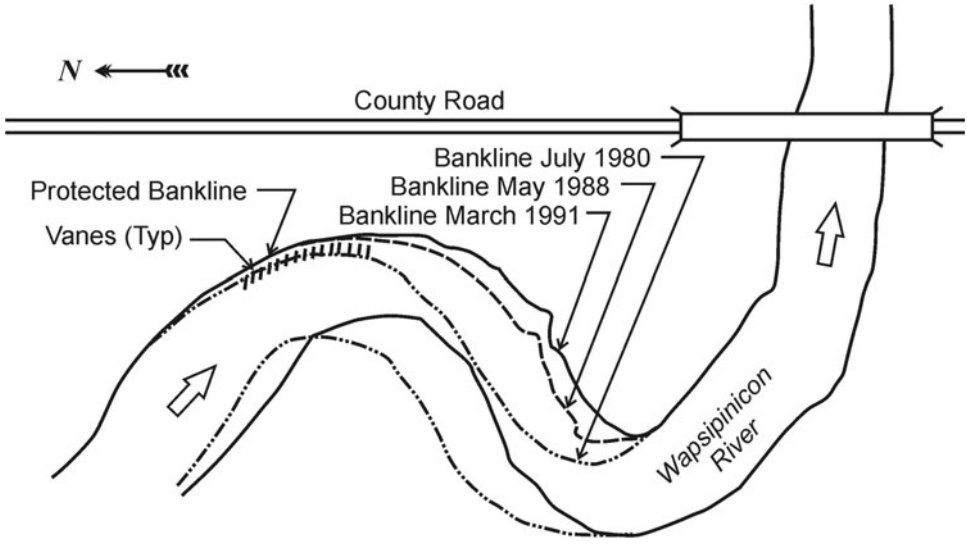

Figure 5-12. Plan of the Wapsipinicon River bend, showing vane system and sequential bank lines. *Source:* DeWitt and Odgaard (1991), ASCE.

the U.S. Geological Survey, and the University of Wisconsin (Fitzpatrick et al. 2005). Submerged vanes were installed to curb the erosion of bluffs along two bends of the creek, Sites 16.4 and 12.2. North Fish Creek is a Wisconsin tributary to Lake Superior that transports a relatively large amount of sediment, about 17,000 tons per year, originating from seventeen 20- to 50-m-tall bluffs like the

Figure 5-13. Wapsipinicon River bend after the 1993 flood. So far (2007), the bank has shown no movement. Courtesy of Robert DeWitt, River Engineering International.

one shown in Fig. 5-14. The bed material in the main channel is a mixture of cobble, gravel, and sand. A photo taken at low flow, Fig. 5-14 also shows one of the vanes at the base of one of the bluffs. At each site a total of 45 vanes were installed in 15 arrays. At Site 16.4, vane height was 0.43 m, about 0.3 times the average bank-full depth as determined from a number of field indicators. Vane length was 0.91 m. Spacings were 0.91 m laterally and 4 to 5 m longitudinally. The innermost vane was placed as close to the bank as possible to ensure that the flow would not cut around the vanes and erode more of the bluff toe. The vane material was 10-mm-thick, white, high-density polyethylene. The vanes were held in place by driving two 19-mm-diameter steel reinforcing bars about 1 m into the streambed and fastening the vanes to the bars with U-bolts. As illustrated in Fig. 5-15, the vanes were installed to capture bank material slumping into the creek and move the thalweg out into the creek, away from the bank.

Channel-cross-section and bluff-erosion surveys were done and stream-flow and stage were measured before, during, and after vane installation to monitor changes in channel morphology and bluff erosion. In April, 2001, about nine months after completion of the vane installation at Site 16.4, a major flood occurred in the creek (recurrence interval of approximately 100 years), peaking at about 100 m^3/s. Large floods also occurred in April and May, 2002 (recurrence in-

Figure 5-14. Downstream view of North Fish Creek at low flow. Submerged vanes protect the toe of the bluff. *Source:* Fitzpatrick et al. (2005), courtesy of U.S. Geological Survey.

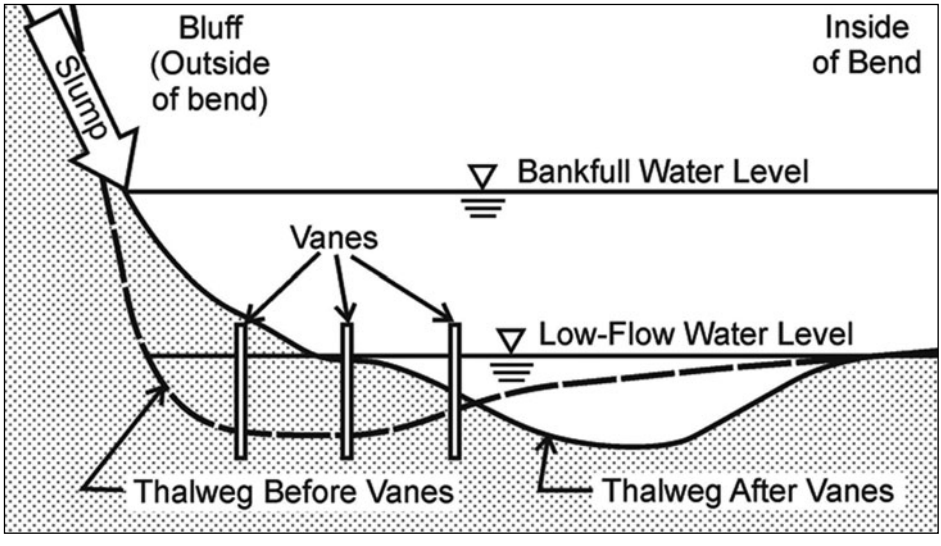

Figure 5-15. Schematic showing changes in channel and thalweg caused by submerged vanes. *Source:* Adapted from Fitzpatrick et al. (2005), courtesy of U.S. Geological Survey.

tervals of approximately 50 years). The vanes at both sites required some maintenance and replacement after the floods. After the April and May, 2002, floods, five near-bank-full or at-bank-full floods occurred (one in October, 2002, and four in April and May, 2003).

The study showed that from 2000 to 2003, the vanes effectively moved the channel away from the base of the bluffs and toward the point bar, allowing sediment to deposit at the base of the bluff. Much of the change in channel morphology resulted from the April, 2001, flood. Over the monitoring period (2000–2003), the 110-m reach at Site 16.4 had a net gain of 200 m^3 of sediment. Deposition along the base of the bluff was about 300 m^3, mainly through the downstream half of the reach. In contrast, the left-bank or point bar side of the channel, channel streambed, and a mid-channel bar eroded.

5.1.2 Gravel-Bed River

Feng-Shan Creek, Taiwan, China

Feng-Shan Creek is 45 km long and drains an area of 250 km^2. Channel slope is 0.0015 and median diameter of the bed sediment is 21 mm.

Vanes have been installed in three consecutive bends in the downstream reach, in Geokang, Maoerding, and Baidi bends. In Maoerding bend, shown in Fig. 5-16, there are eight vane arrays with two vanes in each array. In the other two bends, there is only one row of vanes, 24 vanes in Geokang bend and 18 in Baidi bend. All three installations are performing as intended.

Figure 5-16. Location of submerged vanes in the Maoerding bend of Feng-Shan Creek, Taiwan. Flow is from right to left. Courtesy of Keh-Chia Yeh, National Chiao Tung University.

Figure 5-17 shows the layout plan of the vanes in Maoerding bend, the first bend to be protected. Here, the channel is 180 m wide and minimum radius of curvature is $r_c = 356$ m. The resistance parameter $m = 4.5$, corresponding to a Manning number of $n = 0.035$. The vane system is designed for a 10-year flood, during which the discharge is 1,500 m^3/s, average depth is 3.68 m, and average velocity is 2.26 m/s. Figure 5-18 is a section view showing the vertical dimensions of the vanes and spacings. Because of extreme erodibility, prior to installation of the vanes the bank was stabilized using gabion baskets. As seen in Fig. 5-18, the inner row of vanes is located 5.5 m from the toe of the gabion structure. The outer row is located 3.7 m farther out in the channel. The vanes are made from 6-m-long sheet piles driven to a depth such that the initial vane height in the outer row is 1.6 m and in the inner row 2.6 m.

Figures 5-19 and 5-20 show the vane system in 2007, one year after installation at extreme low flow. During the year, the vanes were subjected to at least one bank-full flow condition. The vanes have been very effective in building up and maintaining a protective berm along the bank. As seen, the berm is now heavily vegetated. The vegetation developed on the berm provides additional protection of the bank. Figure 5-21 is a close-up of a vane showing the configuration of the sheet piles used in this application.

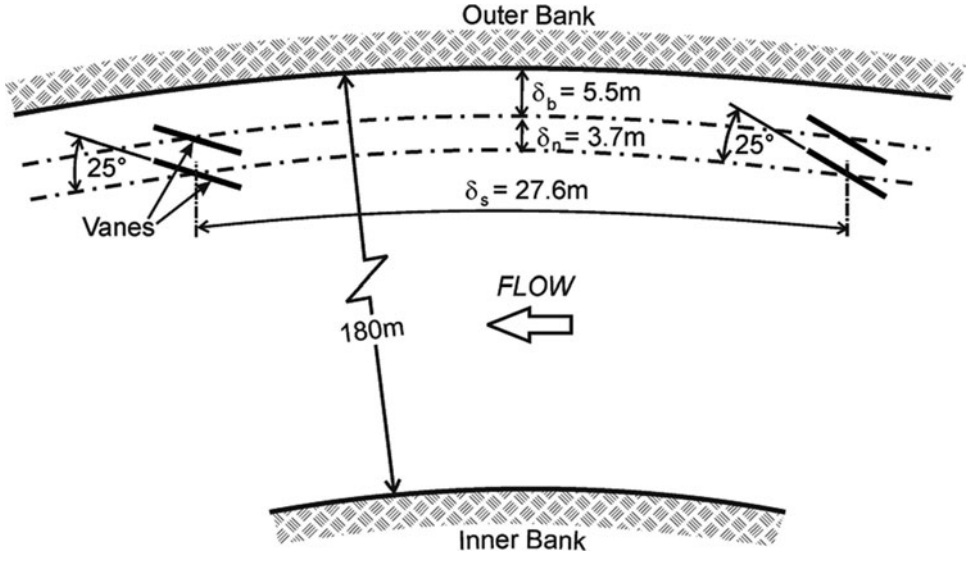

Figure 5-17. Layout of vanes in the Maoerding bend of Feng-Shan Creek. Courtesy of Keh-Chia Yeh, National Chiao Tung University.

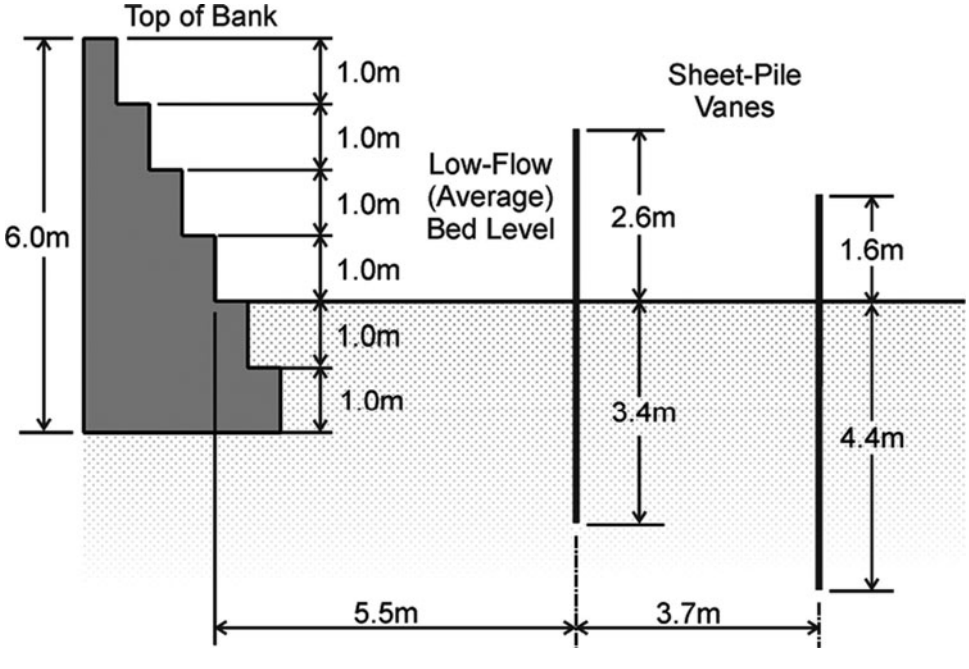

Figure 5-18. Section through vane array in the Maoerding bend, looking upstream. Courtesy of Keh-Chia Yeh, National Chiao Tung University.

Figure 5-19. Upstream view of vane installation in the Maoerding bend, one year after installation, at extreme low flow.

Figure 5-20. Downstream view of vane installation in the Maoerding bend, one year after installation, at extreme low flow.

Figure 5-21. Close-up of vane array in the Maoerding bend, one year after installation, at extreme low flow.

5.2 Stabilization of River Bed/Compound Channel

West Fork Cedar River, United States

The effectiveness of submerged vanes in ameliorating shoaling problems was demonstrated at a highway crossing of the West Fork Cedar River in Butler County, Iowa. The problem at this site developed after a straightening and widening of the river at the time of construction of the bridge (1970). Figure 5-22 shows the excavation plan for the project. The bridge is a 150-m-long, 9-m-wide, six-span, I-beam bridge with the road surface about 5 m above the low-flow streambed. The top width and bank-full depth of the river upstream of the excavation are 30 to 40 m and 1.9 to 2.1 m, respectively. The bed material is sand with a median particle diameter of about 0.5 mm. Annual mean flow in the river is about 14 m^3/s and bank-full flow about 100 m^3/s. A 10-m-wide channel running parallel with the roadway connects the old channel with the new. Aerial photos indicate that the new channel was constructed as shown on the excavation plan. However, the channel parallel with the road was constructed somewhat closer to the roadway than shown on the plan.

By 1984, a considerable portion of the excavation upstream from the bridge had filled in and become vegetated. Figure 5-23(a) shows the 1984 bankline and

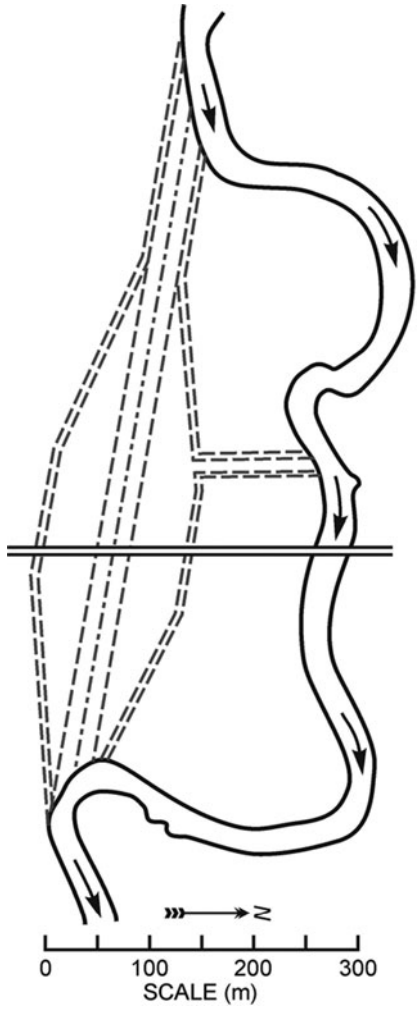

Figure 5-22. Excavation plan for the West Fork Cedar River (Iowa) channel straightening. *Source:* Odgaard and Wang (1991), ASCE.

a sandbar that subsequently developed along the left bank. The sandbar occupied four of the six spans, causing the flow to be thrown toward the right bridge abutment, where it undermined and eroded the bank. Annual dredging was necessary because the sand bar grew in size after each storm. It was clear from aerial photos that the bar formed as part of the river's adjustment to the 1970 channel straightening, which essentially eliminated two meanders and shortened the channel segment by 482 m (from 1,189 m to 707 m). The straightening resulted in a 69% increase in the local channel slope, from 0.00049 to 0.00083.

A system of 12 vanes was installed in the summer of 1984. The layout is shown in Fig. 5-23(b). Each vane consists of vertical sheet piles driven into the streambed and aligned at a 30-degree angle with the main channel. With this angle, the vanes are at about 20 degrees with the 1984 mean flow direction, which is indicated by

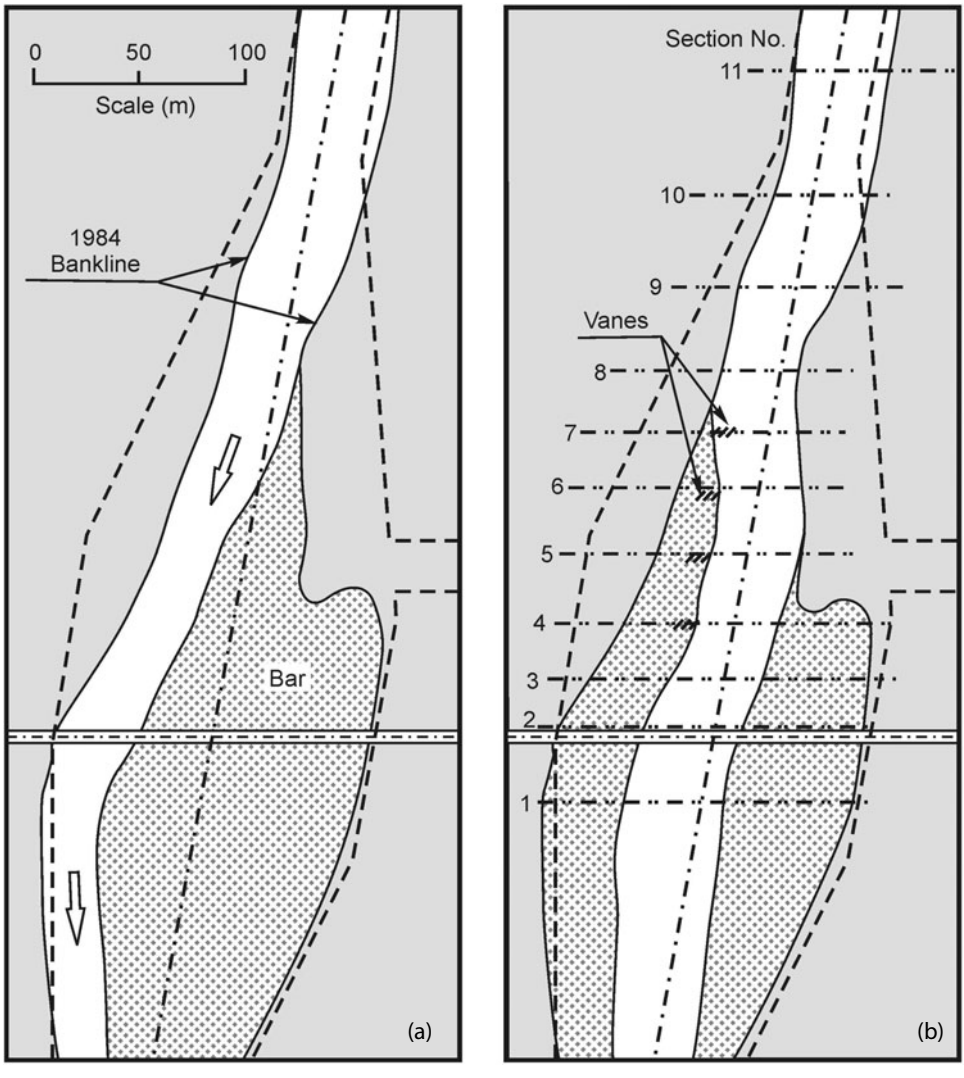

Figure 5-23. Plan of the West Fork Cedar River bridge crossing, (a) prior to vane installation in 1984, and (b) in 1989, five years after vane installation. [Plan (b) shows location of vanes and survey sections.] *Source:* Odgaard and Wang (1991), ASCE.

the arrows in Fig. 5-23(a). Each sheet piling was 3.7 m long, and its top elevation was 0.6 m above the streambed. The vane system was designed to cause flow depth and velocity to decrease along the right bank and increase along the centerline. As seen in Fig. 5-24, the system has accomplished this. A permanent, protective berm now is seen along the bank that was previously eroding (about 450 m). In fact, the vanes are now maintaining a cross-sectional bed profile similar to that designed when the bridge was constructed. Installation cost was $5,000 (in 1984) and, so far, maintenance has not been necessary. Six of the 12 vanes are now permanently covered with sand and vegetation (Fig. 5-25). Figure 5-26 is a photo of the most upstream vane array, which is fully exposed to the flow.

Figure 5-24. Aerial photos of the West Fork Cedar River bridge crossing (left) prior to vane installation in 1984, and (right) in 1989, five years after vane installation. *Source:* Odgaard and Wang (1991), ASCE.

A field survey was conducted on August 22, 1989, to quantify the induced changes in bed topography. The flow in the river was about 0.3 m^3/s on that day. Bed profiles were taken in 10 sections upstream from the bridge and one downstream. The locations of the sections are indicated in Fig. 5-23(b), and the profiles are shown in Fig. 5-27. The vanes caused the bed to aggrade by 0.6 to 1.0 m within the vane-controlled area, which is essentially the old, pre-vane low-flow channel. The aggradation, or berm, starts about 10 m downstream from the first vane array and continues downstream past Section 1. The width of the berm is 20 to 30 m. Between Sections 7 and 1, the vane-induced aggradation amounts to about 3,300 m^3, or 276 m^3 per vane. The aggradation along the bank downstream from Section 1 appears to be of the same order of magnitude.

It is noted that the aggradation straight downstream from the last vane array is decreased and at Section 3 is less than 0.5 m. At this section, and at downstream sections, the major aggradation occurred toward the right bank. The decrease in aggradation straight downstream from the last vane array resulted from the decay of vane-induced circulation. The reason for the enhanced aggradation along the bank downstream from the vanes is that the vanes shifted the main current toward the central portion of the channel, so the velocities along the bank are now considerably less than before.

Figure 5-25. View downstream toward the Butler County (Iowa) bridge, August, 1989. Bank eroding prior to vane installation is by tree line to right in photo. *Source:* Odgaard and Wang (1991), ASCE.

Figure 5-26. Most-upstream vane array of the West Fork Cedar River installation.

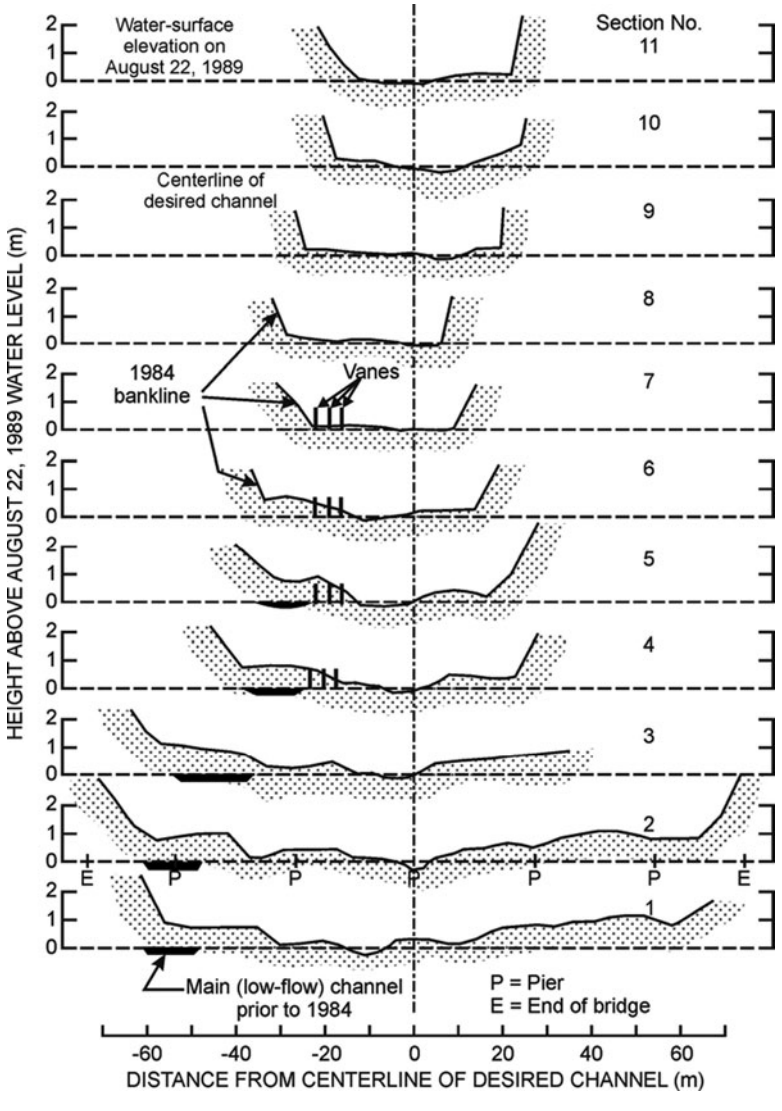

Figure 5-27. Cross sections in the West Fork Cedar River measured on August 22, 1989. *Source:* Odgaard and Wang (1991), ASCE.

The vane-induced aggradation is somewhat better than predicted. At bankfull flow, the velocity at Sections 4 and 5 is about 0.9 m/s, yielding a sediment Froude number of $\mathbf{F}_D = 13$. With a friction parameter of $m = 3$–4, a relative vane submergence of $T/d_o = 0.7$, vane height-to-water depth ratio of $H/d_o = 0.3$, and aspect ratio of $H/L \approx 0.2$, Fig. 2-23 yields $d_o - d_v = 0.6$ m. The reason for the enhanced aggradation is probably the vegetation, which increases flow resistance on the berm and causes the sediment-transport capacity to decrease below that predicted by the theory. The vegetation has continued to increase in the protected area (Fig. 5-28), and today (2008) the system is still fully functional.

Figure 5-28. Views upstream from the bridge at low flow. Above: Old channel along right bank, now a heavily vegetated berm. Below: New channel running straight through center span of bridge.

5.3 Sediment Control at Water Intake/Diversion

There are numerous field installations in place to prevent sediment from being entrained into water intakes. Reference is made to Nakato et al. (1990), Nakato and Ogden (1998), Muste and Ettema (2000), Wang et al. (1996), Barkdoll et al. (1999), Odgaard and Wang (1991), Electric Power Research Institute (1995; 1997; 1998), and Michell et al. (2006). The installations described below are selected to cover a representative range of river-flow rates and sediment sizes. Design-flow rates range from about 100 m^3/s to about 8,000 m^3/s, and median sediment sizes from about 0.3 mm to about 30 mm. The section starts by describing installations in sand-bed rivers and concludes with a description of one in a gravel-bed river.

5.3.1 Sand-Bed Rivers

Cedar River, United States

The water intake for the Duane Arnold Energy Center (DAEC) is located on the Cedar River in Palo, Iowa (Fig. 5-29). The intake draws about 0.7 m^3/s from the river for make-up water for the plant's cooling system. The intake velocity is about 0.04 m/s. At the intake, the river-flow velocity is typically about 0.5 m/s. When the plant started operation in 1972, virtually all of the river flow approached the intake from the meander curve. By 1980, most of the flow had shifted and came through the cutoff. As a result, the intake was no longer situated at the outside of a bend (thus benefiting from ensuing large flow depth), and sedimentation became an increasing problem. By 1989 considerable amounts of sediment were being drawn into the cooling system, leading to maintenance problems. Sediment was accumulating within the intake structure, and the gates at the entrance to the intake were repeatedly buried and made inoperable. At low flow, a sandbar typically

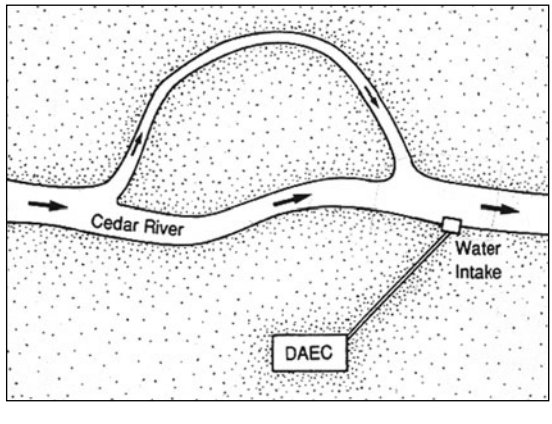

Figure 5-29. The Duane Arnold Energy Center (DAEC) water intake on Cedar River, Iowa.

was visible in front of the downstream portion of the intake (Fig. 5-30). The sandbar connected with the intake structure and blocked the flow into part of the intake. A survey conducted in 1989 (Ettema 1990) showed sediment deposition at the intake being as much as 1 m above the sill elevation.

Figure 5-31 shows the solution that was developed (Odgaard et al. 1990). It consists of a guide wall and a system of nine vanes of the type shown in Fig. 1-19. The guide wall is attached to the upstream corner of the intake and extends upstream as it tapers into the bank-line, thus smoothing the approach flow past the intake structure. The vanes intercept the approaching bed-load and divert it away from the face of the intake. Each vane is supported by a pile driven into the bed to a depth of about 6 m. Details are given in Fig. 5-32.

The performance of the vane system compares well with the theory in Chapter 2. At design flow, average depth, slope, and velocity are $d_o = 2.2$ m, $S = 0.0005$, and $u_o = 0.8$ m/s, respectively. Radius of curvature is $r = \infty$. The bed material is sand with a median grain diameter of $D = 0.3$ mm. The channel's resistance parameter is:

$$m = \frac{\kappa u_o}{\sqrt{gSd_o}} = \frac{(0.4)(0.8)}{\sqrt{(9.81)(0.0005)(2.2)}} = 3.0$$

which corresponds to a Darcy-Weisbach friction parameter of $f = 8\kappa^2/m^2 = 0.133$.

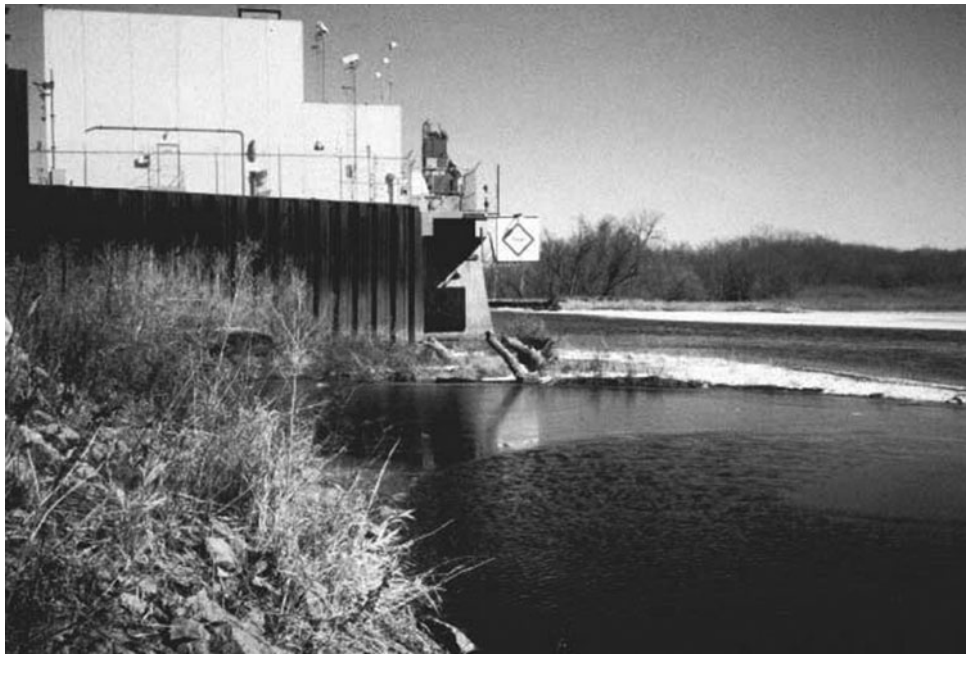

Figure 5-30. View upstream toward the DAEC intake structure, showing a sandbar in front of part of the intake.

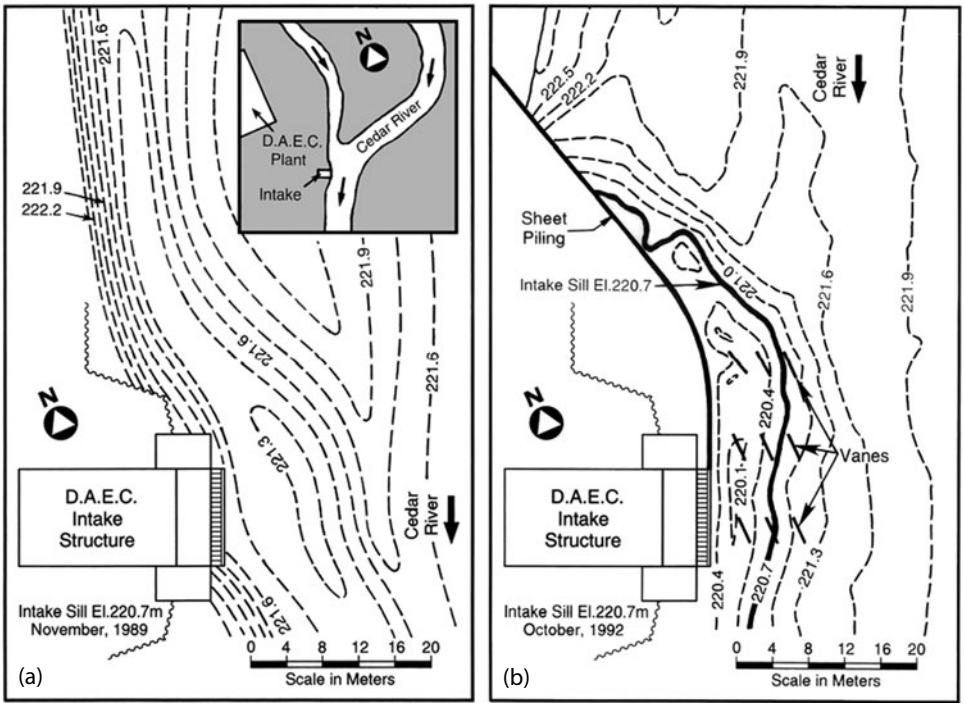

Figure 5-31. Bed-level contours in Cedar River at the DAEC intake structure, (a) in 1989, and (b) in 1992. *Source:* Wang et al. (1996), ASCE.

The sediment Froude number is:

$$\mathbf{F}_D = \frac{u_o}{\sqrt{gD}} = \frac{(0.8)}{\sqrt{(9.81)(0.0003)}} = 14.7$$

The channel's depth–width ratio is $d_o/b = 0.02$, which is small enough that this parameter does not play a role.

With relative vane submergence $T/d_o = 0.59$, vane length $L \simeq 3H$, lateral and longitudinal vane spacings $\delta_n \simeq 3H$ and $\delta_s = 10H$, $\alpha = 20$ degrees or more, and the number of vanes in each array $N = 3$, Fig. 2-23 yields

$$\frac{d_o - d_v}{d_o} = 1.0\left(1 - \frac{T}{d_o}\right) = 0.4$$

that is,

$$d_v = 0.59\, d_o = 1.3 \text{ m}$$

By assuming that $\delta_v \approx \delta_b$, the continuity and Manning equations yield (Eq. 3-4)

$$d_o + \Delta d = 3.3 \text{ m}$$

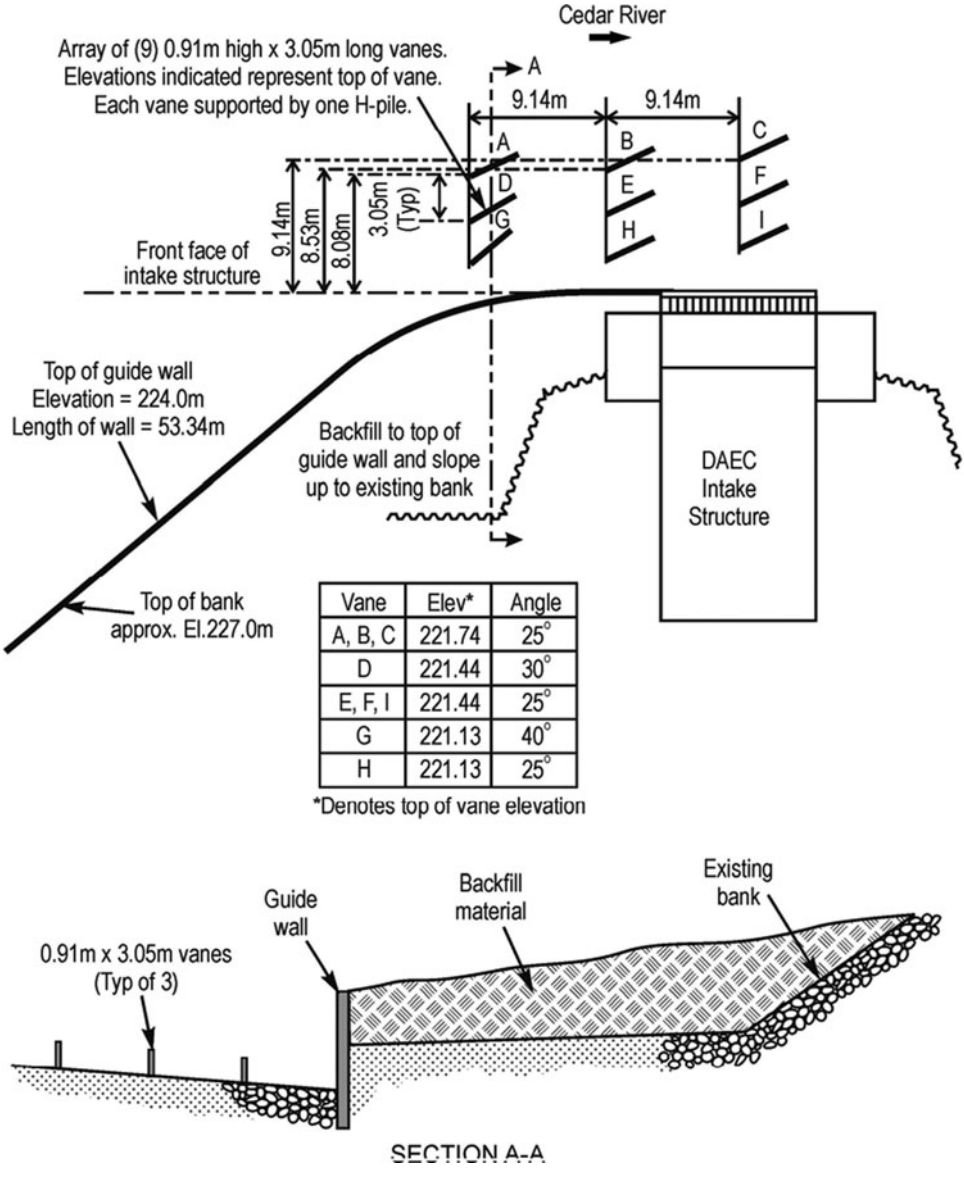

Figure 5-32. Details of vane installation at the DAEC intake on Cedar River. Courtesy of River Engineering International.

or,

$$\Delta d = 1.1 \text{ m}$$

Figure 5-33 shows a comparison between the average bed profile as measured on September 13, 1991, just before the vanes were installed, and the average bed profile as measured on October 12, 1992, one year after installation. The October 12, 1992, profile is in good agreement with the calculated profile. The bed

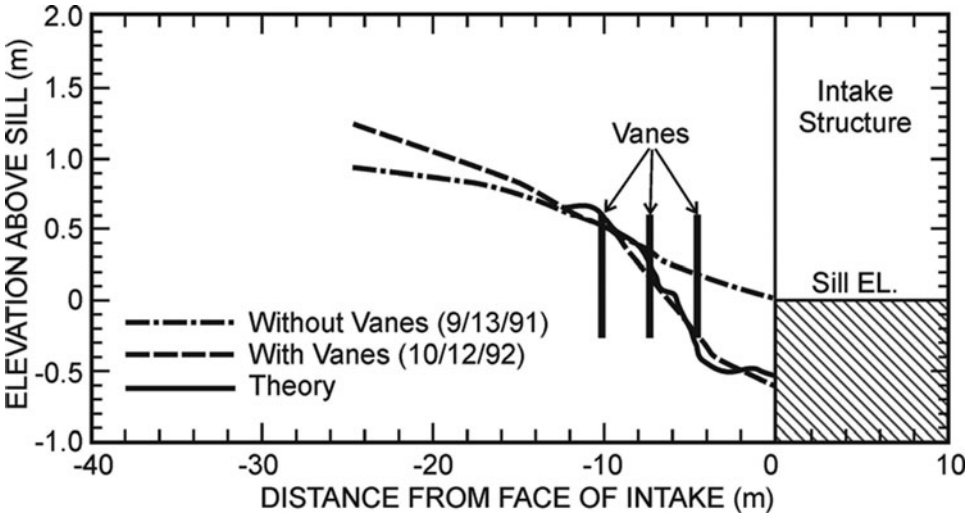

Figure 5-33. Bed profiles outside the DAEC intake structure before and after installation of vanes. *Source:* Wang et al. (1996), ASCE.

along the sill is scoured clear down to the riprap placed at the bottom of the vanes between the innermost row of vanes and the sill (Fig. 5-32).

Construction cost (manufacturing/purchase and installation of vanes and guide wall) was recovered within about two years in terms of reduction in operation and maintenance cost. The cost reduction was estimated based on (a) maintenance at the intake structure and dredging in the river in front of the intake; (b) cleaning maintenance at the cooling tower; (c) pump maintenance; and (d) cleaning of condensers and heat exchangers. The installation was maintenance-free until about 2004.

One of the challenges with the DAEC project was the gradual change in flow split between meander curve and cutoff (Fig. 5-29). By 2005, the flow through the meander curve had decreased to less than 10%. As a result, the channel upstream from the intake had incurred changes that affected the flow approaching the vane field and intake. Between 1990 and 2005, a considerable amount of bank erosion occurred along the right bank about 200 m upstream from the intake in the upstream segment of the cutoff, and an even larger amount along the left bank just upstream of the intake. By 2005, the width of the channel just upstream of the intake had become nearly twice the width in 1980, and shoaling occurred in the channel. A decision was subsequently made to build four spur dikes upstream and opposite the intake (Fig. 5-34) to make the river channel return to its 1980 plan form. The spur dikes caused the flow past the intake to increase and the bed level to return to the level just after the vane installation in 1991.

Rock River, United States

The Byron Station water intake is located on the Rock River in Byron, Illinois (Fig. 5-35). The intake draws 1.8 m^3/s of water from the river for make-up for the cool-

Figure 5-34. Upstream view of Cedar River at the DAEC intake structure. In 2006, four spur dikes were installed on left bank upstream from the intake. The wings of the spur dikes delineate the 1980 left bank of the river. Courtesy of Paul Collingsworth, FPL Energy Duane Arnold.

ing system of the power plant. The intake velocity is about 0.08 m/s, about 20% of the river-flow velocity (0.4 m/s). The sediment problem was partly due to the intake being on the inner bank of a river curve. In 1980, a channel was built into the river bottom to connect the intake opening with the deep portion of the river near the outer bank of the river across from the intake. This channel had to be dredged at frequent intervals. During a survey conducted on August 29, 1990, the bed elevation at the intake was measured to be about 1.3 m above the sill elevation of the intake. Sediment deposits blocked a considerable portion of the intake opening.

A solution was sought that could develop and maintain, in front of the intake structure, a channel with the bed below the intake-sill elevation that could connect to the main channel. Hydraulic model studies were conducted (Melville et al. 1992).

The solution that was developed consisted of (a) removal of a shallow spur on the left bank upstream from the intake structure; (b) reshaping of the river bank downstream from the intake structure; (c) installation of eight arrays of five vanes each in front of the intake structure; and (d) construction of two submerged wing dams (submerged groins) upstream from the intake structure on the opposite bank. The purpose of the wing dams was to ensure that the vane-generated channel along the left bank was connected with the main channel near the right bank. The removal of the spur and the reshaping of the bank caused a smoothening of the flow past the intake. The vanes were located to intercept the approaching bed

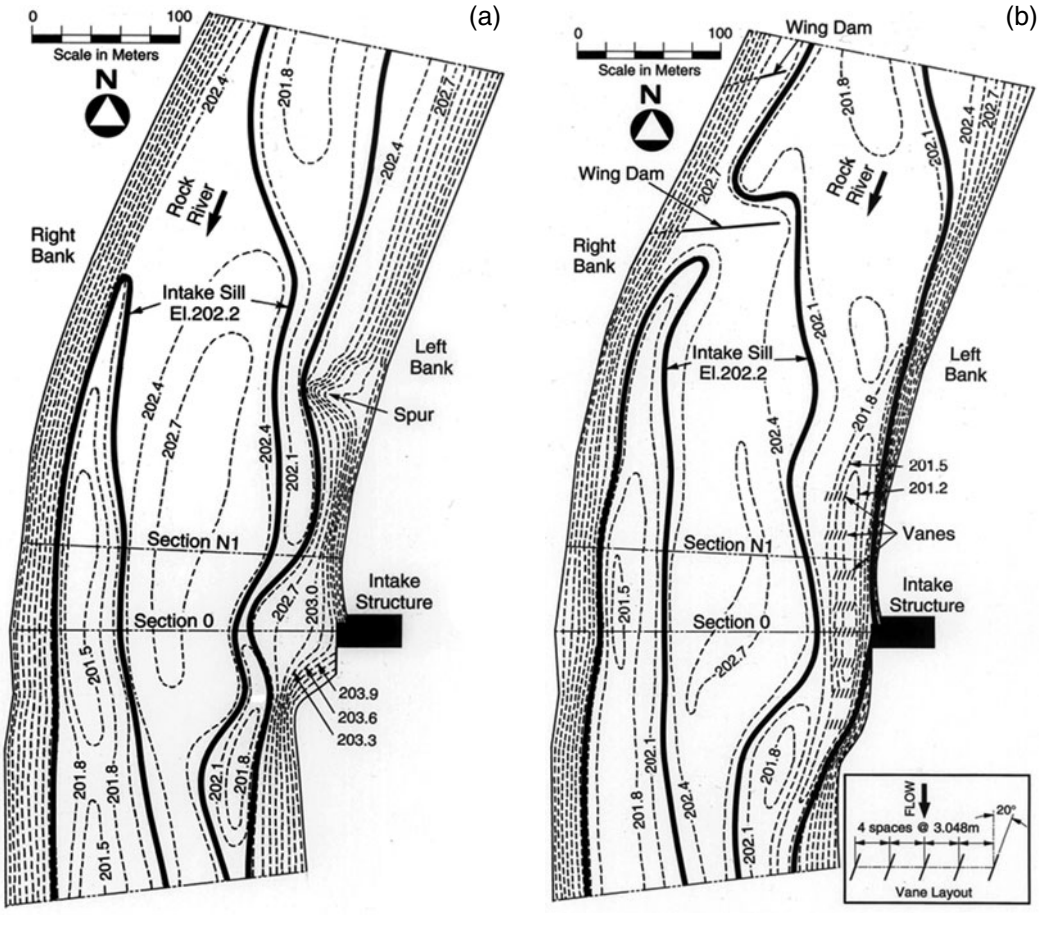

Figure 5-35. Bed-level contours in Rock River at the Byron Station (Illinois) intake structures, (a) in 1990, and (b) in 1994. *Source:* Wang et al. (1996), ASCE.

load and divert it away from the face of the intake. The solution was installed in the fall of 1993.

The performance of the vane system compares well with the theory in Chapter 2: At design stage (204.9 m), average depth and velocity are d_o = 2.7 m and u_o = 0.4 m/s, respectively. Median grain diameter is 0.3 mm and the sediment Froude number is 7.4. The channel's resistance parameter is estimated to be m = 3.0. The vanes are installed so that $T \approx 1.9$ m, yielding $T/d_o = 0.7$. Figure 2-23 and the continuity and Manning equations yield $\Delta d \approx 1.0$ m.

Figure 5-36 shows a comparison of two river cross sections measured in 1990, with the same cross sections measured during a survey conducted on August 2–3, 1994 (Jain et al. 1994). The intake-sill elevation is also shown in Fig. 5-36 for reference. It is seen that the vane system, together with the other channel modifications, very effectively developed a deep channel in front of the intake. The depth is somewhat bigger than calculated. This could be due to the influence of the

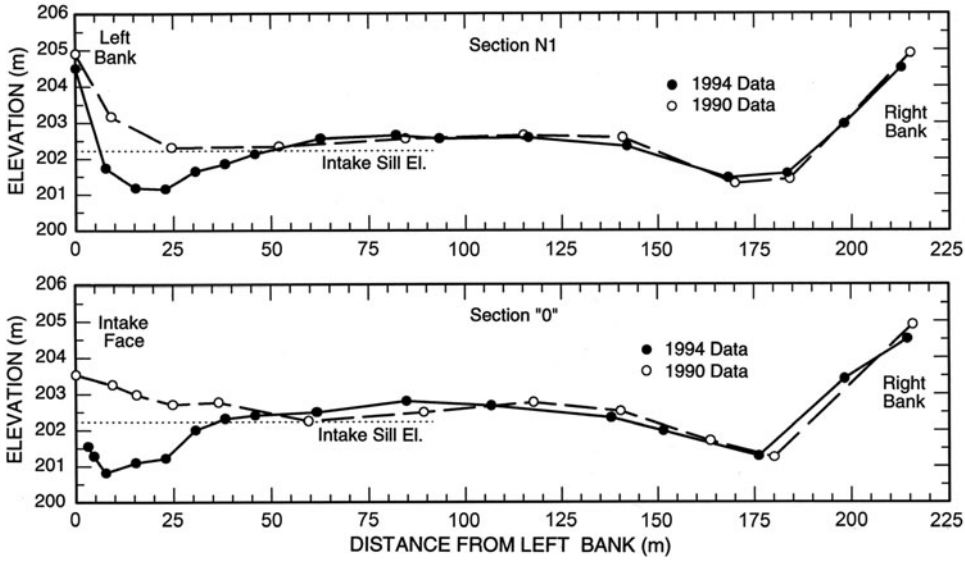

Figure 5-36. Bed profiles in Rock River at the Byron Station intake structure before and after installation of vanes. *Source:* Wang et al. (1996), ASCE.

other components of the solution (removal of spur, reshaping of bankline). Figure 5-35 shows bed-level contours developed based on the data taken in 1990 and in 1994, respectively. The thick line in these figures represents the contour at the intake-sill elevation. There are two channels with the beds lower than the intake-sill elevation—one near the right bank and the other near the left bank. The solution clearly caused an increase in the width of the deep channel near the left bank; the solution created a channel that connects the intake to the main channel and thus achieved the stated objectives. Figure 5-37 shows results of a survey conducted in 2007. It is seen that the vane system continues (14 years after installation) to perform as intended.

Construction cost (manufacturing/purchase and installation of vanes, construction of upstream submerged wing dams, and bankline modification) was recovered within about three years in terms of reduction in operation and maintenance cost. The cost reduction was estimated based on (a) maintenance at the intake structure and dredging in the river in front of the intake; (b) cleaning maintenance at the cooling tower; (c) pump maintenance; and (d) cleaning of condensers and heat exchangers. The installation has so far (since 1994) been maintenance-free.

Missouri River, United States

Submerged vanes have been installed at several intakes on the Missouri River between Sioux City, Iowa and St. Louis, Missouri. Prior to vane installation, the intakes suffered from severe sedimentation problems that required periodic dredging and plant outages. All installations are now performing as intended. The installations were preceded by hydraulic model studies.

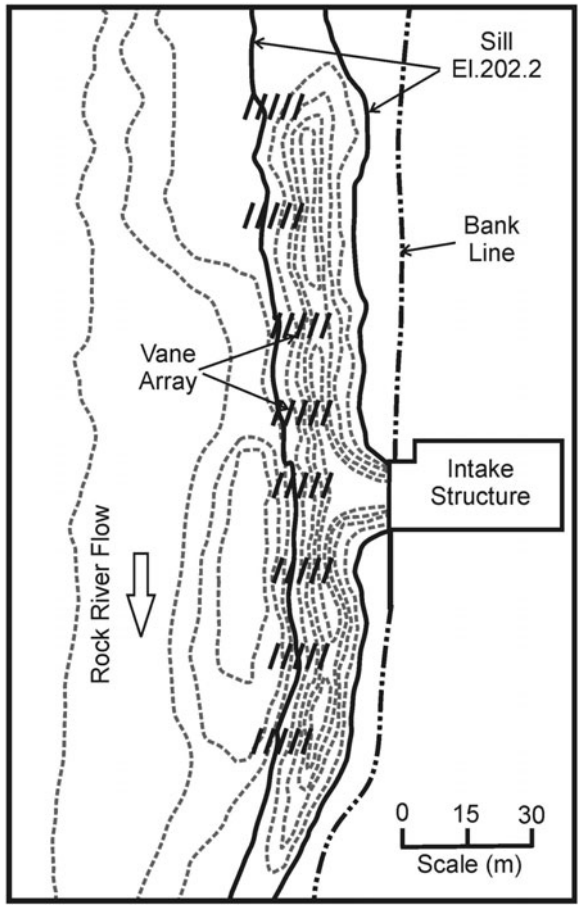

Figure 5-37. Bed-level contours in Rock River at the Byron Station intake structures measured in 2007. Based on survey data used with permission of Exelon Corporation. All rights reserved.

Four of the model studies and installations are described in detail by Nakato and Ogden (1998). Three of the installations include a sediment-barrier wall (skimming wall). Based on the model studies, Nakato and Ogden formulate the following general recommendations for an intake located on a sand-bed river similar to the Missouri River reach (refer to Fig. 5-38):

1. A sediment-barrier wall (skimming wall) should be installed parallel with and within 2.1 m to 3.0 m of the face of the intake. The wall should protrude 0.9 m to 1.5 m above the existing mean bed elevation, and it should flare into the upstream bankline at an angle of 10 degrees to 30 degrees.
2. Two rows of submerged vanes should be constructed outside the wall, as shown in Fig. 5-38. The vanes should be 0.9 m to 3.0 m in length and protrude at least 1.2 m above the existing mean bed elevation. Vane angle of attack should be 20 to 25 degrees relative to the centerline of the channel.

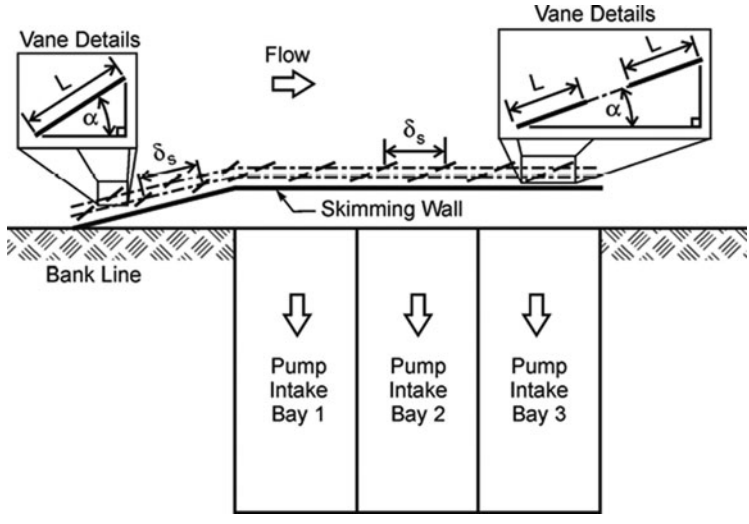

Figure 5-38. Schematic showing general layout of vanes and skimmer wall recommended by Nakato and Ogden (1998) for intakes on the Missouri River. *Source:* Nakato and Ogden (1998), ASCE.

Nakato and Ogden suggest that omission of the barrier wall may be warranted under certain conditions. One of the featured installations is at MidAmerican Energy Company's Council Bluffs Unit 3. Installed in 1985, this installation does not include a barrier wall, and it has maintained the intake free of sediment ever since. This observation is consistent with the guidelines herein. The inner row of vanes is located within the stream tube formed by the intake flow and the bankline. However, the specific discharge ratio, q_r, is only about 0.12, which, according to the laboratory studies by Barkdoll et al. (1999) described in Section 3.4, is sufficiently low that vanes alone can keep the intake free of sediment.

Nakato and Ogden also determine that the reduction in bed level in front of the intakes reduces the suspended-sediment load of the intake flow. This is because the lowered bed level results in lower suspended-sediment concentration at the top of the barrier wall. If it is assumed that the median bed-material size is 0.5 mm, the flow depth is 4.6 m, and the energy slope is 0.0002 (which are typical for the Missouri River reach investigated), Nakato and Ogden calculate that lowering the bed elevation adjacent to the sediment-barrier wall by 0.9 m yields a reduction of suspended-sediment concentration by as much as 90% at the top of the wall, according to the Rouse suspended-sediment concentration curves (ASCE 1975).

In all of the installations, both barrier wall and vanes are constructed of interlocking sheet piling.

Waikato River, New Zealand

The Huntly Power Station is a 1,000-MW coal- and gas-fired power station that draws about 40 m^3/s of cooling water from the nearby Waikato River (Fig. 5-39). Since the station was commissioned in 1982, regular dredging was required to

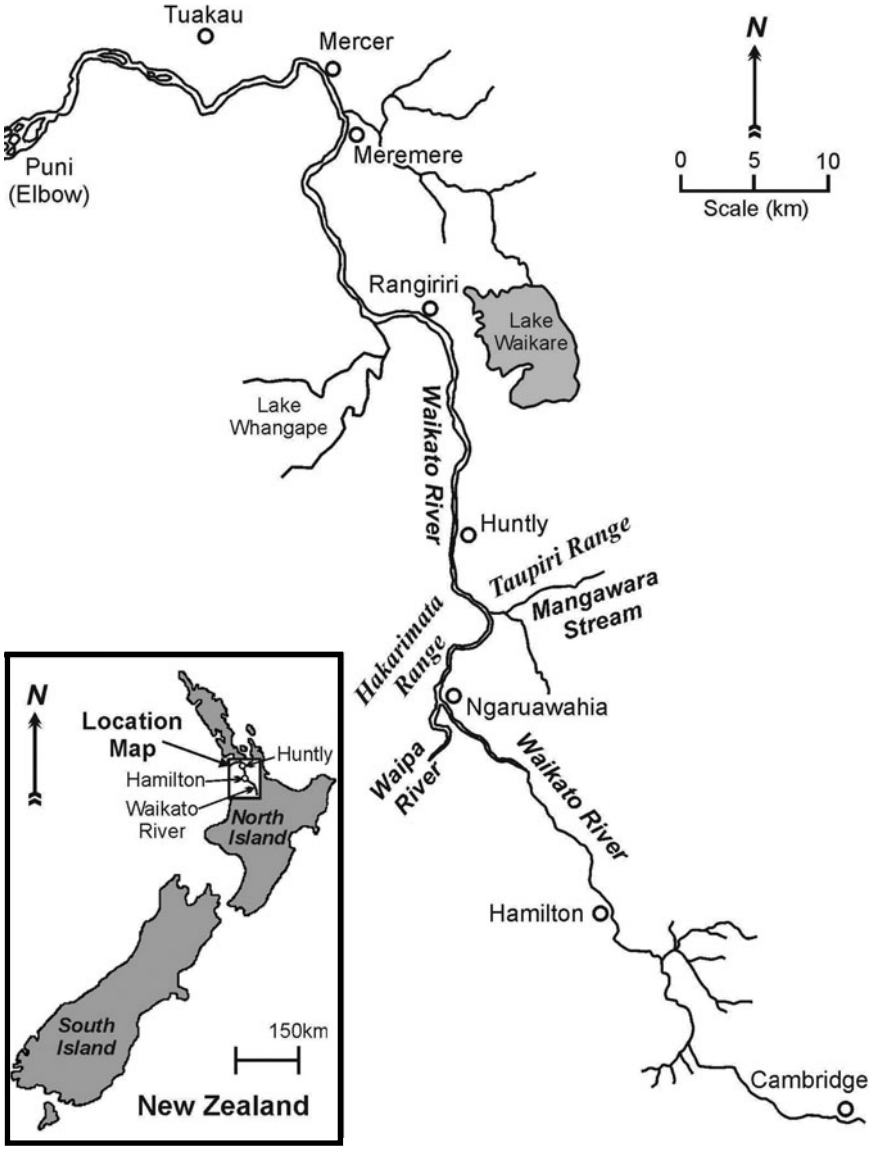

Figure 5-39. Location of Huntly Power Station on Waikato River, New Zealand.

remove sand from the forebay of the cooling water intake. The sediment entrainment was correlated with the passage of large, migrating dunes that periodically filled the channel adjacent to the intake (Dahm and Hume 1989).

In the vicinity of the intake, the width of Waikato River is about 200 m. The low-flow channel occupies 25% to 30% of the river width and meanders with a wavelength of about 3 km (Dahm and Hume 1989). The bed elevation adjacent to the intake ranges from 103.5 m to 105.5 m, with an average of about 104.5 m.

The elevation of the intake sill is 104.5 m. The water level at the intake ranges from 107 m at low flow to 110 m at high flow.

Water-surface slope varies slightly with discharge, from about 0.00018 at a discharge of 220 m^3/s to about 0.000123 at a discharge of 477 m^3/s. The slope decreases with increasing discharge because the bed gets smoother, with bed formations tending to be washed out.

The sediments on the riverbed are moderately sorted, medium-coarse sands that are typically transported as bed load. Median diameter is 0.5 to 0.7 mm. Samples taken from the intake and forebay have textural characteristics similar to the river-bed sediments, suggesting that the bulk of sediment being deposited in the intake is brought in by bed load rather than suspended load.

In their study, Dahm and Hume suggested that sediment withdrawal could be significantly reduced if a deep channel with bottom elevation of 103 m or less could be maintained adjacent to the intake. This finding was confirmed by Odgaard and Keller using a hydraulic scale model at the plant (Keller 1993). A vane system consisting of 26 vanes was subsequently designed to develop and maintain such a channel adjacent to the intake. The design was tested and fine-tuned in the scale model. In addition to the vane system, two upstream weirs were designed and installed on the opposite bank. The purpose of the weirs was to stabilize a natural crossover in the river that occurred just upstream from the intake. Because of the near-braided regime of the river at this location, the crossover was unstable and sandbars tended to form at the intake. These weirs, together with the vanes, now maintain a stable, relatively deep channel along the face of the intake. Figure 5-40 is a plan showing the layout of vanes and weirs. Figure 5-41 shows vane design details. The vanes were installed from a barge using a barge-mounted pile driver and divers to guide the underwater vane assembly (Figs. 5-42 and 5-43).

Muskingum River, United States

The Conesville Station is a 1,900-MW power station located on the Muskingum River, Ohio (Fig. 5-44). When the station is operating at full load, the intake withdraws approximately 13.2 m^3/s of water from the river for cooling and other plant processes. Water enters the intake structure through trash grills and traveling screens. The width of the intake is 26.9 m. At a withdrawal rate of 13.2 m^3/s, the specific discharge (discharge per unit width) is about 0.5 m^3/s per meter of intake width. The station experienced chronic problems with sediment buildup at the intake structure, which adversely affected the station's fuel consumption efficiency. Periodic dredging of the river was necessary.

During the period November through May, the average discharge in the river is about 273 m^3/s. From May to November, the average discharge is about 82 m^3/s. During this period, discharge can be as low as 40 m^3/s. The median diameter of the bed sediment is about 1.5 mm and its geometric standard deviation is 5.2 mm.

The following factors contributed to the sediment problem: (a) At low flow, the unit discharge or velocity in the river past the intake is very low compared with the velocity into the intake; this caused bed sediment to be drawn into the intake

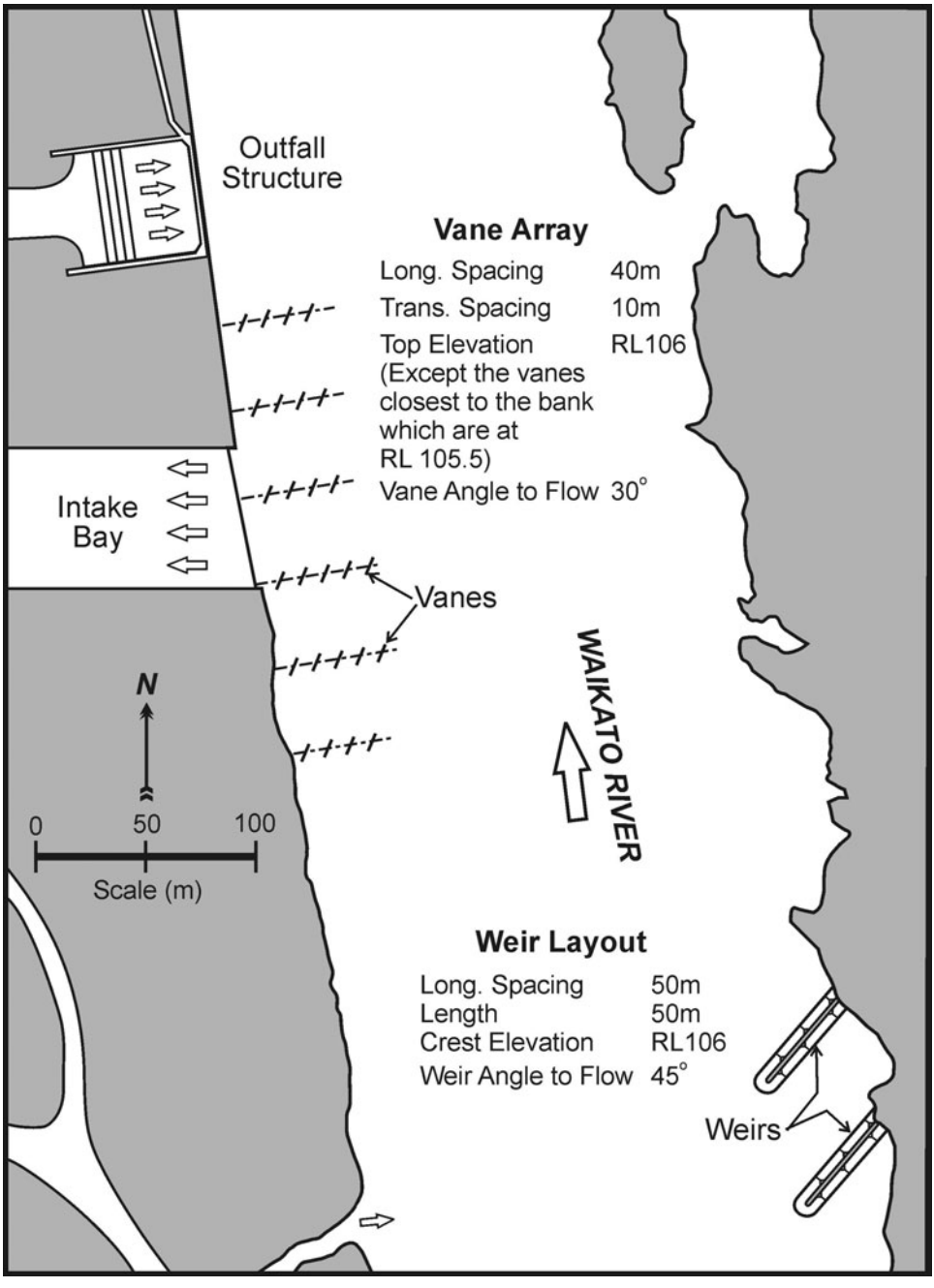

Figure 5-40. Layout of vane system in Waikato River at Huntly Power Station. *Source:* Keller (1993) with permission from Genesis Energy.

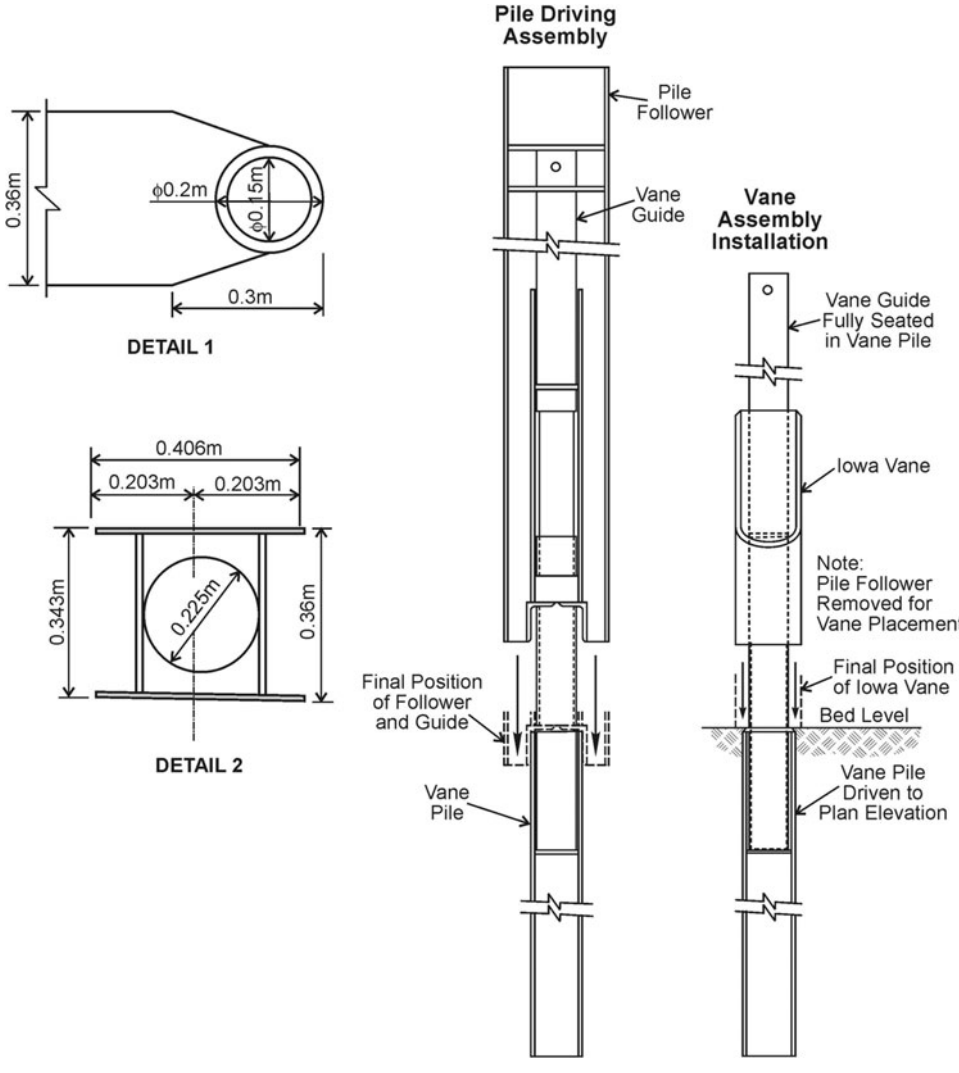

Figure 5-41. Vane design details, Huntly Power Station. Courtesy of Douglas J. Bottorff, Shive-Hattery Group, Inc.

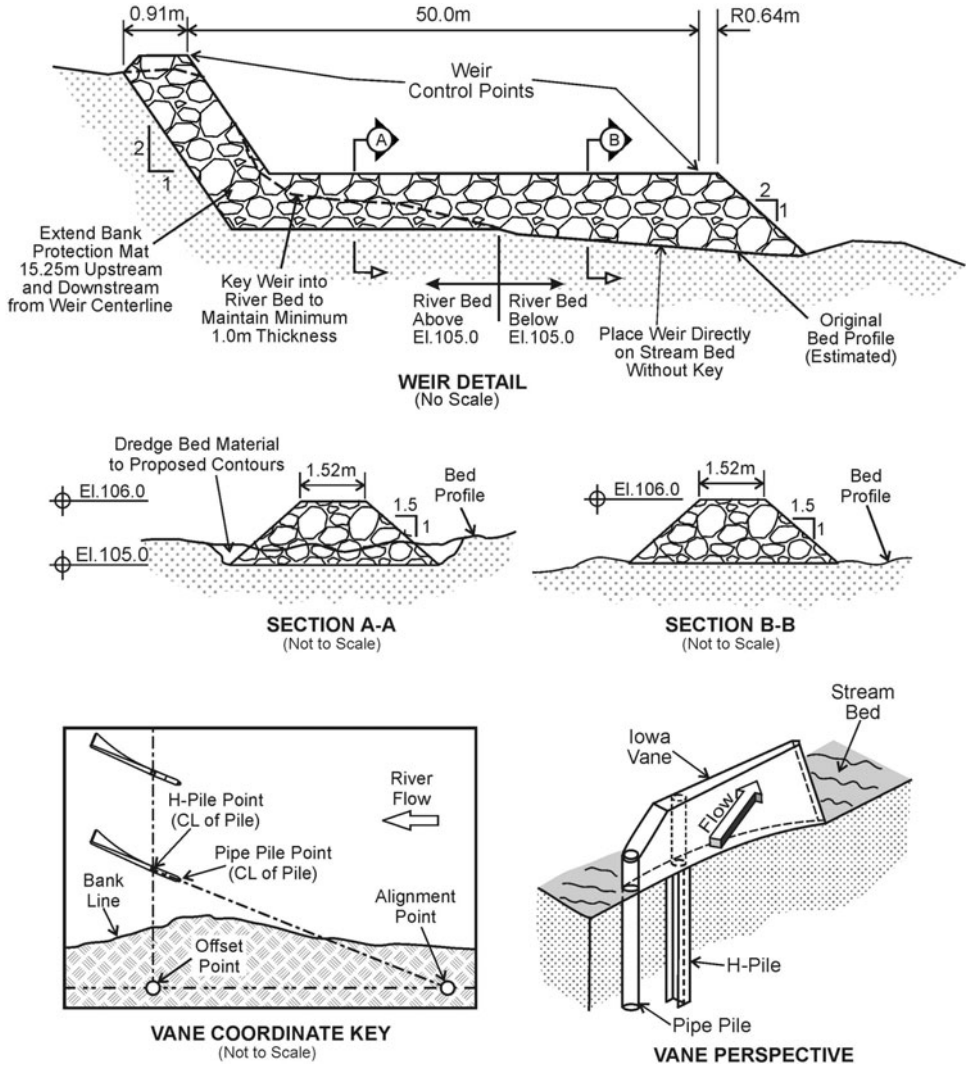

Figure 5-41. Continued.

from a significant width of the river (see illustration in Fig. 5-45). At low flow, the relatively large withdrawal rate caused the formation of a stationary dune to form outside the intake. The dune extending out in the river acted much like a cambered ramp, guiding sediment up to the intake-sill elevation. (b) Erosion of the riverbank immediately upstream of the intake further exacerbated the problem (Fig. 5-46). It caused the upstream river's thalweg (deepest section) to swing out away from the intake and then loop back to the intake entrance. This flow configuration, together with flow separation from the upstream abutment of the intake structure, created a fairly large eddy zone immediately upstream of the intake entrance. At low river flows, the eddy, illustrated in Fig. 5-47, entrapped

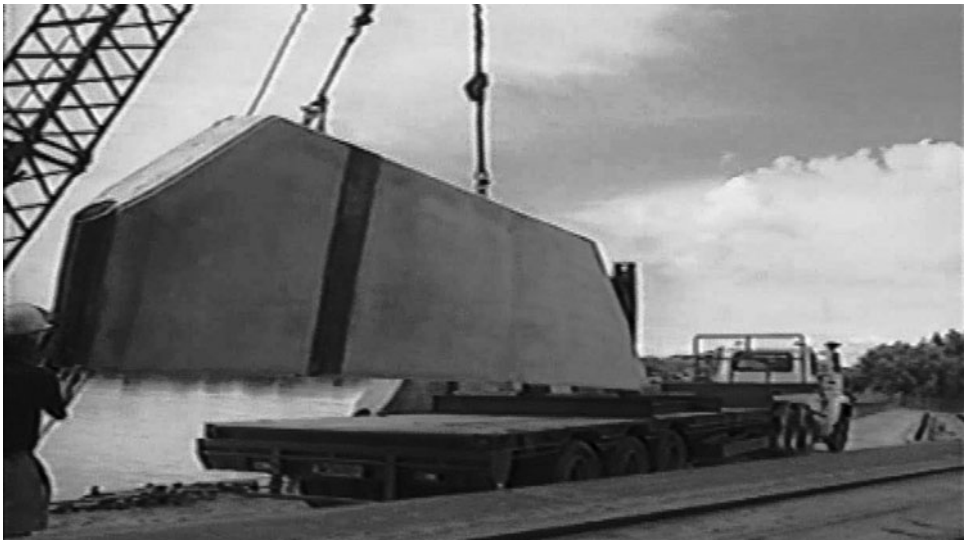

Figure 5-42. Huntly vane nose-pipe and main-pipe sleeve detail. *Source:* Electricity Corporation of New Zealand (1993), with permission from Genesis Energy.

Figure 5-43. Huntly vane, and pipe and pipe follower on barge outside the intake. *Source:* Electricity Corporation of New Zealand (1993), with permission from Genesis Energy.

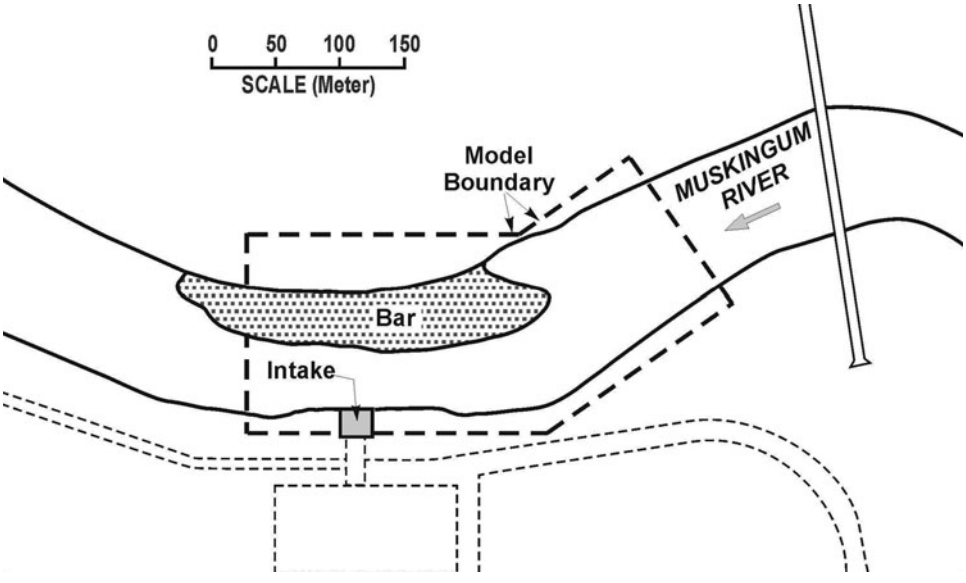

Figure 5-44. Conesville Station intake on Muskingum River, Ohio. Also shown is the area encompassed by a hydraulic model of the intake site. *Source:* Michell et al. (2006), ASCE.

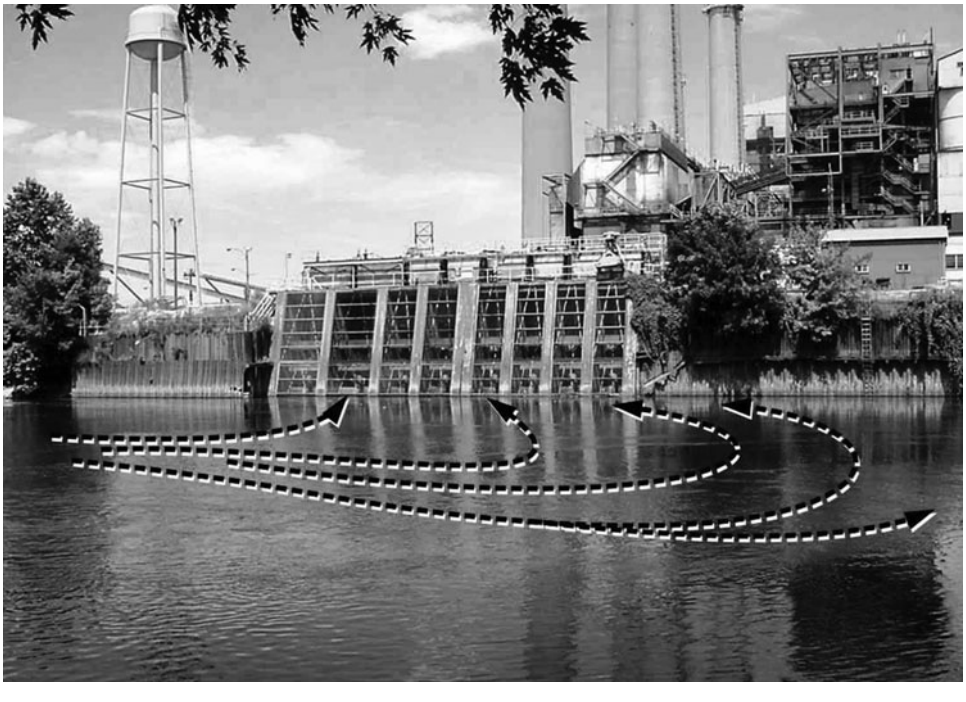

Figure 5-45. View of the intake showing flow lines toward the intake at low flow. *Source:* Michell et al. (2006), ASCE.

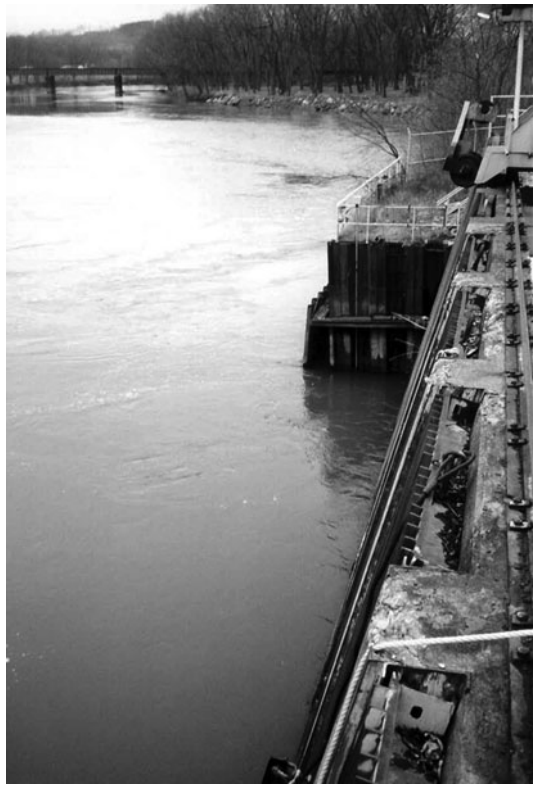

Figure 5-46. View upstream from the intake, showing flow impinging on upstream abutment and being deflected outward away from the intake. *Source:* Michell et al. (2006), ASCE.

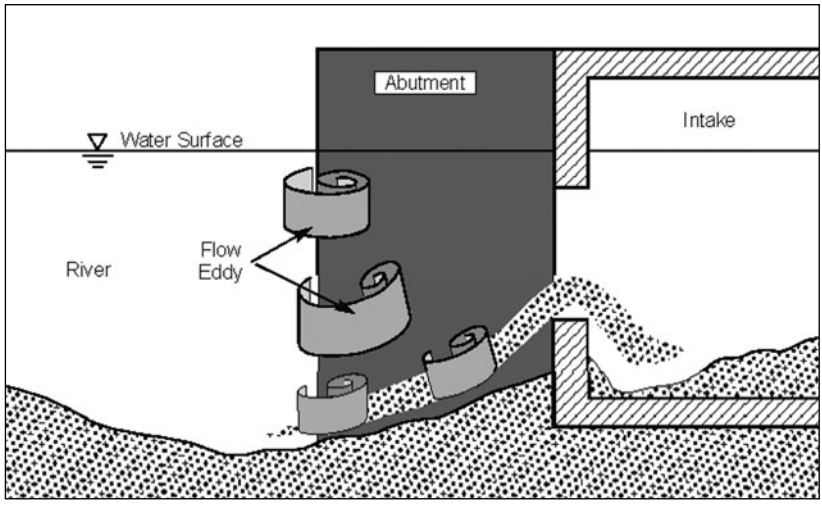

Figure 5-47. Sediment accumulation and ingestion caused by eddies shed from an abutment upstream of the intake. *Source:* Michell et al. (2006), ASCE.

sediment and piled it up in the vicinity of the intake. During subsequent high flows, sediment accumulated in the eddy region was stirred up, entrained in the river flow, and ingested into the intake.

The specific discharge ratio (unit discharge of flow into the intake over unit discharge of river flow past the intake) ranges from 0.1 for a river flow of 273 m^3/s to about 0.4 for a river low flow of 40 m^3/s.

The solution, developed in part by studies in a 1:35 scaled hydraulic model (Muste and Ettema 2000), included the following elements (shown in Figs. 5-48, 5-49, and 5-50): (a) Straightening of the river bank 68 m upstream of the shoulder wall of the intake structure; this eliminated the recirculation region and ensured that the flow passed directly along the face of the intake. (b) Installation of a skimming wall at the face of the intake structure; construction details are shown in Fig. 5-50. The wall helped dislocate the abutment eddies from the bed as indicated in Fig. 5-51. (c) Installation of 13 submerged vanes arrayed in two rows along the intake; construction details are shown in Fig. 5-49. The top elevation of the downstream vanes was increased by 0.3 m above the top elevation of the upstream vanes. This was done to enhance the action of the downstream vanes to compensate for the decrease in flow along the face of the intake. Finally, riprap was placed at the base of the vanes to limit depth of local scour. This was done as a precaution against excessive scour near the foundation of the intake structure. A final test of this solution was conducted in the hydraulic model in which simu-

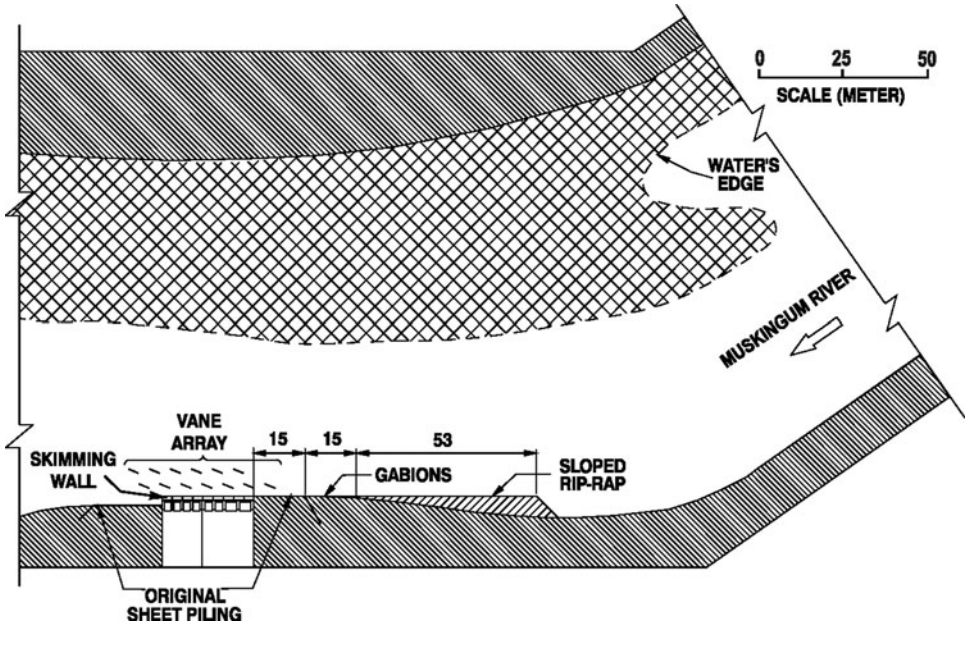

Figure 5-48. Solution consisting of a set of 13 vanes, a skimming wall, and realignment of bankline upstream of the intake. *Source:* Michell et al. (2006), ASCE.

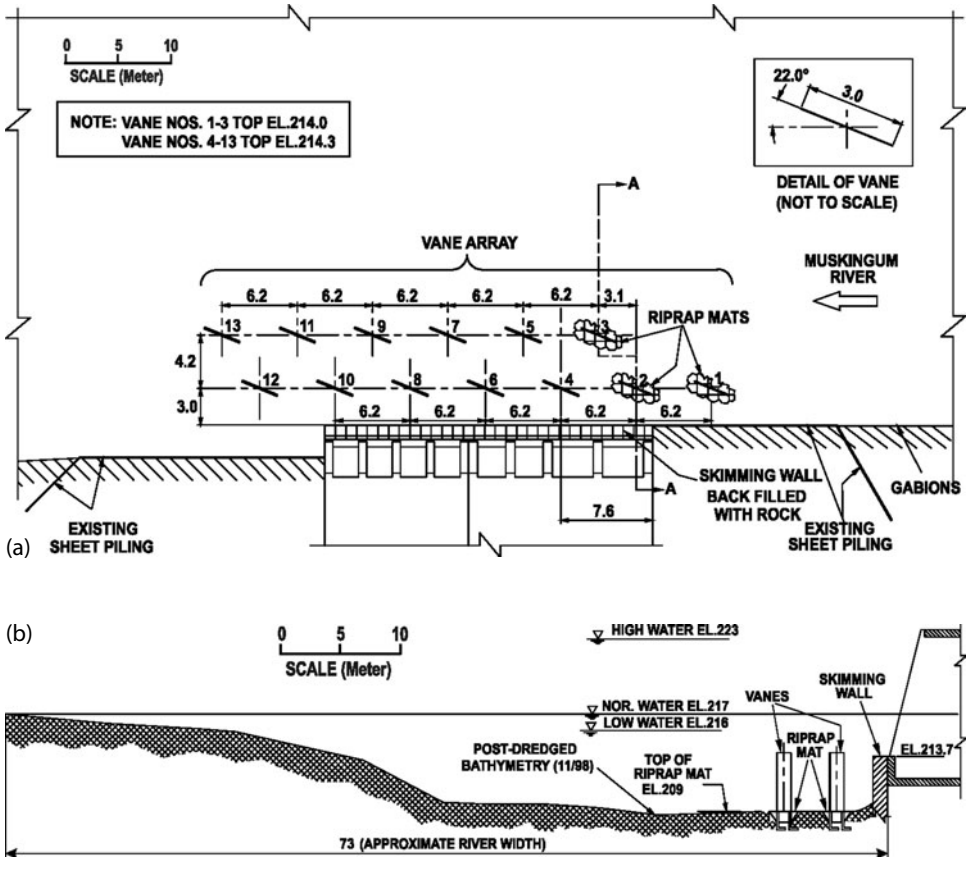

Figure 5-49. Construction details regarding vanes: (a) plan, and (b) section. *Source:* Michell et al. (2006), ASCE.

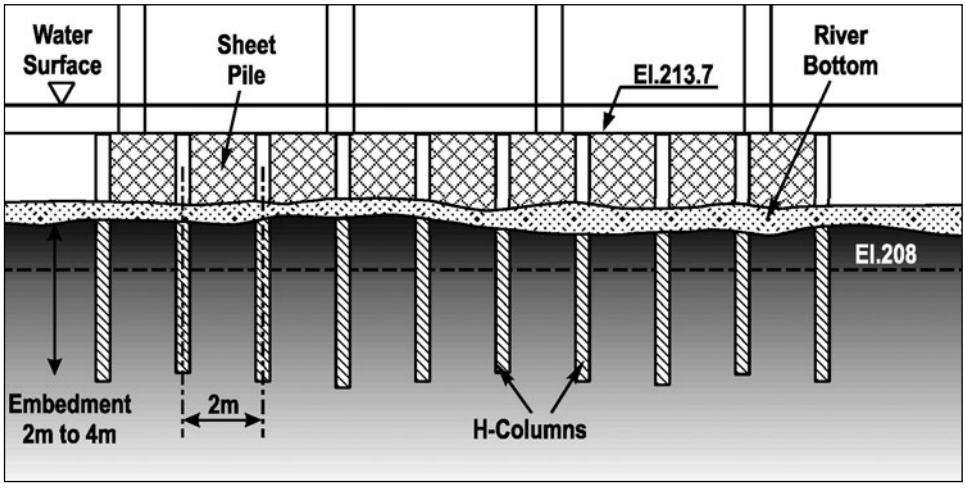

Figure 5-50. Construction details of a skimming wall, composed of sheet-piles and steel H-columns. *Source:* Michell et al. (2006), ASCE.

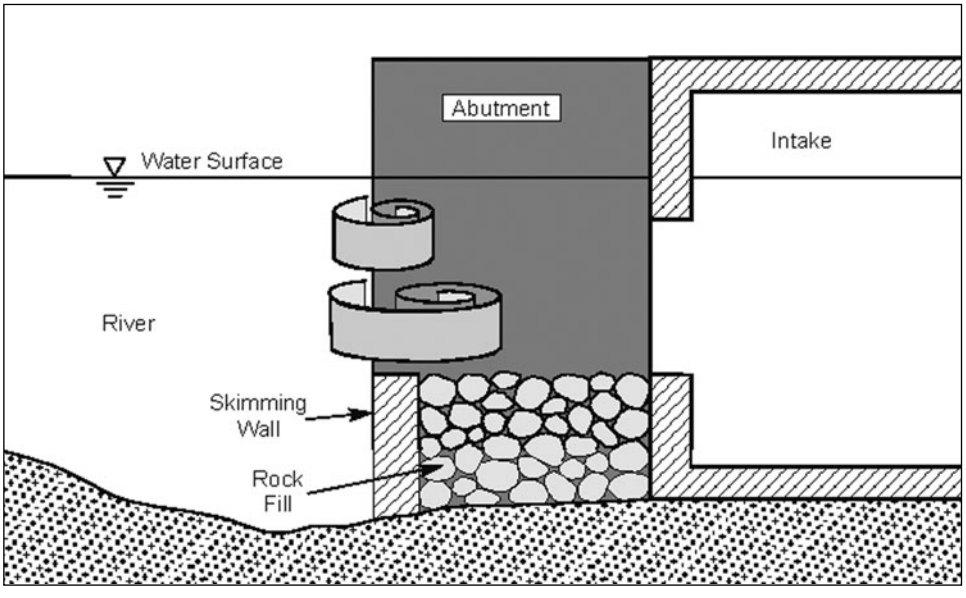

Figure 5-51. Action of a skimming wall to dislocate eddies from the bed.
Source: Michell et al. (2006), ASCE.

lated debris (logs, branches, etc.) was introduced. The test showed that the vanes were sufficiently submerged that debris entanglement would not be a problem.

The sediment control structures were installed during September, 2000 through February, 2001. All the work was accomplished with the station's generating units in service and without the use of divers (i.e., all work was done above the water surface). The work was performed in three phases.

The first phase consisted of straightening the riverbank upstream of the intake (Fig. 5-52). A 50-m-long section of the riverbank was regraded and provided with gabion mats to allow the river to flow smoothly toward the face of the intake.

The second phase consisted of installing the submerged skimming wall in front of the intake structure (Fig. 5-53). Wall alignment was maintained by constructing a temporary frame that extended above the water surface to guide the wall elements into position. A barge-mounted vibratory pile hammer was used to drive the sheet-pile wall sections to the design elevation. The sequence of work in front of the intake structure was closely coordinated with plant operations personnel. When conditions permitted, local flow velocities near the vibratory hammer were reduced by taking the adjacent intake pump out of service.

An unexpectedly high rock formation encountered in the bottom of the river prevented driving several of the skimming wall sheet-pile elements to required embedment. As a result, the design of the skimming wall was modified to incorporate rock socket soldier H-columns spaced approximately 2 m apart. The soldier columns were to provide the necessary support to the sheet-pile wall so no embedment was necessary for the sheet piles below the rock surface (Fig. 5-50).

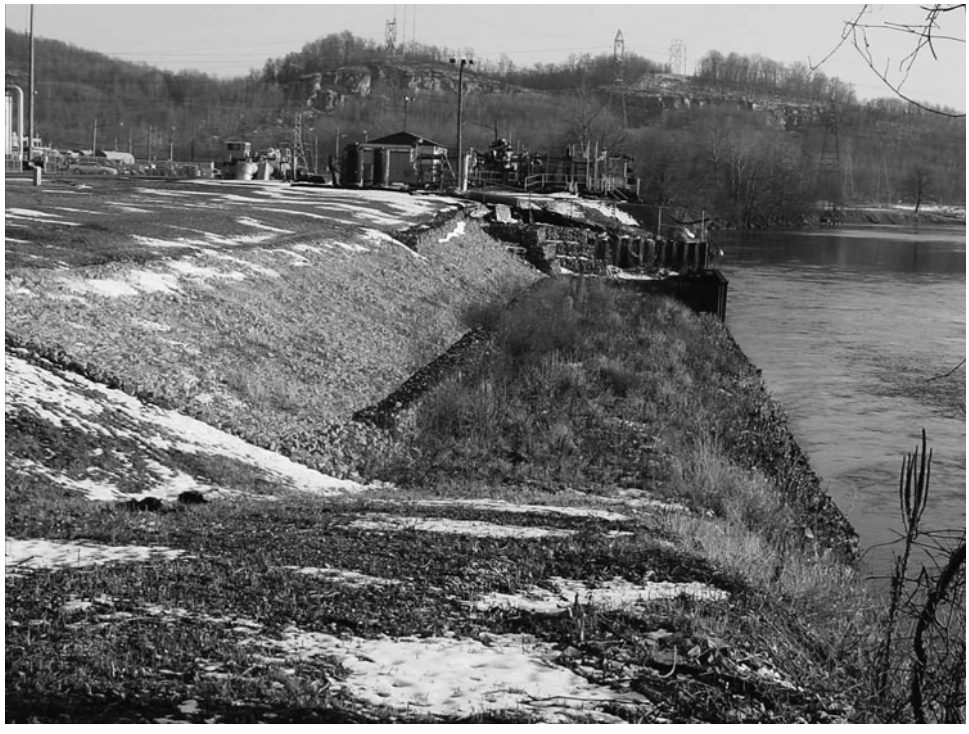

Figure 5-52. View downstream toward the intake. The river bank upstream of the intake was realigned to guide flow directly past the intake. *Source:* Michell et al. (2006), ASCE.

The soldier columns were installed using the barge-mounted drilling rig to core an opening with a diameter slightly less than the nominal diameter of the H-column. The soldier columns were then driven into the holes to provide an embedment ranging from 2 to 4 m. Following the installation of the skimming wall, the area in front of the intake structure was dredged to remove excessive accumulations of sediment to facilitate installation of the submerged vanes.

The third phase of the work included installation of the 13 vanes. The 3-m-long vanes were made up of 0.15-m-thick precast concrete panels secured in place between two 0.20-m H-columns (Fig. 5-54). Steel frames protruding above the water surface were used as guides to ensure that the vanes were located and installed correctly. The tolerance on the vane angle was +/−2 degrees.

As with portions of the skimming wall, at some vane locations rock formations had to be core-drilled to enable installation of the support beam for the precast concrete panel/vane. As mentioned earlier, rock mats were placed at the base of each vane to protect the bed against excessive scour (Fig. 5-55). The mats were placed before the vane panels were slid down the channels of the support columns. The mats and vane panels were placed using a barge-mounted crane. Once the vane was in place, the vane support beams were tied together on top for stability, using a steel channel.

Figure 5-53. Sheet-pile being driven into the bed to form a skimming wall. *Source:* Michell et al. (2006), ASCE.

After only one year of operation, the solution produced immediate improvement in terms of reduced maintenance costs and improved condenser performance. One year after installation, a survey was conducted of the river bottom. It confirmed that the vanes are self-scouring and effective in keeping the sediment moving downstream past the intake. After more than three years, there have been no problems with sediment ingestion. The station no longer budgets funds to dredge the river in front of the intake structure.

5.3.2 Gravel-Bed River

Kosi River, Nepal

Figure 5-56 shows a schematic plan of the area. The location is near Chatra, where the Kosi River turns south toward the Ganges River in India. The performance of the existing intake (for irrigation), shown at the center of the figure, was reduced

Figure 5-54. Precast concrete vane panels being placed between H-pile supports. Placement guides extend temporarily above the H-columns. *Source:* Michell et al. (2006), ASCE.

Figure 5-55. Mat protection being placed at the base of the vanes. *Source:* Michell et al. (2006), ASCE.

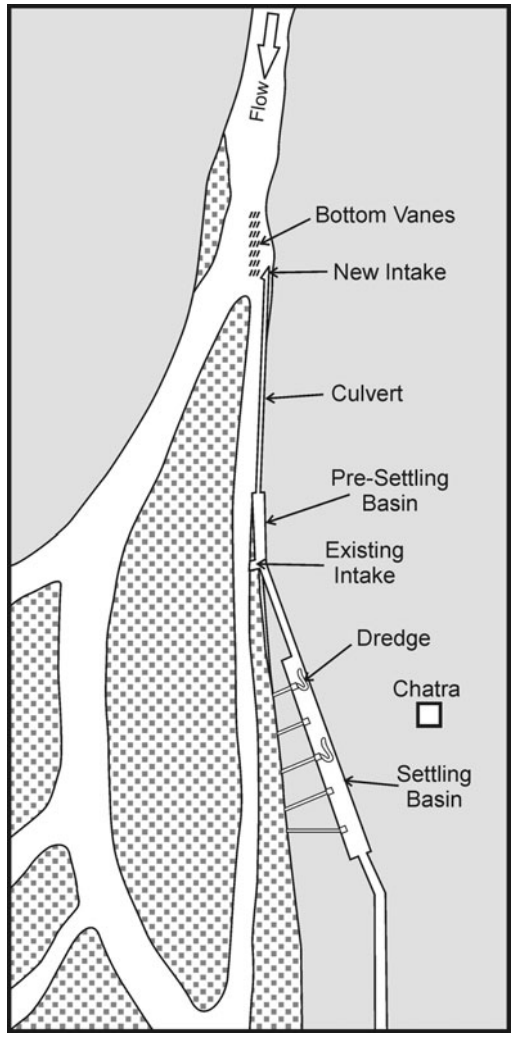

Figure 5-56. Schematic showing old and new intake on Kosi River, Nepal. Courtesy of J. Oosterman, DHV Consulting Engineers.

due to sediment depositions within and near the intake. Every year at the end of the wet season, the existing intake became blocked with sediment and extensive dredging was necessary (Fig. 5-57). Channel instability (braiding) was the cause of the problem. The solution consisted of constructing a new intake 1.3 km upstream closer to a stable (narrower) section of the river. Figure 5-58 is an upstream, pre-construction view of the new intake site. Submerged vanes were installed in front of the intake to maintain a deep channel between the intake and the deeper parts of Kosi River and prevent bed material from entering the intake.

At the new intake, the water level varies from about 109 m at an extreme low flow of 400 to 500 m^3/s to about 113 m at an extreme high flow of 9,000 m^3/s. At the design low-flood flow of 2,000 m^3/s, the water level is at 110.5 m, and at the

Figure 5-57. Dredging at the old intake on Kosi River. Courtesy of J. Oosterman, DHV Consulting Engineers.

Figure 5-58. Upstream preconstruction view of site of the new intake. Courtesy of J. Oosterman, DHV Consulting Engineers.

design high-flood flow of 8,000 m^3/s, the water level is at 112.7 m. At the average-flood flow, the discharge is 4,300 m^3/s and the water level is at 111.7 m. At this condition the average-flow velocity on the left side of the river near the intake is 2 to 2.5 m/s. The slope of the water surface at the intake varies from about 0.0013 at the low-flood condition to about 0.0025 at the high-flood condition. The bed material is broadly mixed (a mixture of pebbles, cobbles, and boulders; see Fig. 5-57). The median diameter is about 30 mm.

The design calculation for the vane installation was based on the following considerations: To ensure that the vanes are effective in generating a secondary circulation of sufficient strength over the range of design-flow conditions (water levels ranging from 110.5 m to 112.7 m), the top elevation of the vanes had to be at 109.0 to 109.5 m. Since the average bed elevation in the vane area is about 107.8 m, vane height had to be H = 1.2 to 1.7 m. The length of the vanes must be at least three times H (i.e., L = 3.6 to 5.1 m). The orientation of the vanes depends on the direction of movement of the bed material and on the local bank configuration. The available data suggest that the vanes' angle with the average bankline should be α = 20 to 25 degrees. A schematic section view is seen in Fig. 5-59.

The final design calculations are summarized in Table 5-4. The calculations are for a vane system in which the vanes extend from elevation 107.8 m to 109.0 m,

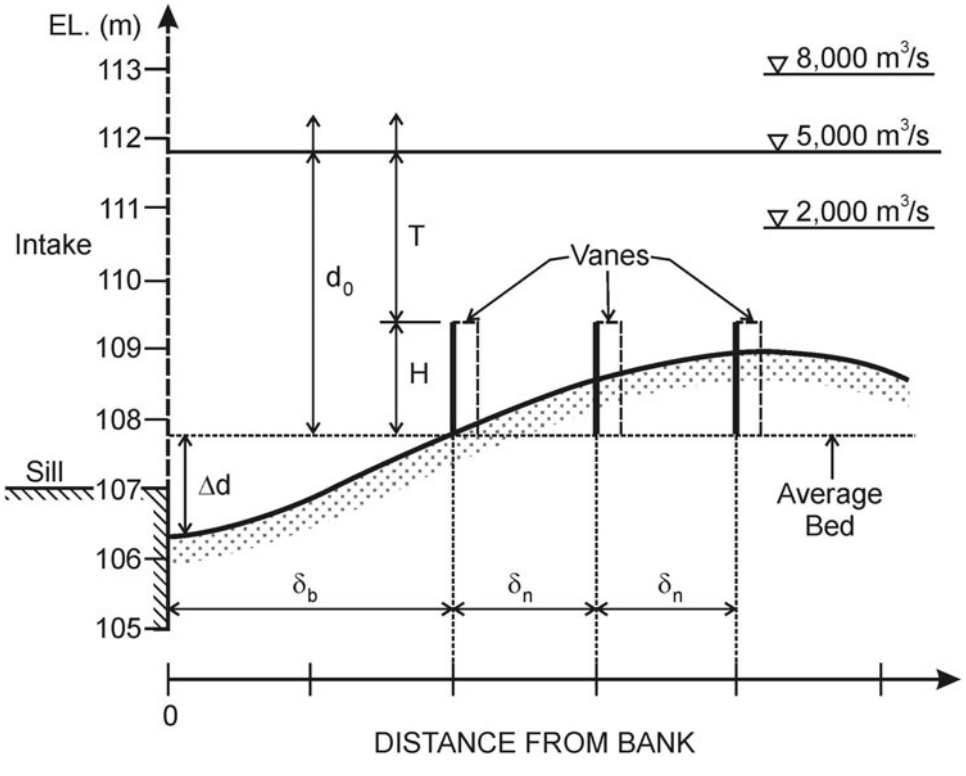

Figure 5-59. Schematic showing design parameters for the Kosi River vane installation.

Table 5-4. Final design calculations for layout defined in Figs. 5-60 and 5-61.

River flow (m^3/s)	*Water level* (m)	*Average water depth,* d_o (m)	*Average velocity,* u_o (m/s)	*Water surface slope*	*Sediment Froude number,* $\mathbf{F}_D$	*Channel resistance, m*	*Vane submergence,* T/d_o	*Maximum bed level change,* $\Delta d/d_o$	Δd (m)
2,000	110.5	2.7	2.0	0.0013	3.7	4.3	0.5	0.2	0.5
3,000	111.0	3.2	2.5	0.0015	4.6	4.6	0.6	0.2	0.6
4,000	111.4	3.6	3.0	0.0017	5.5	4.9	0.7	0.2	0.7
5,000	111.8	4.0	3.4	0.0019	6.3	5.0	0.7	0.2	0.8
6,000	112.2	4.4	3.7	0.0021	6.8	4.9	0.7	0.2	0.9
7,000	112.5	4.7	4.0	0.0023	7.4	4.9	0.7	0.2	0.9
8,000	112.8	5.0	4.3	0.0025	7.9	4.9	0.8	0.2	1.0

their spacing is δ_n = 3.5 to 5.0 m and δ_s = 30 to 40 m, and the vane-to-bank distance is δ_b = 8 to 12 m. The calculations indicate that a vane system can be designed for this site that will generate and maintain a near-bank channel with a bed elevation 0.5 to 1.0 m lower than the average bed level (i.e., the bed in the near-bank channel can be lowered to an elevation of 106.8 to 107.3 m). By increasing the vane height so that the top elevation of the vanes is at 109.5 m instead of 109.0 m, the bed level in the near-bank channel could be lowered to about 106.3 to 106.8 m.

Figures 5-60 and 5-61 show the final vane layout and design. The design consists of 35 vanes in arrays that are located about 30 m from the bank. The distance

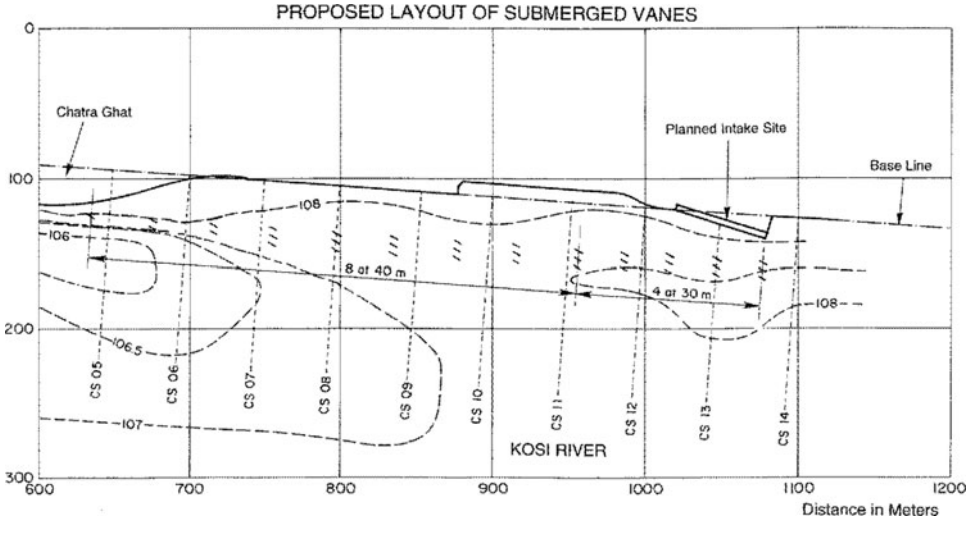

Figure 5-60. Bed topography at the intake, with general layout of the vane system.

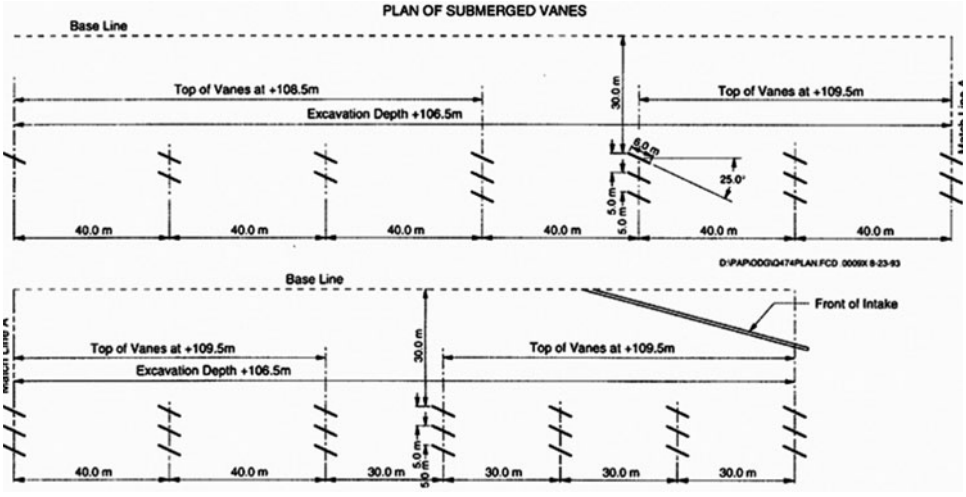

Figure 5-61. Final design layout of the vane system in Kosi River. Courtesy of J. Oosterman, DHV Consulting Engineers.

from the reference line to the vane nearest the bank is $\delta_b = 30$ m. The longitudinal spacing δ_s is 40 m for the upstream vanes and 30 m for the downstream vanes. The lateral spacing is $\delta_n = 5$ m. The vanes are set with a top elevation of 108.5 m upstream and 109.5 m downstream. The length of the vanes is $L = 6$ m and the vanes' angle with the flow is $\alpha = 25$ degrees. The foundation depth of the two river-side vanes is at elevation 100 m. The foundation depth of the vane at the approach channel is at elevation 98 m.

The design vane-to-bank distance is larger than desirable. As a result, the bed level in the approach channel may not be as low as calculated.

Another design concern was the stability of the bed topography. Although the intake was moved to a section that historically had been relatively stable, during design bank erosion was observed on the right bank of the section. Because the section was located so close to the braided part of the river, there was a concern that the pattern of scour and deposition at the section could change with time, causing uncertainty about the long-term performance of the vane system. Consequently, a recommendation was made to construct one or two submerged weirs extending out from the right bank upstream of the intake structure. The weirs would be 40 to 50 m long, angled upstream at about 45 degrees with the flow lines, and would have a top elevation of about 108 m. The weirs would stabilize the bank and bed topography on the right side of the channel and would ensure that sufficient flow be directed toward the left channel. The recommendation was not implemented.

A recommendation was also made to reshape the bankline immediately upstream of the new intake. The field data suggested that the protrusion of the bank into the river at that point might be detrimental at certain stages by promoting deposition in the area between the protrusion and the intake. At other stages, the

protrusion might act as a sediment deflector. A shaving of the bank back to the reference line would create ideal approach-flow conditions for the intake. This recommendation was implemented to some degree. A burial site at the protrusion prevented full implementation.

Figures 5-62, 5-63, and 5-64 show the installation of vanes. A cofferdam was built around the construction site and water inside it was pumped out. As indicated in Fig. 5-62, a reinforced slab was poured to support each array of three vanes. The slab, in turn, was supported by reinforced concrete diaphragm walls extending to an elevation of 100 m. The upstream face of each vane was provided with a steel plate to fender the impact of boulders. Figure 5-63 shows a completed vane array. Figure 5-64 shows the same array as the water level starts to rise. Figure 5-65 is a downstream view of the vane system just as the water level reaches the top of the vanes.

The installation took place in 1994–1995. The installation has performed well ever since. Figure 5-66 shows a 2004 DigitalGlobe image of the site. The image shows the river at extreme low flow, and the tops of the vanes are visible. The figure shows how the vanes are maintaining a near-shore channel toward the new intake. The vanes are "maintaining" a sandbar on the river side of the vanes—a sandbar that without vanes would have been up against the shoreline and intake. The vane system is seen to have reconfigured the bed topography over at least 15% of the channel width.

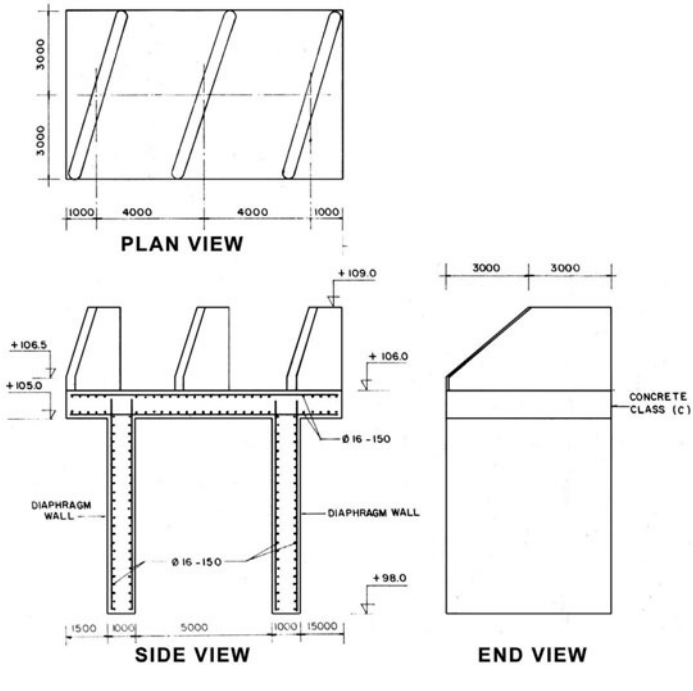

Figure 5-62. Vane details, in plan and elevation view. Courtesy of J. Oosterman, DHV Consulting Engineers.

Figure 5-63. Installation of vane system. View downstream, showing intake on the left, the cofferdam on the right, and the slab with a set of three vanes in the middle. Courtesy of J. Oosterman, DHV Consulting Engineers.

Figure 5-64. View downstream of completed vane installation in Kosi River. The intake is on the left and the cofferdam on the right. Courtesy of J. Oosterman, DHV Consulting Engineers.

Figure 5-65. Vane installation in Kosi River. View downstream shortly after completion, at extreme low flow. Most of the cofferdam has been removed. At elevation 109.5 m, the tops of the downstream vanes are above the water surface. Courtesy of J. Oosterman, DHV Consulting Engineers.

Figure 5-66. 2004 DigitalGlobe image showing low flow in Kosi River near the intake. The image shows the vane system and intake. Flow is from top of image. The vane system is seen to maintain a near-bank channel toward the intake. The vane-induced sand deposit on the far side of the vane system is also clearly visible. Courtesy of DigitalGlobe.

5.4 Stabilization of River Channel Alignment

Des Moines River, United States

Figure 5-67 shows bank erosion in the Des Moines River, Iowa, at River Mile (RM) 105.9. Two legs of a structure carrying power transmission lines are located about 10 m from the eroding bank. The concern is continuing erosion of the bank and eventual undermining of the structure. Figure 5-68 is an aerial photo showing the plan form of the river and the location of the structure relative to the plan form.

To properly design a bank stabilization structure at this site, a channel stability analysis was conducted. The analysis was performed using data on Des Moines River between Tracy at RM 130.4 and Ottumwa at RM 94.1. The data were obtained from studies by the U.S. Army Corps of Engineers (1979), the U.S. Department of the Interior (1995–2000), and Odgaard (1987; 1989b). The reach-averaged, bank-full conditions are (Odgaard 1987): discharge, Q = 900 m^3/s; slope, S = 0.00041; top width, b = 176 m; flow depth, d_o = 4.8 m; average velocity, u_o = 1.07 m/s; friction parameter, m = 3.1; and Froude number, $\mathbf{F}_D$ = 10.1.

The approach is as described in Section 4.6. A review of the aerial photos of the river upstream and downstream from the site indicates that the channel is classified as meandering. This is also confirmed by comparing Q and S with Leopold's and Wolman's (1957) data plotted in Fig. 2-17. With b/d_o = 176/4.8 = 36.7, and m = 3.1, and $\mathbf{F}_D$ = 10.1, Fig. 2-20(a) yields a meander wavelength of λ = 1,900 m.

Figure 5-67. Bank erosion in Des Moines River, Iowa.

Figure 5-68. Aerial view (2000) of Des Moines River at problem site. Courtesy of U.S. Geological Survey.

A meander pattern with this wavelength provides maximum overall channel stability. This is the wavelength the channel would naturally adopt with time if the flood-plain conditions were uniform throughout the reach (i.e., had uniform geological and surface-cover conditions).

The reach under consideration has relatively uniform flood-plain conditions and thus should attain greatest stability at this wavelength (about 1,800 m). Indeed, the three well-defined meander bends just upstream from the reach and the two immediately downstream from the reach fit into a wave pattern with a wavelength of about 1,800 m. Figure 5-69 shows a comparison of the ideal (most stable) meander pattern [Fig. 5-69(a)] and the meander pattern of the reach under consideration [Fig. 5-69(b)]. It is seen that in order for the reach under consideration to fit into the stable wave pattern, the channel should have an eastward meander curve at the site rather than a westward [Fig. 5-69(c)]. An eastward meander curve is also apparent from the topography and vegetation, which suggests that it was the channel-plan form in the past. Figure 5-70 shows the eastward meander curve overlaid on the 2000 channel. The stability analysis suggests that a westward meander curve at the site, which appears to be emerging and causing the erosion problem, is not naturally sustainable unless it is forced by some nonuniformity in the flood-plain characteristics. The nonuniformity could be a rock outcrop, a heavy stand of trees, a manmade structure, or some other obstructive feature.

A channel behavior like the one observed at this site (a meander curve developing in the "wrong" direction) was also observed at a site about one mile upstream some time prior to 1964 [see Fig. 5-69(b)]. Sequential aerial photos show that the upstream site is now returning to a more stable alignment, with a meander wavelength of about 1,800 m. It is not known whether the return to a more stable alignment at that site was triggered by artificial means or whether it happened naturally.

A channel behavior like the one observed at our site (and the upstream site) typically occurs when local, upstream flood-plain features (natural or manmade) restrict the natural meandering process. In this case, the channel restriction at the upstream meander curve could be the cause of the instability at the site. As the flow moves around this curve, the channel narrows from about 180 m just up-

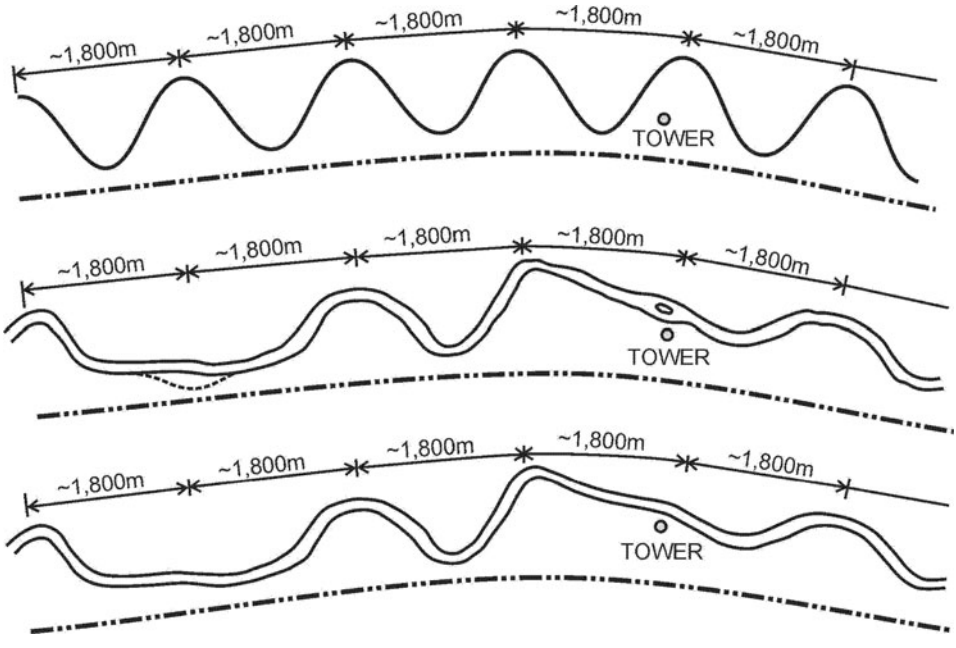

Figure 5-69. (a) Ideal, most stable meander pattern; (b) current meander pattern of reach; and (c) natural evolution of current meander pattern toward greater stability.

stream from the curve to about 120 m just downstream from apex of the curve (Fig. 5-71). This is a 30% reduction in channel cross section. The reduction in width is manmade (a riprap embankment on the left bank). The reduction in width causes a reduction in water-surface slope upstream of the curve and an increase in slope downstream. The increase in water-surface slope downstream from the curve, combined with the expansion of the channel cross section, sets the stage for channel instability. The instability is clearly visible in the bed features seen on the 2000 aerial photo. Some of the bed features are indicated in Fig. 5-71. Immediately downstream from the constriction, the flow is decelerating, and a de-

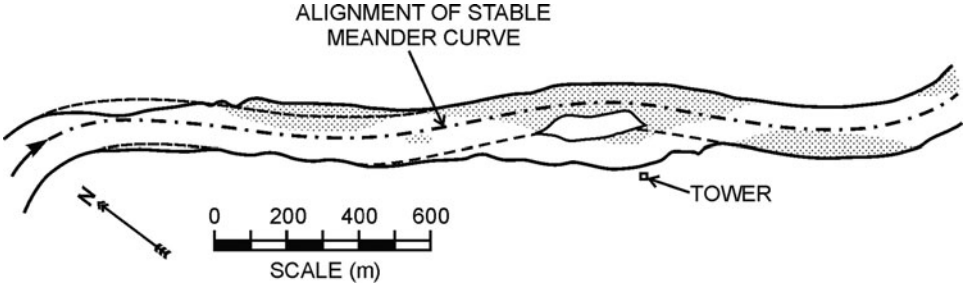

Figure 5-70. Stable meander curve overlaid on the 2000 channel.

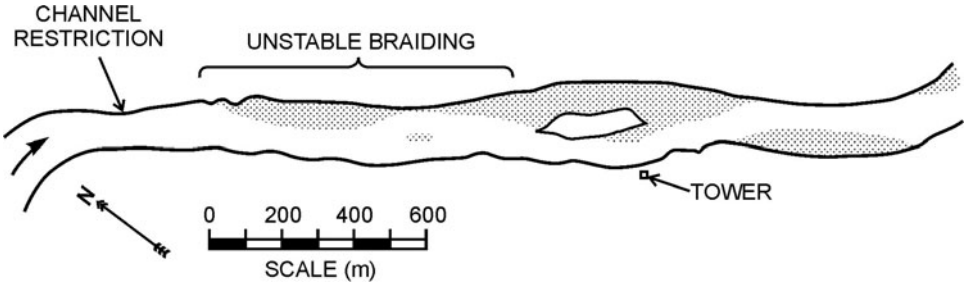

Figure 5-71. 2000 channel. Taken from aerial photo taken October 9, 2000.

celerating flow is inherently unstable—meaning the flow can meander either way or braid, as seen on the aerial photo. In such a reach it would take very little to "swing" the flow one way or the other.

Thus, the stability analysis indicates that the bank erosion at the site should decrease with time. However, two factors work against this indication and suggest that it could continue. First, the bank has been depleted of vegetation and is now more erodible than the bank immediately upstream and downstream. Eddies and secondary currents will likely develop along this section of bank. As a result, a local cavity may develop. This cavity would grow until eddies within it are slow enough to not cause any more erosion. In fact, the aerial photos show evidence of the beginning of such a cavity. Second, the island in the middle of the river upsets the flow pattern. The island may cause local currents to be deflected straight toward the site. Both factors could be significant and could cause the bank at the site to erode at least another 2 to 3 m before reaching equilibrium. Although the stability analysis suggests that it is not likely that the bank will ever erode clear to the structure, the island may induce an unpredictable (and unstable) meander development.

The solution derived from the stability analysis entails installing a flow deflector at the right descending bank at the point where the flow would naturally move away from the right bank toward the left bank (Fig. 5-72). This solution

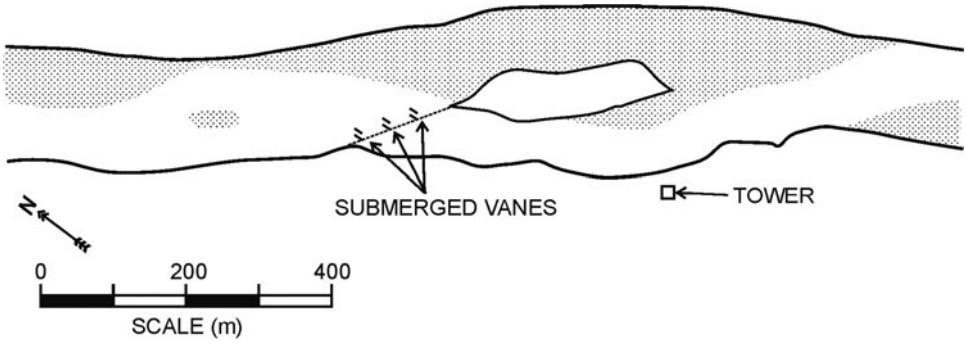

Figure 5-72. Proposed solution. Submerged vanes deflect bed load into the western channel.

would reestablish stability and minimize overall bank erosion along the entire reach. Submerged vanes would be ideally suited to act as a flow deflector. The vane layout would be designed to reestablish the secondary current that would naturally sustain the meander pattern. The vane system would ensure that at medium and high flow a greater portion of the flow is diverted into the eastward channel, the channel east of the big island. The result would be a gradual lowering of flow velocities in the western channel by the eroding bank. The lower velocity would promote deposition of sand in the western channel and reduce the potential for continued bank erosion. The anchoring of the flow deflector would require in situ studies.

It should be emphasized that it would not take a significant structure to trigger the return of the channel to a stable alignment.

A phased construction would be appropriate. Phase I would include the installation of the vane system. The system would need to be laid out so that it provides the correct curvature to the current. The approach would be as described in Section 4.2. Phase II would be implemented only if there is evidence of further erosion damage at the site. Phase II would include the construction of small dikes, hard points, or vanes along the eroding bank to help promote deposition in the western channel. The stability analysis suggests that the Phase II measures would be temporary measures that become redundant once the channel has returned to its natural alignment. Implementation has not begun yet.

CHAPTER 6

Summary of Design Guidelines

The following is a brief summary of (a) typical dimensions, (b) primary design considerations for different applications, (c) vane materials used so far, and (d) limitations to vane use.

6.1 Typical Dimensions

Table 6-1 lists typical dimensions for vane design and layout. These dimensions are based on experience obtained to date.

As indicated in Section 4.1, selection of the design depth of flow, d_o, is probably the most important step in the design process. The effectiveness of a vane system is measured by the system's ability to move bed load, and to reconfigure flow and depth distribution and solve a river training or sediment problem, and at the same time maintain or enhance channel and bank stability. This requires a careful analysis of the relationship between stage, discharge, velocity, bed-load transport, and bank material. Typically, calculations of vane design and layout are required for a range of stages or depths, and final design and layout are selected among several alternatives.

The vane dimensions listed in Table 6-1 are only typical; site-specific conditions may require adjustments to those dimensions. For example, if the bed material is relatively fine, the angle of attack may have to be less than 10 to 20 degrees to avoid unacceptable local bed scour at the leading and trailing edges of the vanes. If the angle of attack is decreased because the bed material is relatively fine, the lateral and/or longitudinal spacing may have to be reduced to compensate for the decrease in induced circulation. A reduction of lateral and longitudinal spacing may also be necessary if vane height is limited due to navigation or other activities on the river. Vane angle of attack would also be less than 10 degrees if the bend is sharply curved. Due to the significant skew of the vertical velocity profile, with near-bed velocity vector strongly skewed toward the inside of the curve, vanes in a sharply curved channel may have an angle of attack of less than 5 to 10 degrees. The distance to bank or intake is also very dependent on local conditions. This distance can only be finalized after a careful study of upstream

Table 6-1. Typical dimensions for vane design and layout.

Variable	*Dimension*
Design depth of flow, d_o	Application-specific (see Section 4.1)
Vane height, H	0.2–0.4d_o (typically 1–3 m)
Vane thickness	0.05–0.20 m
Vane length, L	3H
Lateral spacing, δ_n	3H
Longitudinal spacing, δ_s	10–30H
Distance to bank or intake, δ_b	3H
Angle of attack, α	10–20 degrees

approach-flow patterns, in particular those along the bank immediately upstream from the vane field. A stream stability analysis may be necessary to assess the stability of the upstream portions of the river. The result of such an analysis should be considered in determining the location and configuration of the upstream vanes relative to the bank. If necessary, measures must be taken to stabilize the upstream channel (revetments, submerged weirs). Natural (or manmade) slope of bank is also an important consideration in determining vane-to-bank distance. As a rule of thumb, there should be at least three vane arrays upstream of the section to be stabilized.

Installation technique and tolerances are other variables that must be considered during design. Field experience shows that vane performance is maintained at the desired level when the vanes' angle of attack is within ± 3 degrees of the design angle and linear dimensions are within about 10% of the design dimensions.

6.2 Primary Design Considerations

The most common cause of local bank and bed instability is excessive scour and/or deposition. The first step in determining whether vanes can solve the problem is to estimate the vane design and layout required to change the bed configuration to one that will ensure a stable channel reach.

In a river curve, a vane system consisting of arrays of two or three vanes located close to the outer bank, designed to reduce depth and velocity along the bank to cross-sectional average, would typically suffice. The aforementioned typical dimensions would serve as benchmarks or starters in the design process. Detailed design would proceed as described in Section 4.2.

In straight channels, stability is often achieved by making the vanes develop and maintain a compound channel (i.e., a channel with berms along each bank). In this case, vane height and the number of vanes per array are determined by the cross section that provides the most stable low-flow and high-flow channels. Stable-channel design considerations may be required. Detailed design of the vane installation would proceed as described in Sections 4.3 and 4.4.

At water intakes and diversions, first step should be to locate the stream tube formed by the separating stream surface and the bank line (Eq. 2-33). Ideally, the innermost row of vanes would be located far enough away from the stream tube that any bed load brought in suspension by the vanes will not enter the intake but continue past it. If estimates (Eq. 2-34) show that the vanes are not able to prevent bed load from entering the intake, a skimming wall should be considered. The wall would be parallel with and at a distance from the intake, and the vane field would be located outside the wall. For it to be most effective, the skimming wall should be located such that the stream tube defined by the withdrawal rate lies completely within the channel formed by the skimming wall and the bank line. The wall would be attached (flared) to the river bank upstream of the intake. The angle of the slanting section of the wall should not exceed 10 degrees. The vanes should be placed on the riverside of the wall according to the aforementioned guidelines for vanes alone.

If local considerations limit the outward extent of the skimming wall/vane system, the skimming wall/vane system may fall within the stream tube. In this case, specific discharge ratio determines whether a skimming wall is necessary. If specific discharge ratio is greater than 0.2, a skimming wall should be installed between the vanes and the intake. Optimum distance from the face of the intake would be about 0.12 times the width of the intake opening, and the top of the wall should extend above the intake sill by a distance of about 0.25 to 0.33 times the diversion design flow depth. If the specific discharge ratio is greater than 0.3, considerations should be made to widen the intake to bring the ratio down. Detailed vane design would proceed as described in Section 4.5

When vanes are used for stabilizing a river channel alignment or for remeandering of a reach, it is important that the design be preceded by a channel stability analysis. Such an analysis would consist of either a review of historical, sequential aerial photos of stable upstream and downstream channel reaches, or a formal perturbation stability analysis, or both. The vane system would be designed and installed to preserve the dominant wavelength measured on the aerial photos or calculated by the stability analysis. The phase lag calculated would give the distance from the crossover point to the point where the first vane array should be installed (the point of "first outer-bank erosion occurrence"). In the case of remeandering of a reach, the amplitude of the meanders should be determined such that the water surface slope is, as much as possible, constant through the reach and equal to the slope in the reaches immediately upstream and downstream of the reach. The channel-forming discharge will often be the same as bank-full discharge; however, there are cases where a more comprehensive analysis is required. Dominant wavelength, phase lag, and potential scour depth would be estimated as described in Section 4.6.

Finally, it must be recognized that not all river training and sediment management problems can be solved by a submerged vane system alone. Many projects will require a combination of technologies. The Byron and Huntly projects described in Chapter 5 required upstream flow training by submerged wing dams to create appropriate approach-flow conditions for the vane system. A recently

completed flow and sediment management project at El Kuraimat on the Nile River, Egypt (Odgaard et al. 2006; Odgaard 2008) required, in addition to a vane system, both groins and a riprap embankment in the upstream reach of the river. This project was as much a problem of river channel stability as it was a problem of sediment management. The groins and riprap embankment were constructed to ameliorate a large-scale channel instability problem created some time in the past, whereas the vane system (and skimmer wall) solved the near-field problem of sediment control at a power plant water intake. In this case, the vane system would not have provided a long-term solution to the sediment problem if the channel stability problem had not been solved at the same time. The Nile project is also an example of a project where boundary conditions were too complex for a design by simple analytical calculations. The design required both numerical and hydraulic model studies.

6.3 Typical Vane Materials

So far, the prototype vane material has been either wood, sheet piling, or concrete. In the West Fork Cedar River and Feng-Shan installations, the vanes were constructed from sheet piling (Figs. 5-21 and 5-26). Sheet pile vanes were also used at Missouri River installations, the most recent of which is the Cooper Nuclear Station installation completed in 2006 (Figs. 6-1, 6-2, and 6-3), and at Kureimat Power Station on the Nile River, Egypt completed in 2007 (Fig. 6-4). The vanes in the East Nishnabotna River consist of planks supported by H-piles (Fig. 6-5). In the Kuro River (Fukuoka 1989; Fukuoka and Watanabe 1989), the vanes were constructed from round wood poles (Fig. 6-6). In these cases, the vanes were essentially flat-plate designs. Such a design is effective as long as vane thickness is small compared with vane length and height. Because of the angle of attack, the flow separates at the leading edge of the plates, and local scour occurs. The Kuro River vanes are provided with a relatively large-diameter circular column at the leading edge of the vanes. According to Fukuoka and Watanabe (1989), this column reduces local scour and results in somewhat higher efficiency, as measured by the amount of sand accumulated per vane. This is probably because the rounded nose reduces the size of the separated zone. The leading edge on the East Nishnabotna vanes is a 20-cm-wide flange on the H-piles supporting the vanes. This flange produces considerable separation and local scour and, obviously, inhibits the generation of circulation.

In many installations the vane material is reinforced concrete. Examples include vanes installed in the Kosi River in Nepal described earlier (Fig. 5-63). As mentioned earlier, the vanes in Kosi River are built (in threes) onto a slab, which in turn is supported by reinforced concrete diaphragms that extend into the river bed. The vanes in the Muskingum River are vertical slabs supported by H-piles (Fig. 5-54). In a number of installations, the vane is shaped as a double-curved foil with a twisted rear edge and a rounded nose (Fig. 1-19). Examples include the vanes installed in the Wapsipinicon (Fig. 5-9), Maquoketa, Cedar, and Rock Rivers

Figure 6-1. Vane installation at Cooper Station, Missouri River. The photo shows a barge-mounted guide for vane alignment near the face of the intake (left). Flow is from top left. Courtesy of Rhoël M. Tierra, Nebraska Public Power District.

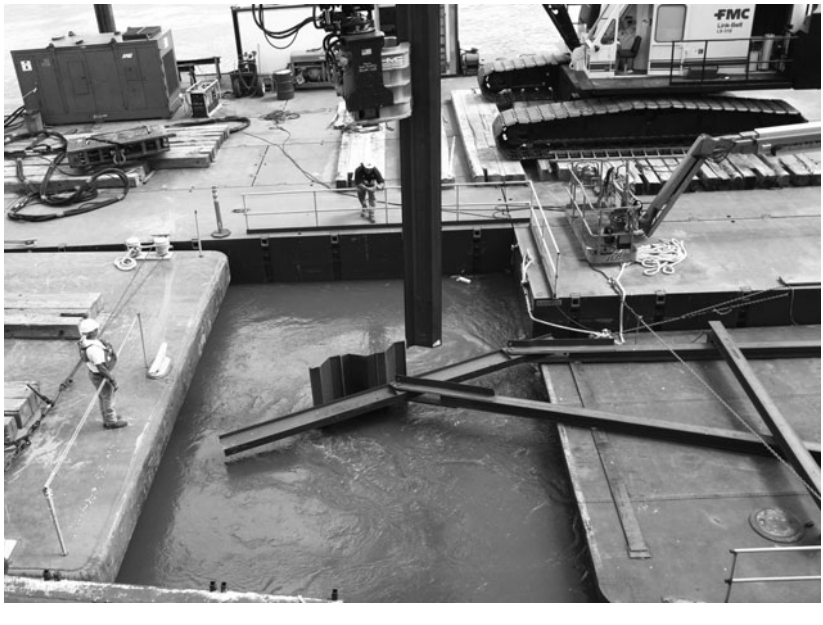

Figure 6-2. Vane installation at Cooper Station, Missouri River. Sheet-pile vanes are being installed along the guide for vane alignment. Flow is from left to right. Face of intake is at bottom of photo. Courtesy of Rhoël M. Tierra, Nebraska Public Power District.

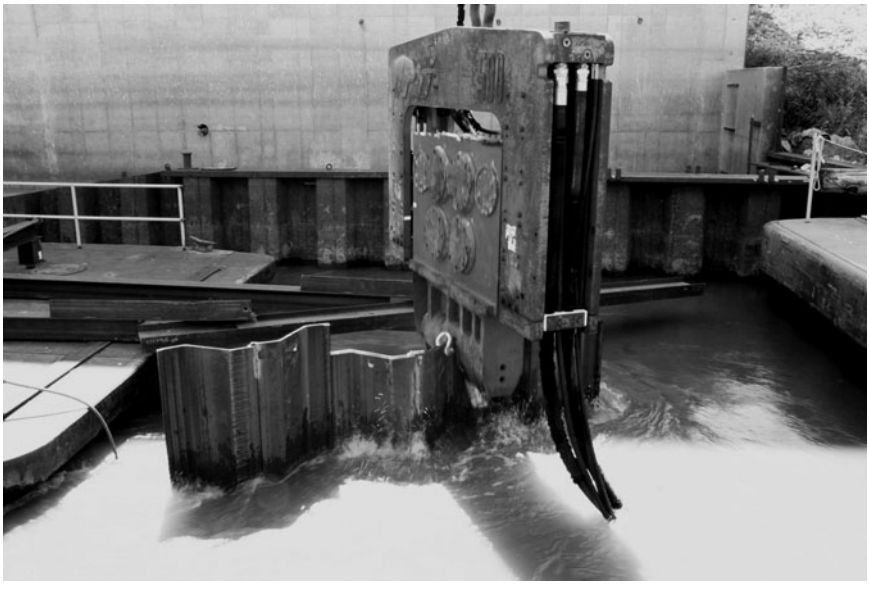

Figure 6-3. Vane installation at Cooper Station, Missouri River. Following alignment along the guide and minimum penetration into the bed (Fig. 6-2), all sheet-piles are driven to final elevation using a vibratory driver. View toward face of the intake. Courtesy of Rhoël M. Tierra, Nebraska Public Power District.

Figure 6-4. Vane installation at Kuraimat Power Station, the Nile River, Egypt, 2007. Photo shows sheet-piles being driven in a template that controls vane orientation. Intake is in the background of the photo. Courtesy of Adnan M. Alsaffar.

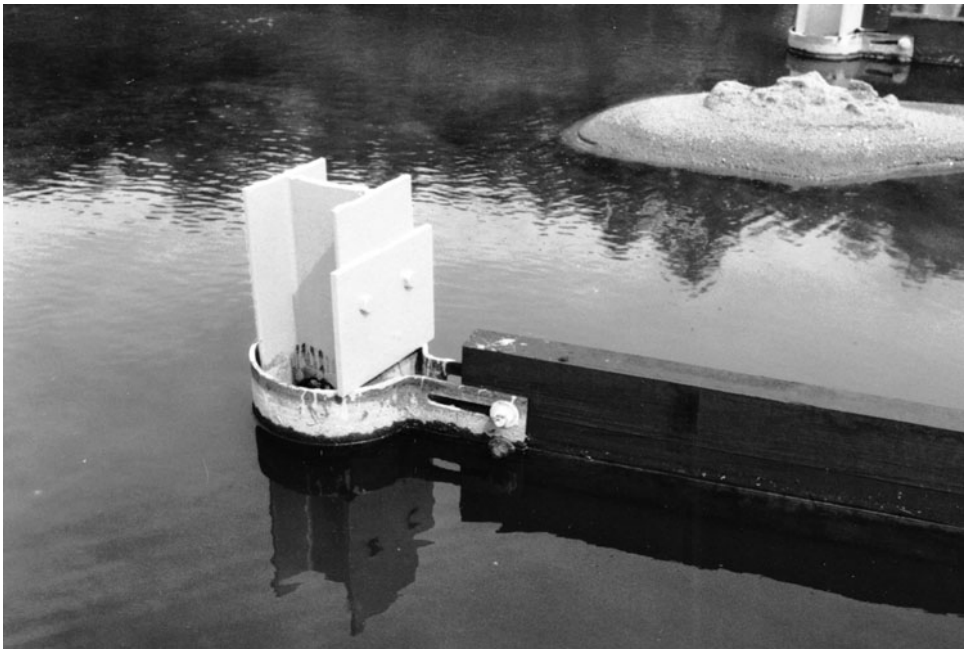

Figure 6-5. Vanes in East Nishnabotna River, Iowa consist of vertical planks supported by H-piles. They are prevented from floating by anchor plates on the flanges of the H-piles.

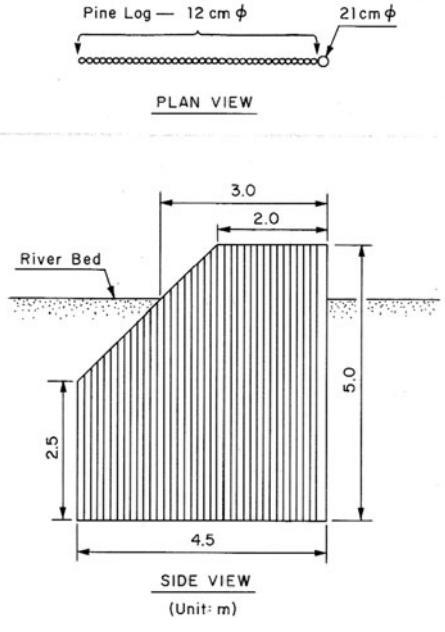

Figure 6-6. Vanes in Kuro River, Japan, constructed from round wood poles. *Source:* Fukuoko (1989), ASCE.

in the United States and in the Waikato River in New Zealand (Fig. 5-41). Figures 6-7 and 6-8 show the installation of such vanes in Clear Creek, Iowa. The shape of these vanes was developed in laboratory tests (Figs. 1-16, 1-17, 1-18, and 1-19). The rounded nose is designed to reduce separation and minimize the impact forces of ice and debris at low flow. The twisted shape occurs as a result of a downward increase in the camber of the vane. This increase in camber is designed so that a certain (elliptical) circulation distribution is maintained along the height of the vane. As the camber increases toward the bed, the effective angle of attack increases. This increase compensates for the decrease in flow velocity near the bed from bed friction, and the resulting circulation distribution is nearly the same as that associated with a thin, flat plate in a uniform velocity field (Odgaard and Spoljaric 1989). Thus, the shape of the vane produces a nearly ideal circulation distribution, despite the fact that the vane is located in a boundary layer. This feature of the vane, and its sturdiness, are the main advantages of the twisted design. The vanes are supported by piles driven into the riverbed (Figs. 6-7 and 6-8).

Typically, the piles are H-piles that fit inside a circular or square cut-out of the vanes. In some designs, the H-pile has a pipe section at the top and the vanes are sleeved, as shown in Fig. 6-9. Once the H-pile is driven to design elevation, the vane is slipped over the pipe connection and locked into the proper orientation.

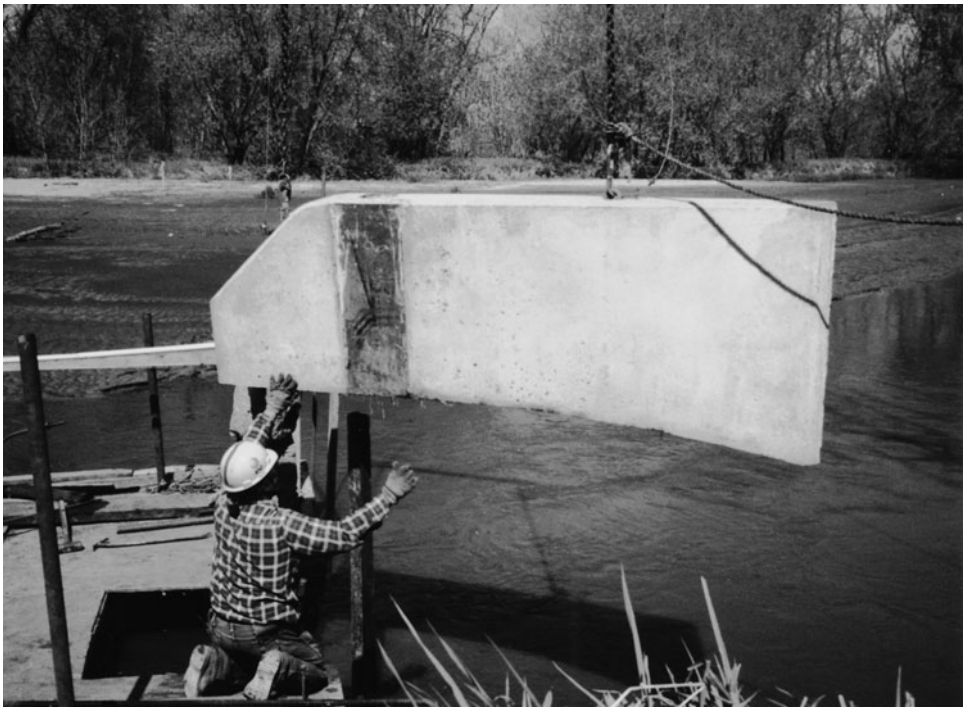

Figure 6-7. Vane installation in Clear Creek, Iowa. The vane is slipped over an H-pile that fits inside a circular cut-out of the vane. Courtesy of Robert DeWitt, River Engineering International.

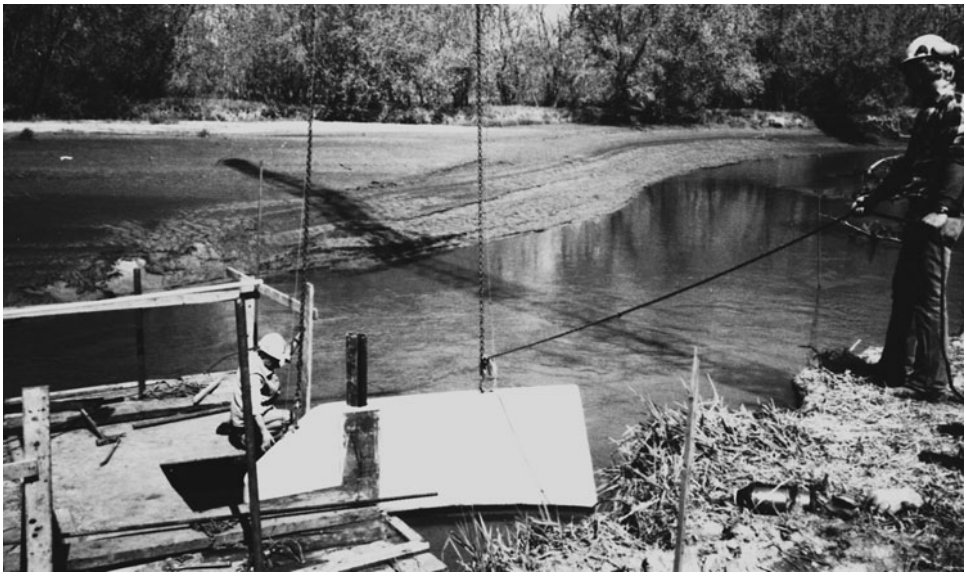

Figure 6-8. Vane installation in Clear Creek, Iowa. Once aligned correctly, grout is poured into the cut-out. Courtesy of Robert DeWitt, River Engineering International.

In some installations, a nose pile is also provided (Fig. 5-41). The nose pile is driven to sufficient depth that it can prevent the vane from being misaligned by side load. The nose pile is also designed so that it can be pulled out and reinserted in case the vane alignment needs to be adjusted. Nose pipe and main pile with pipe connection are shown on the vane sculpture in Fig. 6-10.

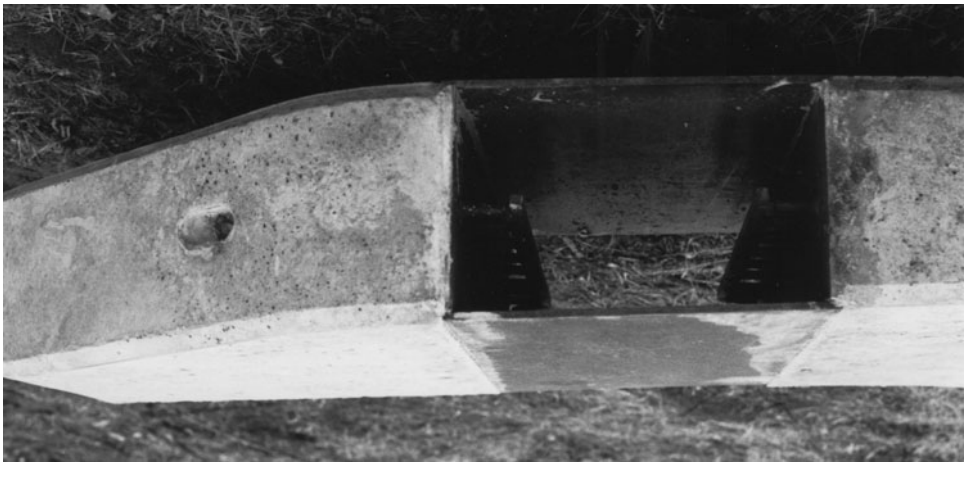

Figure 6-9. Top view of sleeved vane. Courtesy of Robert DeWitt, River Engineering International.

Figure 6-10. Vane display at Huntly Power Station, New Zealand, showing details of nose pipe and main H-pile with pipe connection. *Source:* Electricity Corporation of New Zealand (1993), with permission from Genesis Energy.

It is likely that other materials and designs can also be used. As was mentioned in the Introduction, Odgaard and Kennedy (1983) have suggested that rows of dumped rock with steep side slopes may achieve much the same result, although more and longer vanes of this type would be required because of the smaller transverse force per unit area that would be exerted on them. This solution could be attractive, either in itself or in combination with shaped or plane vanes, in deep water where pile driving is difficult. The design guidelines developed herein do not apply to rock vanes.

6.4 Limitations to Vane Use

As mentioned several times throughout, vane systems can and should be designed to provide flow adjustments that are sustainable. This objective implies certain limitations on design and use. A sustainable adjustment is one that does not cause any significant change in energy grade line. A change would compromise the channel stability and ecosystem. Sustainability limits the total number of vanes relative to the size of the river, and thus puts a limit on what a vane system can accomplish in terms of river training and sediment management. However, both calculations and measurements in laboratory and field show that even if the number of vanes required to accomplish a certain river training job is relatively large, the effect on grade line is often insignificant.

There are practical limitations on the size of vanes and the depth of flow where they can be installed. The limitations are defined by the requirement that

vane height must be between 0.12 and 0.48 times the design flow depth for optimum or near-optimum performance. In installations so far, effective vane height has varied from less than 1 m in rivers in the midwest of the United States to 5.3 m in the Muskingum River, Ohio. The Kosi River vanes are 3 m tall, sitting on a horizontal slab (Figs. 5-62 and 5-63); however, the lowest 1.5–1.8 m of the vanes was designed to be below average bed level. Theoretically, there is no reason why vane height could not be larger than 5 m. For larger vanes, constructability and installation are the limiting factors. If taller vanes are required, considerations may be given to use of rock vanes instead, or a combination of rock vanes and foil-type vanes.

Vane use for bank protection is limited to banks with flow-induced bank failures (i.e., failures due to excessive bank shear stress). Vanes are not effective in preventing failures due to other mechanisms such as piping and over-bank flow. If the failures are flow-induced, vanes provide protection by reducing near-bank depth and velocity to cross-sectional average values. Vanes cannot prevent bank failures associated with natural channel degradation. When a channel degrades, bank height increases and the bank may become structurally unstable. However, in this case, vanes may help retain the slumped bank material at the toe of the bank and help the bank establish and maintain a new equilibrium slope.

For development and maintenance of a navigation and/or flood-flow conveyance channel, vane height and the number of vanes control what depth can be achieved. Maximum achievable depth is determined from continuity and momentum equations given the vane height and the required width of the navigation or flood-conveyance channel. Since vane height and the number of vanes are subject to the aforementioned sustainability criterion, there is an associated limit on the width and depth that can be achieved of the navigation or flood-conveyance channel.

For sediment control at water intakes, the main limitation is also associated with the requirement of sustainability. The objective is to create a near-shore channel with sufficient flow and depth that bed-load bypasses the intake with no chance to enter to intake. A localized cluster of vanes designed to achieve this objective has the potential for upsetting the overall channel stability. Although in most cases the number of vanes is so small that the impact on the channel dynamics is insignificant, a channel stability analysis is always recommended.

In all applications, there are limitations due to other factors besides channel stability. Navigation requirements, ecosystem vulnerability, and aesthetics may limit vane height and/or extent of the vane system. The same would be the case when the river is used for recreational activities such as boating and water skiing. The ultimate indicators of a successful design are that it enhances the river and its environment and facilitates sustainable developments around the river.

This page intentionally left blank

References

American Society of Civil Engineers (ASCE). (1975). *Sedimentation engineering*, ASCE Manuals and Reports on Engineering Practice No. 54, ASCE, New York, N.Y.

Barkdoll, B. D., Ettema, R., and Odgaard, A. J. (1999). "Sediment control at lateral diversions: Limits and enhancements to vane use," *J. Hydraul. Eng.*, 125(8), 862–870.

Biedenham, D. S., Elliot, C. M., and Watson, C. C. (1997). "The WES stream investigation and streambank stabilization handbook," U.S. Army Corps of Engineers, Vicksburg, Miss.

Bledsoe, B. P., and Watson, C. C. (2001). "Logistic analysis of channel pattern thresholds: Meandering, braiding, and incising," *Geomorphology*, 38, 281–300.

Chabert, J., Remillieux, M., and Spitz, I. (1961). "Application de la circulation transversale a la correction des rivieres et a la protection des prises d'eau," *Proc., Ninth Conv.*, IAHR, Dubrovnik, Yugoslavia, 1216–1223 (in French).

Chang, H. H. (1988). *Fluvial processes in river engineering*, John Wiley & Sons, New York, N.Y.

Dahm, J., and Hume, T. M. (1989). "An investigation of sediment intake problems at Huntly Power Station," Electricity Corporation of New Zealand, Production Division, Huntly Power Station, Huntly, New Zealand.

DeWitt, R. J., and Odgaard, A. J. (1991). "Submerged vane projects for bank stabilization and sedimentation management," *Proc. National Conf. on Hydraulic Engineering*, ASCE, Nashville, Tennessee, July 29–August 2.

Doyle, M. W., Shields, D., Boyd, K. F., Skidmore, P. B., and DeWitt, D. (2007). "Channel-forming discharge selection in river restoration design," *J. Hydraul. Eng.*, 133(7), 831–837.

Eibeck, P. A., and Eaton, J. K. (1987). "Heat transfer effect of a longitudinal vortex embedded in a turbulent boundary layer," *J. Heat Transf.*, Transaction of the ASME, 109(1), 16–24.

Electric Power Research Institute (EPRI). (1995). "Review of river-bed sediment problems at intakes," EPRI Report No. TR-105201, EPRI, Palo Alto, Calif.

EPRI. (1997). "A laboratory study of sediment control at riverside water intakes," EPRI Report No. TR-108621, EPRI, Palo Alto, Calif.

EPRI. (1998). "Bed-sediment control at riverside water intakes: A guide for utility engineers," EPRI Report No. TR-110551, EPRI, Palo Alto, Calif.

Ettema, R. (1990). "Bathymetric survey of the Cedar River at the Duane Arnold Energy Center," IIHR LD Report No. 166, The University of Iowa, Iowa City, Iowa.

Fitzpatrick, F. A., Peppler, M. C., Schwar, H. E., Hoopes, J. A., and Diebel, M. W. (2005). "Monitoring channel morphology and bluff erosion at two installations of flow-deflecting vanes, North Fish Creek, Wisconsin, 2000–03," Scientific Investigations Report 2004-5272, U.S. Department of the Interior, U.S. Geological Survey, Reston, Va.

Flokstra, C. (2006). "Modeling of submerged vanes," *J. Hydraul. Res*., 44(5), 591–602.

Fukuoka, S. (1989). "Groins and vanes developed basing upon a new concept of bank protection," *Proc., Natl. Conf. on Hydraulic Engineering*, ASCE, New Orleans, La., 224–229.

Fukuoka, S., and Watanabe, A. (1989). "New bank protection methods against erosion in the river," *Proc., Japan–China Joint Sem. on Natural Hazard Mitigation*, Kyoto, Japan, 439–448.

Henderson, F. M. (1963). "Stability of alluvial channels," *Trans. Am. Soc. Civ. Eng.*, 128(Part I), 657.

Ikeda, S., and Nishimura, T. (1985). "Bed topography in bends of sand-silt rivers," *J. Hydraul. Eng*., 111(11), 1397–1411.

Jain, S. C., Kundert, M., and Goss, J. (1994). "Field survey of the Rock River. Commonwealth Edison Byron Nuclear Power Station," IIHR LD Report No. 225, The University of Iowa, Iowa City, Iowa.

Jansen, P. Ph., van Bendegom, L., van den Berg, J., de Vries, M., and Zanen, A. (1979). *Principles of river engineering*, Pitman Publishing Ltd., London, U.K.

Keller, R. J. (1993). "Huntly heat rejection project. Stabilization of river bed," Electricity Corporation of New Zealand, Ltd., Huntly Power Station, Huntly Thermal Group, Huntly, New Zealand.

Lamb, H. (1932). *Hydrodynamics*, 6th ed., Cambridge University Press, Cambridge, U.K.

Lane, E. W. (1957). "A study of the shape of channels formed by natural streams flowing in erodible material," M.R.D. Sediment Series Report No. 9, U.S. Army Engineer Division, Missouri River, Corps of Engineers, Omaha, Nebraska.

Leopold, L. B., and Wolman, M. G. (1957). "River channel patterns—braided, meandering and straight," U.S. Geological Survey Professional Paper 282B, U.S. Geological Survey, Washington, D.C.

Leopold, L. B., and Wolman, M. G. (1960). "River meanders," *Bull. Geolog. Soc. Am.*, 71, 769–794.

Marelius, F. (2001). "Vane applications and vane induced flow," thesis presented to the Royal Institute of Technology, at Stockholm, Sweden, in partial fulfillment of the requirements for the degree of Doctor of Philosophy.

Melville, B. W., Odgaard, A. J., Wang, Y., and Sinha, S. K. (1992). "Hydraulic model study of sediment management alternatives. Commonwealth Edison Byron Station River Water Intake Structure," IIHR Limited Distribution Report No. 198, The University of Iowa, Iowa City, Iowa.

Michell, F., Ettema, R., and Muste, M. (2006). "Case study: Sediment control at water intake for large thermal-power station on a small river," *J. Hydraul. Eng.*, 132(5), 440–449.

Milne-Thomson, L. M. (1966). *Theoretical aerodynamics*, Dover Publications, Inc., New York, N.Y.

Muste, M., and Ettema, R. (2000). "River-sediment control at Conesville Power Station, on the Muskingum River, Ohio," Report No. 410, Iowa Institute of Hydraulic Research, The University of Iowa, Iowa City, Iowa.

Nakato, T., Kennedy, J. F., and Bauerly, D. (1990). "Pump-station intake-shoaling control with submerged vanes," *J. Hydraul. Eng.*, 116(1), 110–128.

Nakato, T., and Ogden, F. L. (1998). "Sediment control at water intakes along sand-bed rivers," *J. Hydraul. Eng.*, 124(6), 589–596.

Neary, V. S., Sotiropoulos, F., and Odgaard, A. J. (1999). "Three-dimensional numerical model of lateral-intake flows," *J. Hydraul. Eng.*, 125(2), 126–140.

Odgaard, A. J. (1987). "Streambank erosion along two rivers in Iowa," *Water Resour. Res.*, 23(7), 1225–1236.

Odgaard, A. J. (1989a). "River-meander model. I: Development," *J. Hydraul. Eng.*, 115(11), 1433–1450.

Odgaard, A. J. (1989b). "River-meander model. II: Applications," *J. Hydraul. Eng.*, 115(11), 1451–1464.

Odgaard, A. J. (2008). "Stability analysis in stream restoration," *World Environmental and Water Resources Congress 2008 Ahupua'a*, ASCE/EWRI, Honolulu, Hawaii, May 12–16.

Odgaard, A. J., and Abad, J. D. (2007). "River meandering and channel stability." *Sedimentation engineering: Processes, measurements, modeling, and practice*," M. Garcia, ed., ASCE Manuals and Reports on Engineering Practice No. 110, ASCE, Reston, Va.

Odgaard, A. J., and DeWitt, R. J. (1989). "Sediment control by submerged vanes," *Proc., 20th Annual Conf., Intl. Erosion Control Assoc.*, Vancouver, British Columbia, Canada.

Odgaard, A. J., and Kennedy, J. F. (1983). "River-bend bank protection by submerged vanes," *J. Hydraul. Eng.*, 109(8), 1161–1173.

Odgaard, A. J., and Lee, H. Y. E. (1984). "Submerged vanes for flow control and bank protection in streams," IIHR Report No. 279, Iowa Institute of Hydraulic Research, The University of Iowa, Iowa City, Iowa.

Odgaard, A. J., and Mosconi, C. E. (1987). "Streambank protection by submerged vanes," *J. Hydraul. Eng.*, 113(4), 520–536.

Odgaard, A. J., and Spoljaric, A. (1986). "Sediment control by submerged vanes," *J. Hydraul. Eng.*, 112(12), 1164–1181.

Odgaard, A. J., and Spoljaric, A. (1989). "Sediment control by submerged vanes. Design basis," in "River meandering," S. Ikeda and G. Parker, eds., Water Resources Monograph No. 12, American Geophysical Union, Washington, D.C., 127–151.

Odgaard, A. J., and Wang, Y. (1990). "Sediment control in bridge waterways," Report No. 336, Institute of Hydraulic Research, The University of Iowa, Iowa City, Iowa.

Odgaard, A. J., and Wang, Y. (1991). "Sediment management with submerged vanes. I: Theory," *J. Hydraul. Eng.*, 117(3), 267–283.

Odgaard, A. J., and Wang, Y. (1991). "Sediment management with submerged vanes. II: Applications," *J. Hydraul. Eng.*, 117(3), 284–302.

Odgaard, A. J., Wang, Y., and Neary, V. S. (1990). "Hydraulic-laboratory model study of river intake at Duane Arnold Energy Center," IIHR Limited Distribution Report No. 177, The University of Iowa, Iowa City, Iowa.

Odgaard, A. J., Abdel-Fattah, S., Ali, A. M., El Ghorab, E. A. S., and Alsaffar, A. (2006). "Sediment management at a water intake on the Nile River, Egypt," *Conf. Proc., An International Perspective on Environmental and Water Resources*, ASCE/EWRI, New Delhi, India, December 18–20.

Ouyang, H., Weber, L., and Odgaard, A. J. (2006). "Design optimization of a two-dimensional hydrofoil by applying a genetic algorithm," *Eng. Optimization*, 38(5), 529–540.

Pauley, W. R., and Eaton, J. K. (1987). "Experiments on the development of longitudinal vortex pairs in a turbulent boundary layer," *AIAA J.*, 26(7), 816–823.

Petersen, M. S. (1986). *River engineering*, Prentice-Hall, Englewood Cliffs, N.J.

Potapov, M. V., and Pyshkin, B. A. (1947). "Metod poperechnoy tsirkulyatsii i ego primenenie v gidrotekhnike" ["The regulation of water streams with the method of artificial cross circulation"], Izd. Ak. Nayk. SSSR, Publishing House of the Academy of Sciences of the USSR, Moscow, Leningrad, the Soviet Union (in Russian).

Raudkivi, A. J., and Ettema, R. (1985). "Scour at cylindrical bridge piers in armored beds," *J. Hydraul. Eng.*, 111(4), 713–731.

Sabersky, R. H., and Acosta, A. J. (1964). "Fluid flow," MacMillan Publishing Co., New York, N.Y.

Spoljaric, A. (1988). "Mechanics of submerged vanes on flat boundaries," thesis presented to the University of Iowa, at Iowa City, Iowa, in partial fulfillment of the requirements for the degree of Doctor of Philosophy.

U.S. Army Corps of Engineers. (1979). "Des Moines river bank erosion study, Iowa and Missouri, Stage 2," Final Feasibility Report, Rock Island District, U.S. Corps of Engineers, Rock Island, Ill.

U.S. Army Corps of Engineers. (2008). "River engineering basics", St. Louis District Applied River Engineering Center, <http://www.mvs.usace.army.mil/engcon/expertise/arec/basics_elements.html>

U.S. Department of the Interior. (1995–2000). " Water resources data for Iowa," U.S. Geological Survey Water Data Reports, Water Resources Division, U.S. Geological Survey, U.S. Department of the Interior, Washington, D.C.

van Zwol, J. A. (2004). "Design aspects of submerged vanes," thesis presented to Delft University of Technology, at Delft, The Netherlands, in partial fulfillment of the requirements for the degree of Master of Science.

Voisin, A., and Townsend, R. D. (2002). "Model testing of submerged vanes in strongly curved narrow channel bends," *Can. J. Civ. Eng.*, 29, 37–49.

Wang, Y. (1989). "Bank protection with submerged vanes," *Proc., XXIII Cong., Intl. Assoc. for Hydraulic Research*, Vol. S, 17–23.

Wang, Y. (1990). "Sediment control with submerged vanes," thesis presented to the University of Iowa, at Iowa City, Iowa, in partial fulfillment of the requirements for the degree of Doctor of Philosophy.

Wang, Y., and Odgaard, A. J. (1993). "Flow control with vorticity," *J. Hydraul. Res.*, 31(4), 549–562.

Wang, Y., Odgaard, A. J., Melville, B. W., and Jain, S. C. (1996). "Sediment control at water intakes," *J. Hydraul. Eng.*, 122(6), 353–356.

Ward, J. V., Tockner, K., Uehlinger, U., and Malard, F. (2001). "Understanding natural patterns and processes in river corridors as the basis for effective river restoration," *Regulated Rivers: Research & Management*, 17(4–5), 311–323.

Zeller, J. (1967). "Meandering channels in Switzerland," *Proc. Symp. on River Morphology*, Intl. Assoc. of Scientific Hydrology, Bern, Switzerland, 75, 174–186.

Zimmermann, C., and Kennedy, J. F. (1978). "Transverse bed slopes in curved alluvial streams," *J. Hydr. Div.*, 104(1), 33–48.

This page intentionally left blank

Index

About the Author

A. Jacob Odgaard is Professor of Civil and Environmental Engineering at the University of Iowa and Research Engineer at IIHR-Hydroscience and Engineering. He is also a former Associate Dean for Research and Graduate Studies in the College of Engineering, University of Iowa. Prior to coming to the United States, he was Senior Research Engineer at the Danish Hydraulic Institute. His expertise includes environmental fluid mechanics, river mechanics, hydraulic structures, and hydraulic modeling. In 2001, he received the Hydraulic Structures Medal from the American Society of Civil Engineers (ASCE) in recognition of his innovations in experimental and engineering design. Previous honors include ASCE's Karl Emil Hilgard Hydraulic Prize, and being named Editor and Associate Editor of ASCE's *Journal of Hydraulic Engineering*. He is a Fellow of ASCE and a registered Professional Engineer in Iowa. His consulting activities span the globe. He is also an FAA-certified flight instructor and captain in the Civil Air Patrol.